I. PATTERNING OF SILICALITE-1 FILMS USING CO_2 LASER ABLATION

II. IMPACT OF DEPOSITION AND LASER DENSIFICATION OF SILICALITE-1 FILMS ON THEIR OPTICAL CHARACTERISTICS

Dissertation by

Swarnasri Mandal

In Partial Fulfillment of the Requirements for the

Degree of

Doctor of Philosophy

UNIVERSITY OF MISSOURI

Columbia, Missouri

May 2015

The undersigned, appointed by the dean of the Graduate School, have examined the dissertation entitled

I. PATTERNING OF SILICALITE-1 FILMS USING CO_2 LASER ABLATION

II. IMPACT OF DEPOSITION AND LASER DENSIFICATION OF SILICALITE-1 FILMS ON THEIR OPTICAL CHARACTERISTICS

Presented by Swarnasri Mandal, A candidate for the degree of

Doctor of Philosophy in Bioengineering

And hereby certify that, in their opinion, it is worthy of acceptance.

Assistant Professor Heather K. Hunt (Chairperson of the Committee)

Professor Fu-hung Hsieh

Professor Sheila Grant

Professor John A. Viator

Professor Kevin L. Shelton

ACKNOWLEDGMENTS

The time I have spent at Mizzou has been equally challenging and enjoyable days of my life, and I know that I will always remember Mizzou and the wonderful people that I have met here with great affection. Over the last five years, I have been privileged to interact and work with truly inspiring and talented educators, researchers, mentors, authors, and administrators, and I am sincerely grateful to all of them for their guidance and support. This thesis is the culmination of several years of effort that would not have been possible without them.

First and foremost, I would like to thank my advisor, Professor Heather K. Hunt, for being the most encouraging advisor I can imagine. I'm thankful for her support, financial and otherwise, throughout my time here. I have been very fortunate to work in her lab, and this work would not have been possible without her efforts, suggestions, and patience when not everything worked perfectly. I will always be grateful to her for giving me this opportunity and showing immense trust and confidence in me and for providing a healthy, learning and exciting working environment. She will always be a source of inspiration in my life. I'm fortunate to be the first Doctorate student from her Lab.

I would also like to thank the members of my Candidacy and Thesis Committees, Professor Fu-hung Hsieh, Professor Sheila Grant, Professor John A. Viator and Professor Kevin L. Shelton for their suggestions, support, and kindness. Professor Shubhra and Keshab Gangopadhyay have been very kind and provided me with advice, guidance in addition to access to Dr. Shubhra's lab. Dr. Cherian J. Mathai has trained me in using

several characterization tools and has provided essential insight into these techniques. To all of you, thank you. Additionally, I would like to thank members of Electron Microscopy Core at Mizzou for their help and advises during the long and excruciating hours of electron microscopy. I'm thankful to Professor Shantanu Bhattacharya and Professor Amitabha Ghosh for being my mentors in IIT, Kanpur and intriguing the sense of scientific research and for believing in my potential.

I would like to thank all the members of the Hunt group, past and present, who have made my time here at Mizzou both educational and entertaining. Specifically, I would like to Thank Dylan, Ali, Heather, Anna, Charissa, Emily, Paul and Ben for being wonderful lab mates. I would like to thank Bala, for his constant support and willingness to drop anything if I needed help. With him, I have experienced all the joys and anguish of life and research at Mizzou and have become friends for life.

Finally, I thank my parents, Asok Kumar and Banani Mandal, without their encouragement, support and faith I would not have the courage to move across the globe and made it to Mizzou. I'm thankful to my sister, Srirupa and brother-in-law, Sourendra for being my best friends and standing by me whenever I needed from across the world, listening in hardship, sorrow and laughter and truly caring for me. I'm thankful to my niece, Annika for being the only person who can lighten me up at any given point and is a source of great joy in my life. I'm thankful to my Grandma for her prayers, blessings and inspiration. I'm thankful to God for all of them. To all of you, I owe a debt of gratitude that I can only hope I can repay.

God bless all of you.

TABLE OF CONTENTS

LIST OF FIGURES

LIST OF TABLES

ABSTRACT

Although the field of integrated optics has advanced tremendously, the state-of-the-art still lags behind its electronic counterpart. One of the main challenges that consistently arises is the creation, characterization, and evaluation of new material systems for this field. For instance, nanostructured materials, like carbon nanotubes, graphene, quantum dots, and a plethora of oxide-based materials have properties that could be beneficial to integrated optics; however, very few of these materials have been evaluated for this purpose. This limits their use in integrated optical systems. Porous, nanostructured oxide materials, like zeolites, have unique and complex relationships between structure and physicochemical properties that can be tuned during their synthesis by interchanging framework atoms such as Zn, Ti, etc. or by introducing guest molecules, such as small organic molecules or nanoparticles. In particular, zeolites have uniform microporosity and structural symmetry, and can be produced in a variety of topologies that result in desirable physicochemical properties, such as high surface area, thermal stability, and shape and size selectivity, in addition to unique optoelectronic properties tailored by guest/host interactions. Using the same model zeolite system and composition (topology MFI), in thin film form we evaluate its potential for integrated optics.

The synthesis and patterning of nanostructured materials in a controlled fashion is of great interest for application in electronic devices, photonics, energy storage, and biological/chemical analysis. Recently, porous, nanostructured materials, such as silicalite-1 zeolite films, have been used to form 2D and 3D structures for building nano-containers and other intricate assemblies for harvesting light, for sensing applications or

for creating microreactors. Traditionally, these films have been synthesized as multilayers of randomly oriented crystals; however, these types of new applications require precise control of the crystal orientation, surface coverage, film thickness and, most importantly, post-synthetic patterning. The standard methods used to pattern such nanostructured materials are based on either typical microfabrication techniques, which involve several complex steps of long duration, or organization of pre-formed seeds/crystals arranged uniformly by chemical linkages, which requires precise control and positioning and could result in pore clogging. To avoid these challenges, we evaluate the use of CO_2 laser ablation, which has earlier shown good potential for patterning of sol-gel materials. Here, we demonstrate the effects of this technique on the patterning of a model zeolite thin film system, silicalite-1 (MFI), to evaluate its potential for patterning complex, multicrystalline, nanostructured materials.

The effects of CO_2 laser irradiation on silicalite- films i.e. densification effects to cause changes in degree of porosity, crystallinity which in turn results in changes in transmission and absorption characteristics of the films (IR and Raman spectrum) and the evolution these properties on account of changes in laser irradiation power were also studied. The results of this study will help determine the suitability of zeolites for optoelectronic materials and introduces a one-step, non-destructive and rapid technique to pattern materials with specific framework structures and subnanometer pore sizes thus broadening their usage in areas of optical sensing, optical signal processing or optical computing.

Chapter 1: Introduction and Organization of Thesis Presentation

1.1 Introduction to Zeolites and Molecular Sieves

Zeolites are a group of nanostructured microporous materials that have been studied extensively due to their ultra-high surface-to volume ratio, which is typical of nanomaterials. Their pore size ranges from 0.2-2 nm and their crystalline structure forms a three-dimensional network made up of atoms like Si, Al, Ga, Ge, Zn, Be, etc. These atoms (also called T-atoms) are tetrahedrally linked to four oxygen atoms, and through these shared oxygen atoms, to their adjacent T-atoms, thus keeping the framework ratio of oxygen to T-atoms as 2. Compared to compositionally equivalent amorphous materials, zeolites exhibit appreciable acid activity with shape-selective features. Elements iso-electronic with Al^{+3} or Si^{+4} have been proposed to substitute into the framework lattice during synthesis including B^{+3}, Ga^{+3}, Fe^{+3} and Cr^{+3} in place of Al^{+3}, and Ge^{+4} and Ti^{+4} in place of Si^{+4}. The acidity of the materials is modified by the incorporation of transition elements such as Fe^{+3} for framework Al^{+3} cations. The general empirical formula for the composition of a zeolite is: $Al_2O_3 \bullet x\ SiO_2 \bullet y\ H_2O \bullet M_{2/n}O$, where M is a cation. The ratio of silica (SiO_2) to alumina (Al_2O_3) is variable; however, since aluminum tetrahedra do not sit in adjacent positions owing to the bond angle strain that would impose, it is always equal to or greater than two. From these tetrahedral building blocks, one- , two- , and/or three dimensional structures are formed, which in

turn may be interconnected to create microporous cages and channels of different sizes and shapes for which zeolites are famous [1, 2].

Zeolites are named based on three letter structure codes representing their specific framework type (structure). As of December 2013, 217 different framework types of zeolites, many with multiple compositions, have been successfully created, with many more theoretically predicted [3]. The International Zeolite Association (IZA) assigns a three letter code to each kind of framework and the codes are adapted from the manner in which the basic units, i.e. tetrahedral arrangement of atoms, are connected to one another irrespective of the kind of atom or chemical composition or unit cell size [1, 4].

Zeolites are a material of high-commercial value owing to the three primary molecular sieve properties: they act as (1) selective and strong absorbers, (2) selective ion-exchangers, and (3) excellent solid-state catalysts. The importance of most zeolites in terms of their industrial use is based on their ability to selectively absorb one component from a mixture over another. Because of their unique porous, crystalline nanostructure, as well as the molecular sieving properties mentioned previously, zeolites have been widely used in a variety of applications, such as separations, catalysis, ion-exchange, and heavy metal adsorption, etc. processes, primarily as powders or powder-coatings of structural materials [5, 6].

1.2 Introduction to Patterning Techniques

In past few decades, several powerful tools have been designed and developed for making structures and devices in the micro/nano-domain. It is established that 'miniaturization' is one of the key factors by which major challenges associated with cost of raw material, processing and efficiency can be addressed. Miniaturization, particularly at the nanoscale, causes quantum confinement of electrons, which in turn would provide us control over the materials' electrical, optical, magnetic, and thermoelectric properties. Worldwide, researchers are interested in the development of information storage devices with dimensions of a few nanometers, thus compelling the need to convert information into either magnetic or optical energy.

With the successful growth and applications of carbon-nanotubes, and graphene-based, one dimensional materials such as nanotubes and nanowires in electronics, mechanics, and optical devices, there has been an increasing focus on creating novel materials as highly ordered nanostructure arrays [7-9]. Features in micro- and nano-domain are created with the techniques of microelectronic fabrication, 'lithography', which impose several technological as well as economical limitations. Currently available techniques like; wet-chemical etching, chemical vapor deposition (CVD), xenon fluoride etching (XeF_2), ion-beam etching, e-beam etching (electron), LIGA (Lithography, Electroplating, and Molding), multi-lamination, laser micromachining, dip-pen lithography etc. have evolved from microelectronics fabrication processes which have been successfully translated to the micromechanics and micro-optics industries.

In order to fabricate features in the sub-nanometer level (the next big requirement) researchers worldwide are looking for newer fabrication modalities with lot of focus on nanostructure formation by self-organization techniques, since the use of expensive lithographical tools such as, electron beam (e-beam) exposure systems etc. can be eliminated for mass production of nanofabricated materials. By using block copolymers, one-dimensional structures have been created where basically regular arrays of patterns (rods, cylinder etc.) were first formed by self-assembly which is later selectively decorated with desired components like metals, semiconductors through physical or chemical bonds thus acting as templates [10-12].

Features in nanometer sizes have also been fabricated by using naturally occurring structures as hosts which have proven to be beneficial for obtaining large-area and nanometer sized structures with greater aspect ratio, which are otherwise challenging to fabricate with conventional lithography [13-15]. For making nanosized materials templates like nanorods, nanowires, nanodots, porous silicate, mesoporous zeolites, carbon nanotubes (CNT), polycarbonate membranes, electro-spun polymer fibers, pre-existing nano-structured materials etc. have been used extensively [16-28]. Another highly investigated template is that of anodic aluminum oxide (AAO), which acts by directing growth of features in nano-dimension owing to their precisely aligned nano-sized porous structures [13, 29, 30].

According to existing reports, when amorphous colloidal silica polymerized with fulfurl alcohol and triblock polymer (pluronic P123) were carbonized and mixed and kept under hydrothermal conditions, caused transformation of the previously amorphous silica

to crystalline zeolite. On purification and removal of the carbon matrix by combustion, the zeolite crystals obtained were of mean sizes 103 nm [10, 31-33]. These hard-templates used to direct the growth of the nanostructures provides the benefit of imposing controlled and uniform dimensions at large scale. The basic goal is to fill the intrinsic pores with the precursor materials by methods like vapor phase deposition, dipping, liquid injection, creation of negative pressure etc. and the final nanostructures simply adopt the dimensions of the pores and channels of the template [34-36]. However, the use of hard template technique also encumbers certain limitations imposed by harsh post-synthetic treatments, fixed number of template sizes which restricts large-scale manufacturing.

Until now, the properties of zeolite films or coatings that have been put to applications are through the fabrication techniques common to electronic industry for making microstructured supports, mostly on silicon substrates. However, the methods for creating patterned zeolite coating (by pre-modification of the substrate surfaces) have also been explored for e.g. by immersing a gold patterned surface into a synthesis solution of zeolite it is possible to obtain patterned films [37]. Reports exist where mesoporous silica were selectively deposited on patterned substrates but this technique requires precise control and positioning of the substrate between the air and the reaction mixture [12].

Recently, zeolite thin films have been used to form different two-dimensional and three-dimensional structures, such as microreactors, microseperators, micromixers, combinatorial catalysts and as low-dielectric packing materials for integrated circuits. In

most cases zeolite microreactors/microstructures are made by first making the micropatterns (by different means) followed by deposition or coating of zeolite crystals using *ex situ* or *in situ* processes [6, 38].

Though development of features at two-dimensional and one-dimensional using zeolite like materials have been carried out from quite some time with advanced nano-lithographic techniques like; e-beam, focused-ion beam, proximal-probe patterning, X-ray and extreme-UV; however, extensive use of these techniques are debarred from wide-spread and easy access owing several factors already discussed e.g. to cost, material specificity, throughput and limited-scale production. Thus, the need for one-step, less complicated, less expensive; however, applicable to wide variety of materials with satisfactory resolution and feature sizes for creating one-dimensional structure cannot be denied. Certain chemical synthesis methods for creation of one-dimensional structures does take care of some factors like, cost, materials diversity, high-scale production and greater throughput [39]. One of the main objectives of this research is to use the already studied and verified filed of zeolite synthesis (powders or *in situ*) and collaging with another area of patterns making so as to convert zeolite material into the usable form of waveguides and integrated optics.

Patterning of zeolites has been done with several techniques; however; most of these techniques have been stymied by limitations. Our goal is to study the various techniques which have been adapted from various conventional patterning methods, to make micro-scale patterns with zeolite like materials. **Figure 1-1** is a schematic

representation of the various existing zeolite patterning techniques that we have studied extensively, by dividing them into distinct categories namely, top-down and bottom-up.

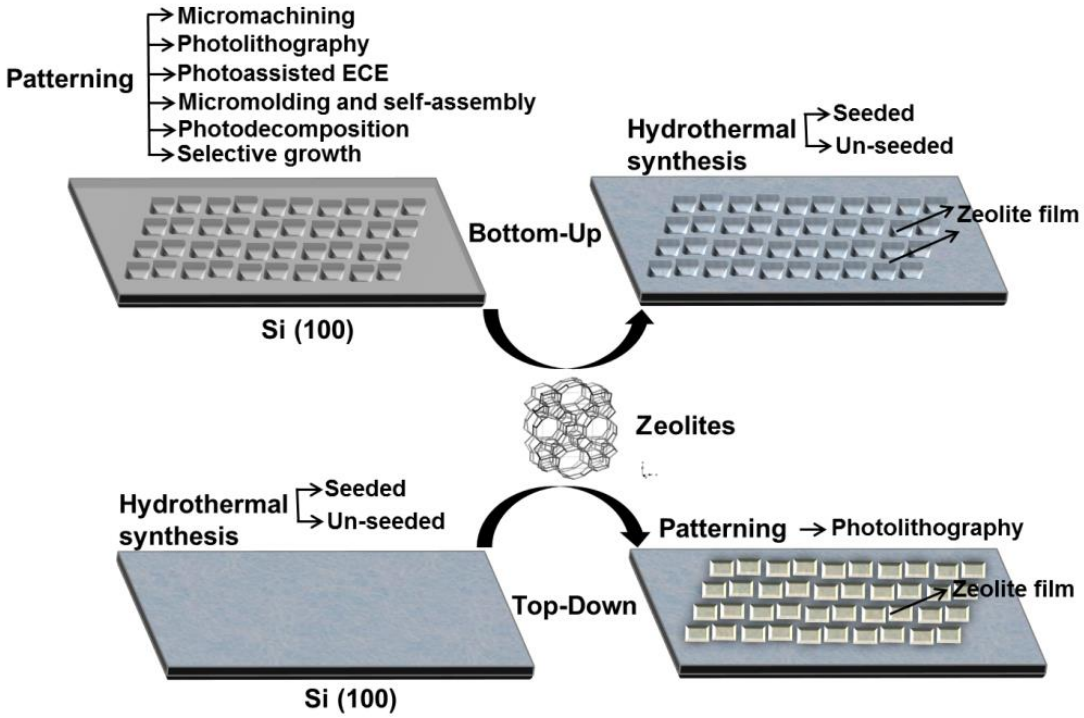

Figure 1-1: Schematic representation of various existing zeolite patterning techniques.

1.3 Introduction to the Synthesis and Formation of Zeolites

The microstructures in zeolites that can be found naturally are also synthesized in the laboratory with the aid of high temperature ovens and autoclaves. Extensive research in this area has confirmed that by using different synthesis temperatures and times it is possible to obtain zeolite crystals ranging from nanometers to several centimeters. By changing the composition of the reaction gel zeolites of modified properties can also be obtained [40]. Typically zeolites can be synthesized in low-temperature processing conditions with high purity, at the same time offering control over its composition, properties, physical structure, pore size and distribution, and can be made in the form of coatings, membranes, films and nanocrystalline powders [41, 42]. Although zeolite has been used more commonly in the form of powders from the beginning, the acts of converting them into two-dimensional structures i.e. films have improved its applications in some major areas like chemical analysis, reactor engineering and molecular separations. In order to increase the strength of the bond between thin films with its corresponding substrate several techniques have been utilized so far [43, 44]. Several reports in the literature suggest that these materials can be deposited or grown on previously patterned substrates using hydrothermal techniques [45-50].

Scientists have used various techniques to synthesize zeolites and most of these processes are now standardized to form desirable zeolite crystal composition, orientation, form and yield. Zeolite like materials (Zeolite Y and ZSM-5) have been synthesized to attain its morphology in nano domain by using CNT with internal diameter of 20-30 nm, where simply the CNT were filled in with reaction gel and the crystallization is done

using autogeneous conditions, later the CNT were removed by combustion [31, 51-53]. The silica content of diatoms has been converted to zeolite ZSM-5 to create or adapt microporous and mesoporous hierarchical structure by the process of 'zeolitization' [28].

It is known that synthesis of zeolite occurs in closed systems with a reaction gel of known composition and the reaction occurring between each component that leads to nucleation followed by its growth in the direction of the most favorable phase [54]. With fine control of the steps of nucleation and growth we can voluntarily direct zeolite growth. By controlling the nucleation it is possible to tune the number and sizes of crystals growth. Based on theory and Ostwald's growth mechanism it have been proven that once the supply of nutrient required for crystal growth is exhausted, growth of crystals ceases to occur [54].

Zeolite nuclei formation at temperature below 100 ^{o}C with the aid of nanoparticles (secondary hydrothermal growth) is typical of silicalite-1 type of zeolites. However, when implied for synthesis of ZAM-12 or other forms of zeolite with different (from TPA) structure directing agent (SDA), did not lead to any crystallization when subjected to low temperatures. When the temperature is raised to above 150 ^{o}C there were formation of typical organized zeolite microporous structures [55, 56].

Apart from the most commonly used TPA as SDA, other organic templates have also been used for attaining similar crystals. Using sol-gel system and low temperature Persson *et al.* synthesized nanosized ZSM-5 (silicalite-1). Several groups reported successful attempts of using the same TPA and obtained much smaller zeolite crystals by increasing the rate of crystallization but lower crystallization time [57]. Valtechev *et al.*

have pointed out that with reduction in the sizes of zeolite crystals it is highly probable that interesting, novel and intrinsic properties are emancipated, which in turn will govern its application in newer field [31].

Use of zeolite nano-seeds to govern growth of zeolite nanocrystals instead of the SDA's or other templates have been investigated [31]. Use of zeolite seeds in order to synthesize zeolite nanocrystals causes aggregation of higher degree, hence it can be stated that this technique is less efficient compared to clear sol gel synthesis at hydrothermal conditions in presence of TPA. Controlled synthesis of ZSM-5 (silicalite-1) has been achieved without using SDA in the presence of silicalite-1 nanocrystals. It is interesting to note that methylene blue (MB) have been used to control the size and yield of nanocrystals of silicalite-1 and it was found that with trace amount of MB the crystals size reduces and the yield increases astonishingly by 20% and 54% respectively [58]. Other groups have also reported the use of acidic amino acids, L-glutamic acids (proved to be most efficient) to control the size of silicalite-1 and titanium silicalite-1 (TS-1) type of zeolites. P. Sharma *et al* have reported that in order to obtain nanocrystals of sizes below 100 nm we can play with the composition of the primary gel or the source of silica [59].

There aren't many publications wherein zeolite materials are used in microfabrication processes. In most cases zeolites are used by embedding/organizing them with high spatial resolution (micrometer scale). To be compatible with this technique large zeolite crystals are required, which impose challenges thus rendering the methods of film or powder growth by deposition or *in situ* the most widely studied areas.

1.4 Introduction to Applications of Zeolite as Material and Patterned Components

The growing interest on nanostructured materials comes from their peculiar, superior and interesting properties compared to their bulk counterparts and these characteristics have been exploited to the most by the microelectronics industry which has unquestionably led to greater performance, which typically burgeoned with integrated chips. Similar to other nanostructured materials zeolites have peculiar, superior and interesting properties compared to their bulk-counterparts which could be exploited by the microelectronic industry. Novel properties of zeolites have rendered them as one of the most widely studied nanostructured materials which can be efficiently synthesized in the form of powders, films, membranes and coatings. The various application can be broadly classified into fields like-membrane reactors, microreactors, chemical sensors, separation membranes, low dielectric constant films (applicable for electronics and computer chips) and hydrophilic coatings (useful in space ships/stations) [38, 60, 61]. For practical applications and better understanding of growth and formation of zeolites the greatest impact have been laid by formation of zeolite films both supported and free-standing. Zeolites in the form of films and membranes are typically useful in separation devices, membrane reactors, and chemical sensors where they act by hosting specific guest molecules that in turn can govern and tune the ultimate optical, electrical or magnetic property of the film.

The advantages of using nanosized zeolite crystals as opposed to micrometer sized for catalytic application are the increase in external surface area by orders of

magnitude and significant reduction in diffusion path length, thus corresponding diffusion time which in turn increases the rate of desired reaction. Application of zeolite nanocrystals in sensing, in Nafion© membranes for proton exchange fuel cells due to increase in conductivity have been established [6, 31, 35, 38]. Frisch *et al.* studied that there is increase in ion-conductivity when the sizes of ZSM-5 (silicalite-1) crystals falls to nano- domain compared to micro- thus giving us the hope of being able to observe improved and novel optical properties as well [62].

Zeolites act as suitable optical and electronic device materials due to its sustainable crystal structure and stability at temperatures of range 550-650 ^{o}C. The end applications of zeolite crystals can vary depending on the crystal orientation on the surface of substrate/membrane not only when they are used for sensing, molecular sieving or separation but also when we are trying to study the electronic or optical properties of the materials [63, 64]. However, the number of available techniques to prepare such devices using zeolite/zeolite like materials is not plenty.

In order to extend the applications of zeolites to such areas it is essential to be able to pattern thin films on different types of supports. Extensive use of zeolite as nanostructured material for most of the stated applications is largely governed by successful production of well-controlled zeolite thin films/coatings with ability to pattern either pre- or post- synthesis. The scale of patterning, quality, resolution and thickness of the device also determines efficiency and effectiveness of the end application.

1.5 Thesis Organization

In this thesis our research is divided into two distinct areas where first **(Part I)** we study techniques used to pattern zeolite (silicalite-1) films to make them into useful components and we also dwell further into material properties of zeolites (silicalite-1) to determine its suitability as optical material. However, both studies are rooted in the development of zeolite (silicalite-1) films.

Chapter 2: provides a general introduction into silicalite-1 materials and their synthesis. In this chapter we discuss in details the theories behind reaction kinetics and synthesis of silicalite-1. This chapter contains information on how silicalite-1 films are created, including support choice, synthetic strategies for films and nanocrystals, spin-coating techniques using different dispersion media, characterization techniques, defect identification and elimination and a short discussion of selecting methods based on application intended.

Chapter 3: provides a comprehensive study of the various existing patterning techniques which is divided into bottom-up, top-down and deposition approaches. The bottom up approaches is subdivided into micromachining, photolithography, photo-assisted electrochemical etching, micromolding and self-assembly and selective growth techniques. The Top-down approach comprise of photo-lithographical approaches. Under deposition approaches; we discuss arranging zeolite crystals through molecular linkers, their alignment by mechanical vibration and optical tweezers and pulse-laser deposition.

Chapter 4: introduces the concept of using CO_2 ablation for patterning of silicalite-1 films, a short discussion on the importance and advantages of using CO_2 laser for patterning silicalite-1 films, synthesis and characterization of silicalite-1 films with applications of such patterned films. We further discuss as-prepared film characteristics, impact of laser properties on patterning characteristics and pattern morphology, the effects of laser raster scanning and beam shadowing. The resulting quality, pattern size and surface roughness of the patterns are also discussed. The effects of densification on silicalite-1 films on account of laser irradiation were also reported. This observation of silicalite-1 film densification and their corresponding alteration of film nature/properties led to further studies conducted in **Part II** of this thesis.

Part II presents the various methodologies studied for making silicalite-1 films for their application as optoelectronic materials. We also studied the optical properties and their variations on account of changes in microporous nature of the film when irradiated with CO_2 laser at different power density.

Chapter 5: provides a general introduction to various non-traditional applications of zeolites. We also provide a brief introduction to application of zeolites as optoelectronic materials and synthesis strategies for silicalite-1 films for such applications. This chapter also discusses the characterizations conducted to evaluate optical properties of zeolites by introducing for the first time studies on *in situ* grown films and comparing them with *ex situ* grown films. Determination of refractive index (RI), infra-red (IR) and Raman spectrum of silicalite-1 films were also discussed. Based on the methodology of patterning silicalite-1 film using CO_2 laser irradiation developed

in **Chapter 3**: we densify *in situ* grown silicalite-1 films using different power density of CO_2 laser and study their transmission and absorption property changes. We also discussed in details and importance of CO_2 laser irradiation of silicalite-1 films and their effects on film properties.

Chapter 6: discusses in details the impact of deposition and laser densification of silicalite-1 films on their optical characterization. We discuss the importance of differentially densified silicalite-1 films as graded refractive index (GRIN) and Bragg stack material owing to changes in microporous nature of the films and release of internal stress when irradiated with CO_2 laser at 10, 20 and 30% power. It also contains a brief review on the importance and ability of zeolite films for hosting dye molecules, semiconductor nanoparticles etc. with applications as antireflective coatings, micro-lasers etc. **Chapter 6**: uses the methodology and strategies developed in **Chapter 4:** to demonstrate the silicalite-1 film synthesis.

Using these films, we investigate their refractive index and compare them based on deposition technique. Through this investigation, we demonstrate that by studying refractive index of *in situ* grown films over *ex situ* grown films various limitations like formation of internal cracks, peeling effects, non-uniform film thickness associated with multiple coatings can be eliminated at the same time superior optical properties can be achieved. We also investigate refractive index variation with respect to changes in nanocrystal sizes for *ex situ* grown films. The transmission and absorption characteristics along with changes in degree of crystallinity (water content, ratio of amorphous to crystalline) of the material on CO_2 laser densified silicalite-1 films were also investigated

for the first time. Here, we propose the application of such materials as non-linear optical material materials with applications as Bragg stacks, gradient refractive index material (GRIN) and optical coatings

Chapter 7: concludes the thesis, summarizes Parts I and II, and discusses future opportunities of using the introduced technique of laser based patterning of zeolite (silicalite-1) films and of further studying effects of patterning and densification of zeolite films by changing zeolite compositions, molar ratio of synthesis gel, dispersion media for *ex situ* synthesis etc. for variation in transmission and absorption characteristics for novel applications primarily, optoelectronic materials.

1.6 References

[1] R. Szostak, Molecular sieves, Springer1998.

[2] M.E. Davis, R.F. Lobo, Zeolite and molecular sieve synthesis, Chemistry of Materials, 4 (1992) 756-768.

[3] http://www.iza-online.org/

[4] M.E. Davis, A. Katz, W.R. Ahmad, Rational catalyst design via imprinted nanostructured materials, Chemistry of Materials, 8 (1996) 1820-1839.

[5] M.E. Davis, Zeolites and molecular sieves: not just ordinary catalysts, Industrial & Engineering Chemistry Research, 30 (1991) 1675-1683.

[6] M. Pina, R. Mallada, M. Arruebo, M. Urbiztondo, N. Navascués, O. De La Iglesia, J. Santamaria, Zeolite films and membranes. Emerging applications, Microporous and Mesoporous Materials, 144 (2011) 19-27.

[7] S. Iijima, Helical microtubules of graphitic carbon, nature, 354 (1991) 56-58.

[8] A.M. Morales, C.M. Lieber, A Laser Ablation Method for the Synthesis of Crystalline Semiconductor Nanowires, Science, 279 (1998) 208-211.

[9] X. Wang, G.-R. Han, Fabrication and characterization of anodic aluminum oxide template, Microelectronic Engineering, 66 (2003) 166-170.

[10] L. Huang, Z. Wang, J. Sun, L. Miao, Q. Li, Y. Yan, D. Zhao, Fabrication of Ordered Porous Structures by Self-Assembly of Zeolite Nanocrystals, Journal of the American Chemical Society, 122 (2000) 3530-3531.

[11] K. Ha, J. Seon Park, K. Sun Oh, Y.-S. Zhou, Y. Sung Chun, Y.-J. Lee, K.B. Yoon, Aligned monolayer assembly of zeolite crystals on platinum, gold, and indium–tin oxide surfaces with molecular linkages, Microporous and Mesoporous Materials, 72 (2004) 91-98.

[12] K. Ha, Y.-J. Lee, D.-Y. Jung, J.H. Lee, K.B. Yoon, Micropatterning of oriented zeolite monolayers on glass by covalent linkage, Advanced Materials, 12 (2000) 1614-1617.

[13] H. Masuda, K. Fukuda, Ordered metal nanohole arrays made by a two-step replication of honeycomb structures of anodic alumina, Science, 268 (1995) 1466-1468.

[14] H. Masuda, F. Hasegwa, S. Ono, Self-Ordering of Cell Arrangement of Anodic Porous Alumina Formed in Sulfuric Acid Solution, Journal of The Electrochemical Society, 144 (1997) L127-L130.

[15] H. Masuda, K. Nishio, N. Baba, Fabrication of a one-dimensional microhole array by anodic oxidation of aluminum, Applied Physics Letters, 63 (1993) 3155-3157.

[16] M.S. Sander, A.L. Prieto, R. Gronsky, T. Sands, A.M. Stacy, Fabrication of high-density, high aspect ratio, large-area bismuth telluride nanowire arrays by electrodeposition into porous anodic alumina templates, Advanced Materials, 14 (2002) 665-667.

[17] N. Yasui, A. Imada, T. Den, Electrodeposition of (001) oriented CoPtL10 columns into anodic alumina films, Applied Physics Letters, 83 (2003) 3347-3349.

[18] T. Seki, T. Shima, K. Yakushiji, K. Takanashi, G.Q. Li, S. Ishio, Dot size dependence of magnetic properties in microfabricated L10-FePt (001) and L10-FePt (110) dot arrays, Journal of Applied Physics, 100 (2006) -.

[19] C.T. Rettner, M.E. Best, B.D. Terris, Patterning of granular magnetic media with a focused ion beam to produce single-domain islands at >140 Gbit/in², Magnetics, IEEE Transactions on, 37 (2001) 1649-1651.

[20] K. Naito, H. Hieda, M. Sakurai, Y. Kamata, K. Asakawa, 2.5-inch disk patterned media prepared by an artificially assisted self-assembling method, Magnetics, IEEE Transactions on, 38 (2002) 1949-1951.

[21] M. Albrecht, G. Hu, I.L. Guhr, T.C. Ulbrich, J. Boneberg, P. Leiderer, G. Schatz, Magnetic multilayers on nanospheres, Nat Mater, 4 (2005) 203-206.

[22] Z. Huang, J. Zhu, Growth and enhanced emission of silicon-germanium hemisphere shell arrays, Applied Physics Letters, 91 (2007) -.

[23] C. Kim, T. Loedding, S. Jang, H. Zeng, Z. Li, Y. Sui, D.J. Sellmyer, FePt nanodot arrays with perpendicular easy axis, large coercivity, and extremely high density, Applied Physics Letters, 91 (2007) -.

[24] Y.C. Sui, W. Liu, L.P. Yue, X.Z. Li, J. Zhou, R. Skomski, D.J. Sellmyer, Template-mediated assembly of FePt L10 clusters under external magnetic field, Journal of Applied Physics, 97 (2005) -.

[25] K. Liu, J. Nogués, C. Leighton, H. Masuda, K. Nishio, I.V. Roshchin, I.K. Schuller, Fabrication and thermal stability of arrays of Fe nanodots, Applied Physics Letters, 81 (2002) 4434-4436.

[26] Y. Lei, W.-K. Chim, Shape and Size Control of Regularly Arrayed Nanodots Fabricated Using Ultrathin Alumina Masks, Chemistry of Materials, 17 (2005) 580-585.

[27] Y. Zhao, B. Liu, L. Pan, G. Yu, 3D nanostructured conductive polymer hydrogels for high-performance electrochemical devices, Energy & Environmental Science, 6 (2013) 2856-2870.

[28] M.E. Davis, Ordered porous materials for emerging applications, nature, 417 (2002) 813-821.

[29] H. Gao, C. Mu, F. Wang, D. Xu, K. Wu, Y. Xie, S. Liu, E. Wang, J. Xu, D. Yu, Field emission of large-area and graphitized carbon nanotube array on anodic aluminum oxide template, Journal of Applied Physics, 93 (2003) 5602-5605.

[30] S. Shingubara, Fabrication of Nanomaterials Using Porous Alumina Templates, Journal of Nanoparticle Research, 5 (2003) 17-30.

[31] V. Valtchev, L. Tosheva, Porous Nanosized Particles: Preparation, Properties, and Applications, Chemical Reviews, 113 (2013) 6734-6760.

[32] L. Huang, Z. Wang, H. Wang, J. Sun, Q. Li, D. Zhao, Y. Yan, Hierarchical porous structures by using zeolite nanocrystals as building blocks, Microporous and Mesoporous Materials, 48 (2001) 73-78.

[33] Z. Huang, Y.-h. Guo, T.-m. Zhang, X.-h. Zhang, L.-y. Guo, Fabrication and Characterizations of Zeolite β–filled Polyethylene Composite Films, Packaging Technology and Science, (2012) n/a-n/a.

[34] Advances in top–down and bottom–up surface nanofabrication: Techniques, applications & future prospects, Advances in Colloid and Interface Science, 170 (2012) 2.

[35] M. Zaarour, B. Dong, I. Naydenova, R. Retoux, S. Mintova, Progress in zeolite synthesis promotes advanced applications, Microporous and Mesoporous Materials, 189 (2014) 11-21.

[36] Engineering of Micro- and Nanostructured Surfaces with Anisotropic Geometries and Properties, Advanced Materials, (2012) n/a.

[37] S. Li, C. Demmelmaier, M. Itkis, Z. Liu, R.C. Haddon, Y. Yan, Micropatterned Oriented Zeolite Monolayer Films by Direct In Situ Crystallization, Chemistry of Materials, 15 (2003) 2687-2689.

[38] C.M. Lew, R. Cai, Y. Yan, Zeolite Thin Films: From Computer Chips to Space Stations, Accounts of Chemical Research, 43 (2009) 210-219.

[39] Y. Xia, P. Yang, Y. Sun, Y. Wu, B. Mayers, B. Gates, Y. Yin, F. Kim, H. Yan, One-Dimensional Nanostructures: Synthesis, Characterization, and Applications, Advanced Materials, 15 (2003) 353-389.

[40] T. Humplik, J. Lee, S. O'Hern, B. Fellman, M. Baig, S. Hassan, M. Atieh, F. Rahman, T. Laoui, R. Karnik, Nanostructured materials for water desalination, Nanotechnology, 22 (2011) 292001.

[41] Y. Haruvy, S. Webber, Supported sol-gel thin-film glasses embodying laser dyes. 1. A new fast method for the preparation of optically clear polysiloxane thin-film glasses, Chemistry of Materials, 3 (1991) 501-507.

[42] Y. Haruvy, S.E. Webber, Fast sol-gel preparation of glasses, Google Patents1993.

[43] A. Kulak, Y.-J. Lee, Y.S. Park, H.S. Kim, G.S. Lee, K.B. Yoon, Anionic surfactants as nanotools for the alignment of non-spherical zeolite nanocrystals, Advanced Materials, 14 (2002) 526.

[44] J.R. Agger, N. Pervaiz, A.K. Cheetham, M.W. Anderson, Crystallization in Zeolite A Studied by Atomic Force Microscopy, Journal of the American Chemical Society, 120 (1998) 10754-10759.

[45] O. de la Iglesia, V. Sebastián, R. Mallada, G. Nikolaidis, J. Coronas, G. Kolb, R. Zapf, V. Hessel, J. Santamaría, Preparation of Pt/ZSM-5 films on stainless steel microreactors, Catalysis Today, 125 (2007) 2-10.

[46] E.V. Rebrov, G.B.F. Seijger, H.P.A. Calis, M.H.J.M. de Croon, C.M. van den Bleek, J.C. Schouten, The preparation of highly ordered single layer ZSM-5 coating on prefabricated stainless steel microchannels, Applied Catalysis A: General, 206 (2001) 125-143.

[47] E. Mateo, R. Lahoz, G.F. de la Fuente, A. Paniagua, J. Coronas, J. Santamaría, Preparation of Silicalite-1 Micromembranes on Laser-Perforated Stainless Steel Sheets, Chemistry of Materials, 16 (2004) 4847-4850.

[48] E. Mateo, R. Lahoz, G.F. de la Fuente, A. Paniagua, J. Coronas, J. Santamaría, Preparation and application of silicalite-1 micromembranes on laser-perforated stainless steel sheets, Journal of Membrane Science, 316 (2008) 28-34.

[49] J.C. Jansen, J.H. Koegler, H. van Bekkum, H.P.A. Calis, C.M. van den Bleek, F. Kapteijn, J.A. Moulijn, E.R. Geus, N. van der Puil, Zeolitic coatings and their potential use in catalysis, Microporous and Mesoporous Materials, 21 (1998) 213-226.

[50] Y.S.S. Wan, J.L.H. Chau, K.L. Yeung, A. Gavriilidis, 1-Pentene epoxidation in catalytic microfabricated reactors, Journal of Catalysis, 223 (2004) 241-249.

[51] V. Valtchev, Silicalite-1 Hollow Spheres and Bodies with a Regular System of Macrocavities, Chemistry of Materials, 14 (2002) 4371-4377.

[52] V. Valtchev, S. Mintova, Layer-by-layer preparation of zeolite coatings of nanosized crystals, Microporous and Mesoporous Materials, 43 (2001) 41-49.

[53] V. Valtchev, B.J. Schoeman, J. Hedlund, S. Mintova, J. Sterte, Preparation and characterization of hollow fibers of silicalite-1, Zeolites, 17 (1996) 408-415.

[54] J.D. Wright, N.A. Sommerdijk, Sol-gel materials: chemistry and applications, CRC press2000.

[55] J.D. Rimer, J.M. Fedeyko, D.G. Vlachos, R.F. Lobo, Silica Self-Assembly and Synthesis of Microporous and Mesoporous Silicates, Chemistry – A European Journal, 12 (2006) 2926-2934.

[56] C.-H. Cheng, D.F. Shantz, Silicalite-1 growth from clear solution: effect of the structure-directing agent on growth kinetics, The Journal of Physical Chemistry B, 109 (2005) 13912-13920.

[57] A.E. Persson, B.J. Schoeman, J. Sterte, J.E. Otterstedt, Synthesis of stable suspensions of discrete colloidal zeolite (Na, TPA)ZSM-5 crystals, Zeolites, 15 (1995) 611-619.

[58] C.M. Lew, Z. Li, S.I. Zones, M. Sun, Y. Yan, Control of size and yield of pure-silica-zeolite MFI nanocrystals by addition of methylene blue to the synthesis solution, Microporous and Mesoporous Materials, 105 (2007) 10-14.

[59] P. Sharma, P. Rajaram, R. Tomar, Synthesis and morphological studies of nanocrystalline MOR type zeolite material, Journal of Colloid and Interface Science, 325 (2008) 547-557.

[60] Z. Wang, H. Wang, A. Mitra, L. Huang, Y. Yan, Pure-Silica Zeolite Low-k Dielectric Thin Films, Advanced Materials, 13 (2001) 746-749.

[61] Z. Wang, Y. Yan, Oriented zeolite MFI monolayer films on metal substrates by in situ crystallization, Microporous and Mesoporous Materials, 48 (2001) 229-238.

[62] S. Frisch, L.M. Rösken, J. Caro, M. Wark, Ion conductivity of nano-scaled Al-rich ZSM-5 synthesized in the pores of carbon black, Microporous and Mesoporous Materials, 120 (2009) 47-52.

[63] M. Trau, N. Yao, E. Kim, Y. Xia, G. Whitesides, I. Aksay, Microscopic patterning of orientated mesoscopic silica through guided growth, nature, 390 (1997) 674-676.

[64] P. Yang, D. Zhao, D.I. Margolese, B.F. Chmelka, G.D. Stucky, Generalized syntheses of large-pore mesoporous metal oxides with semicrystalline frameworks, nature, 396 (1998) 152-155.

Chapter 2: Introduction to Silicalite-1 (MFI) Material and Synthesis

2.1 Introduction

The first synthetically developed zeolites were commercialized in 1954 and were identified as types A (LTA), X (FAU) and Y (FAU) [1]. It is still common to designate many of the molecular sieves by more than one name. To indicate different chemical composition having same topology different names are assigned. ZSM-5 (MFI) is used for aluminosilicate composition with varying Si/Al ratios; however, silicalite-1 (MFI) is used for pure-silica polymorph [defined in Mobil patent of Mobil Oil Corporation] [1].

The structure of silicalite-1 (MFI) zeolite is made up of double five- ring secondary building units (SBU's) and these can be assembled to create a "pentasil" structure **(Figure 2-1A)** whose compositions might vary from purely silicate, aluminosilicate, phosphosilicate etc. but the crystal structure always remains unchanged. The structure is composed of zig-zag pore network running along [100] and an intersecting straight cylinder pore system along [010]. The lattice parameters of Zeolite MFI are following: a = 20.048, b = 19.884, c = 13.352, α, β, $\gamma = 90°$, lattice parameters of silicalite-1 are little varied. The structure contains relatively big pores which run through the structure in (100) and (010) directions. The dimensions of the zig-zag pore openings are 5.1 Å X 5.5 Å while those of the straight cylinder are slightly larger and are 5.4 Å X 5.6 Å [1]. Zeolite containing pores are referred to as small (8-member ring), medium (10-member ring) **(Figure 2-1B)** and large (12-member ring). The finer details of the channel

system are important and needs to be considered after the initial consideration of the pore sizes of zeolite. The second level of complexity includes two features, the dimensions of the pores and pore mouth shape.

Mostly zeolites are categorized based on the number of T atoms forming the pore mouth opening (ring size). Typically the size and shape of the pore opening is found to be governed by the following five factors: (1) configuration of the T and O atoms relative to each other; (2) silica/alumina ratio; (3) size of the cation; (4) location of the cation and; (5) temperature. The pure-silica materials (silicalite-1) we are interested in investigating has Si^{4+} ion as the T-atom which leads to neutral electronic structure, which is not true with Al^{3+} as the T-atom, in which case an extra framework cation is required to balance the net charge on the framework.

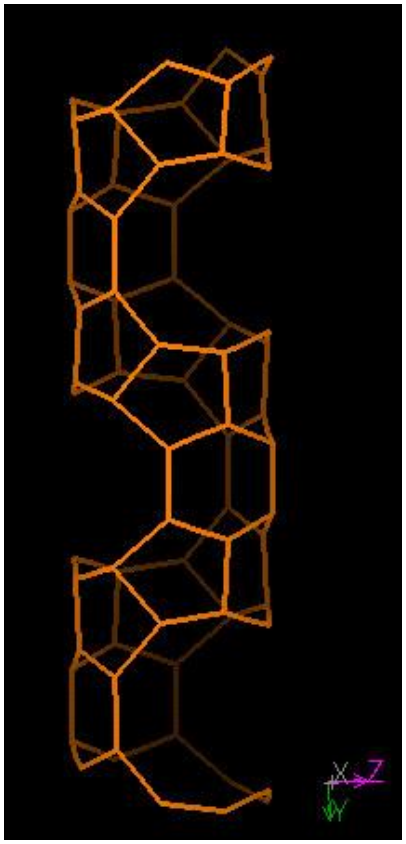

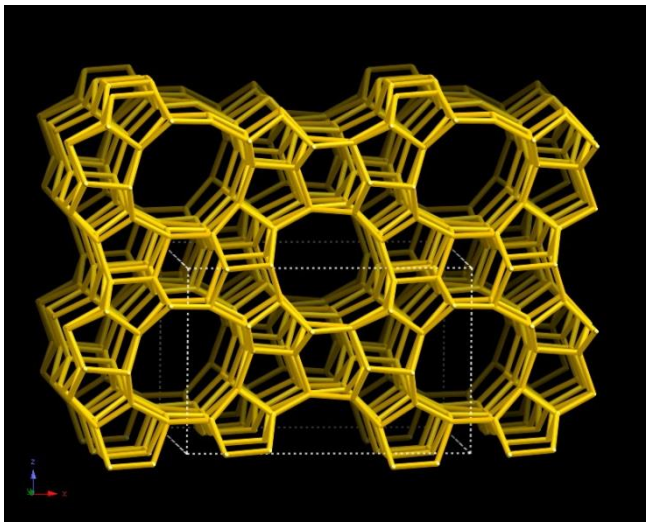

Figure 2-1: (A) Double 5-ring for MFI zeolite forming Pentasil structure [10 ring straight channel] (B) 10-membered ring .Viewed along [010] (courtesy IZA).

2.2 Silicalite-1 (MFI) Film Synthesis Strategies

One of the most commonly used technique to create one-dimensional nanostructures is through templates which simply acts as scaffolds inside or around which the growth of nucleated material i.e. crystal growth; takes place. The nanostructure can grow as being either complementary to the substrate or the template can only be physically involved to direct growth in which case it needs to be selectively removed through post-synthetic processes, nanostructures in zeolite-like materials are made following this methodology [2, 3].

Zeolites form through a combination of nucleation and growth processes, which begins with formation of energetically unstable nuclei and goes on to formation of thermodynamically stable larger particles owing to reduction in the surface to area ratio. The observed zeolite crystal thus grown at the expense of several small crystals which provide essential content for the growth and themselves gets disappeared [3]. This phenomenon can be considered comparable to micelles in an aqueous solution when the concentration of the active ingredient reaches a value typically known as critical micelle concentration (cmc) or critical aggregation concentration (cac) before proceeding to further growth. It can also be stated, that owing to heat the nanoparticles/nuclei grows by Ostwald ripening mechanism and the density of nuclei reduces relatively. Hence zeolites are basically thermodynamically metastable phase of the components where according to Ostwald's law the first phase produced gets replaces due to consumption by the second phase which is more stable and this trend continues until the most stable phase is formed [4]. As stated from kinetic perspective sometimes a relatively less stable thermodynamic

phase can continue to exist by crystallizing if it encounters large energy barrier in the tryst to transcend to the more stable phase [3, 4]. Details of the gel system and the crystallization kinetics of zeolites and can be found in several sources [1, 4].

The fundamental methodology that governs zeolite crystallization/synthesis includes the following factors: (1) gel composition; (2) pH; (3) temperature and time; and (4) nature of the starting material [1, 5, 6]. The reagents for synthesis upon mixing forms a gel which in turn gets converted into zeolite crystals upon application of autogeneous condition for certain amount of time and thus separating the gel into two phases: a solid and a liquid. It can be observed that with progress of crystallization there is increase in density of the reaction gel which begins to settle to the bottom of crystallization vessel, which accounts for successful zeolite crystallization.

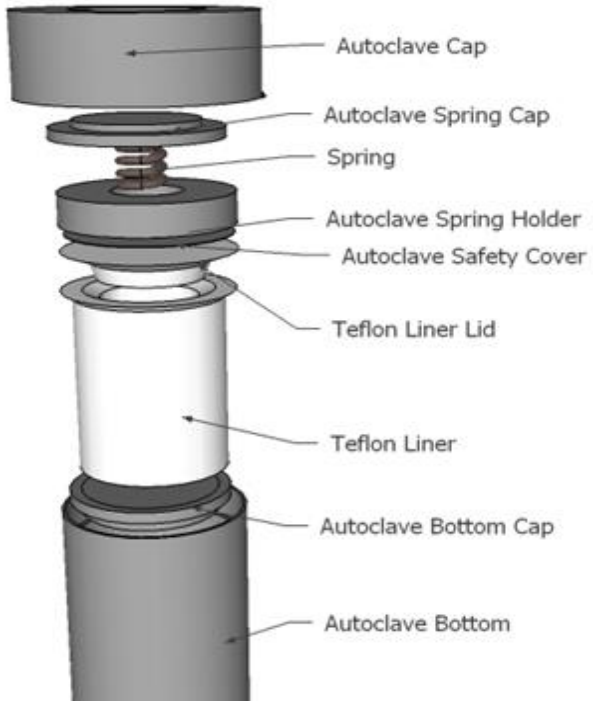

Figure 2-2: Parts of a Teflon© line autoclave.

Hydrothermal synthesis of zeolite is carried out using specialized crystallization vessels; autoclaves purchased from variety of sources (Parr Autoclave). **Figure 2-2** shows schematic of a typical autoclave. Under synthesis conditions (temperature above boiling point of water) small stainless steel autoclaves with Teflon© liners are used. To remove residues of synthesis special cleaning agents and methods are used like; soaking in sodium hydroxide solution or 5% hydrofluoric acid (HF) is used. Extreme cautions with specialized training are required for using HF, owing to its highly corrosive nature.

Zeolite synthesis in laboratory includes a protocol that includes a mixture containing a source of silica, water, usually an organic cation as SDA and a base as catalyst which are heated to hydrothermal conditions (70-200 ^{o}C) under autogenous pressure, which leads to formation of highly crystalline materials having exquisite structures after few hours to several days. Post synthesis calcination of the crystalline product is carried out to open the pore structures and revealing outstanding chemical and physical properties upon removal of the SDA, originally occluding the pores and channels. By choosing different structure directing agent and T-atoms like Ge, Al, B, Be, Zn etc. zeolites with several other geometry has been synthesized [3].

The batch compositions for zeolite synthesis are most commonly written in their oxide components for e.g. M_2O. Al_2O_3. $x SiO_2$. yOrganic. $zH_2O + q$ (anything else added). It is important that all the reagents that have been added to the final reaction gel are included in the final molar composition. The importance of retaining the information about purity and composition of the reagents used for zeolite synthesis has been emphasized over and again [1]. Since zeolite synthesis is carried out in high alkalinity

conditions, it becomes detrimental to use non-reactive laboratory ware, which does not end up contaminating the zeolite reaction gel e.g. Teflon©, plastic or stainless steel. During synthesis of zeolite nanocrystals, while using a mixed solvent; e.g. while adding ethanol in case of formation of nanocrystals it should be included in the molar composition. The reaction gel is subjected to aging by allowing it to stand at room temperature under slow shaking/agitating conditions. The purpose of this step is to equilibrate and generate seeds/nuclei in the reaction mixture which, upon attaining the desired temperature and at increase rate of crystallization will form the desired crystal phase. The act of keeping the reaction gel in static or agitating condition along with type of movement i.e. stirred, rolled, vibrated, shaken has shown to have effects on the product distribution, hence is required to be documented.

Factors which determine the finally crystallized structure are: SiO_2/Al_2O_3 ratio; the hydroxide content of the gel, presence of inorganic cation and organic additive (SDA). The inorganic/organic cation also influences the properties of morphology and crystal size of the final crystalline product. It is desirable to minimize the concentration of hydroxide (OH^-) in the molar composition of the reaction gel, since at higher OH^- concentration the yield of the crystalline material is lowered. The pH of the reaction gel mixture affects the concentration of free OH^- present on the reaction gel. The reaction mixture is alkaline before beginning of crystallization; however, there is marked change in pH with starting of crystal growth i.e. increase in pH is observed owing to incorporation of SiO_2 units into the silicate framework accompanied by release of free OH^- in the surrounding gel mixture, which further grows with crystal growth. Water

becomes part of the 'template' for structure directing by interacting strongly with the cations present in the solution. The transport properties and the viscosity of the reaction gel is determined by the water content, for e.g. in MFI synthesis the water content of the reaction gel determines synthesis of large-port. The mineralizing agent provides the essential alkaline pH condition to the reactants for crystallization to occur at specific rate (also determined by the molar composition of the reaction gel and the temperature provided). OH^- is also used to solubilize silicate and aluminate species in the gel. It has been observed that when F^- is used as mineralizing agent instead of OH^- for zeolite synthesis the crystals thus synthesized are hydrophobic in nature they are also free of defects [7].

Earlier high temperatures were administered to the reaction gel in order to simulate the conditions of natural growth of these zeolite minerals, however, nowadays at low temperature < 200 ^oC and low pressure with modified and more reactive reactants in suitable molar ratio are used for successful and repeatable crystallization of zeolites. The administered temperature influences the factors like; zeolite phase obtained, time of crystallization, rate of crystallization and composition range of certain zeolite phase. Three of the heating methods most commonly used for zeolite synthesis are: hot air oven, hot sand/water bath, microwave.

2.2.1 Substrate Choice and Modifications

Synthesis of zeolite films and membranes have been accomplished using various supports for e.g. silicon, glass, quartz, ceramic, alumina, polymeric membranes, stainless

steel, clay, and Teflon [8-12]. The most common method used for pre-processing/modification of the silicon substrates are using Piranha Solution [volume ratio; 1Hydrogen Peroxide (H_2O_2, 40 wt%): 4Sulphuric Acid (H_2SO_4, 98 wt%)] and drying under N_2. Clean room grade wafers has also been used without any further processing for synthesis of silicalite-1 thin films [13]. Under circumstances when silicalite-1 nanocrystals are spin-coated on silicon wafers to make thin films a chemical cleaning procedure with two different solutions ethanol and acetone are used [14].

2.2.1.1 In situ Hydrothermal Techniques for Silicalite-1 Films

Although silicalite-1 has been used more commonly in the form of powders from the beginning the acts of converting them in the form of two dimensional structures i.e. films has improved its applications in some major areas like chemical analysis, reactor engineering and molecular separations. The rate of crystal formation and its consequent deposition on a substrate to form films can be tuned by modifying several of the synthesis parameters. It is has been seen through investigations that by controlling the time of aging of the reaction gel and/or crystallization of reaction gel under autogeneous conditions, films of various thickness can be deposited on various substrates. This allows us to have silicalite-1 of very high thickness or in the form of thin films based on applications and end use. By controlling the reaction parameters in the hydrothermal synthesis it is also possible to have silicalite-1 films or deposited crystals with tunable pore sizes, structures, thickness, orientation and intergrowth. New crystals are formed either by surface nucleation or by adsorption of the nuclei from the solution, preferential

site of nucleation being the surface of seed which controlled the direction of the crystal growth comprising of epitaxial growth. Since in concentrated solution the phenomenon of nucleation is governed by the solution the SDA molecule interacts with the inorganic silica due to van der Waals forces upon loss of its hydrations sphere [3, 15-17]. When this reaction gel is subjected to hydrothermal condition and there is increase in temperature the pH and conductivity raises causing nuclei formation. Due to dissociation of silicic acid in the solution at the initial stage the pH drops, later it equalizes; however, again on addition of TEOS there is change in pH. This suggests that at high temperature the particles tend to be more condensed. With increase in sizes of the nuclei i.e. crystal growth the silica source starts getting exhausted and the pH of the solutions doesn't change much; however, it again starts to increase before getting at equilibrium value of high pH [3]. In some cases, pre-formed seeds of small zeolite particles can be added to the reaction gel to speed up the reaction process by decoupling the nucleation and growth phases. Improved and rapid crystallization can be observed in presence of seed crystals compared to unseeded crystallization.

We have adopted various silicalite-1 synthesis techniques established to obtain uniformly oriented silicalite-1 crystals both as films and nanocrystals **(Table 2-1).** Using most of these synthesis strategies we have focused on achieving *in situ* grown thin films of dimension ranging from 200-500 nm with a monolayer of *b*- oriented silicalite-1 (MFI) film on silicon (Si) and quartz (Q) substrates and nanocrystals with sizes < 100 nm [18].

Figure 2-3 illustrates schematically the various substrate orientation used in this research along with the different recipes listed in **Table 2-1**.

Table 2-1: Summarizes the various recipes used to synthesize silicalite-1 films and nanocrystals (NC).

Molar Ratio	Aging time (h)	Substrate	Temp. (^oC)	Time (h)	Orientation	Post Processing	Ref.
0.32TPAOH*/TEOS*/165H_2O	3, 4	Si-V Q-V	165	2	(*b*-)	calcination 450 ^oC for 2 h in air	Wang-2001
0.32TPAOH/TEOS/165H_2O	3, 4	Si-H Q-H	165	3, 4, 5	random	calcination 450 ^oC for 2 h in air	Wang-2001
99H_2O/0.14TPAOH/0.84TEOS	1	Si-H Q-H	165	2-19	(*a, b*)	Dried at 80 ^oC, calcination at 400^oC for 4h with ramping rate 0.5^oC/min	Exter-1997
99H_2O/0.23TPAOH/0.84TEOS	1	Si - Slant	165	2	(*b*-)	Air dry, calcination- 400 ^oC, 4h ,ramping rate 0.5^oC/min	Exter - 1997
6TPABr*/3TPAOH/25SiO_2/4500H_2O	12 – 14 (Added TPABr)	Si - H	100	7 days	(*b*-)	Rinse in 0.025 M TPAOH, DIW, acetone, Dry at RT***, calcination- 600 ^oC, 2h, 1 ^oC/min.	Schoeman-1997
9TPAOH/25SiO_2/408H2/100EtOH	24	-	90	12,15, 19,22, 24	Powder	Series of centrifugation and ultrasonication	Mintova-2001
9TPAOH/25SiO_2/680H2/100EtOH	24	-	90	27, 36, 48	Powder	Series of centrifugation and ultrasonication	Mintova-2001

*TPAOH is Tetrapropylammonium hydroxide, TEOS is tetraethylorthosilicate, TPABr is Tetrapropylammonium bromide

**DIW is Deionized water

***RT is Room temperature

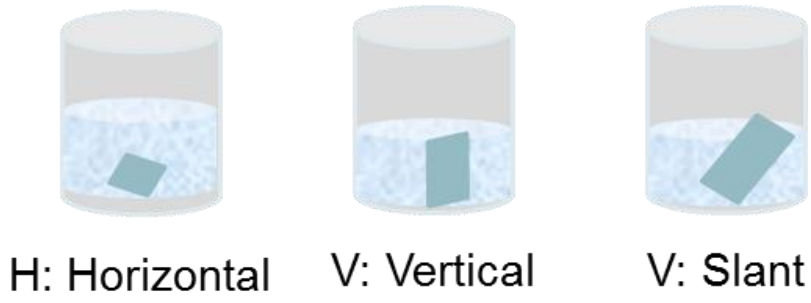

Figure 2-3: Shows a schematic representation of the different substrate orientation, depending on which the final thickness of the film along with the crystal orientation can be modified.

The typical synthesis steps includes (1) Prepare clear gel solution; (2) Age the reaction gel under stirring e.g. magnetic; for different amount of time **(Table 2-1)**; (3) Dip cleaned substrate in the reaction gel for films at different orientations **(Figure 2-3)**; (4) Carry out crystallization in a convection oven in a Teflon©-lined Parr autoclave **(Table 2-1)**; (5) Remove substrates from autoclave and rinse in deionized water and blow-dry in air for films; (6) Calcine under air **(Table 2-1)** [11]. The details of the steps are further illustrated in **Figure 2-4**.

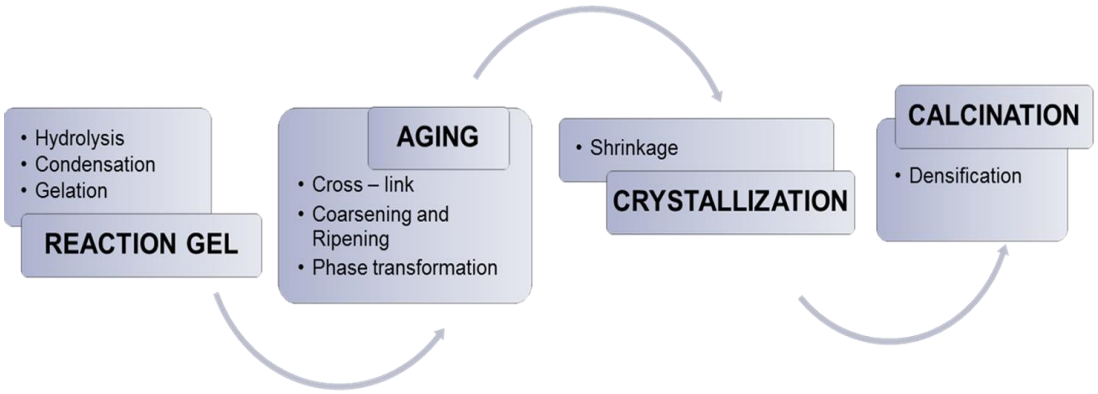

Figure 2-4: Schematic representations of the steps of hydrothermal synthesis.

The films formed using various strategies listed in **Table 2-1** when checked for their crystals structure shows MFI crystals framework at different orientations on the surface of the substrate (Si), some of the XRD patterns are shown in **Figure 2-5** and **Figure 2-6**. Details of characterization techniques performed on each film can be found in **section 2.2.2**.

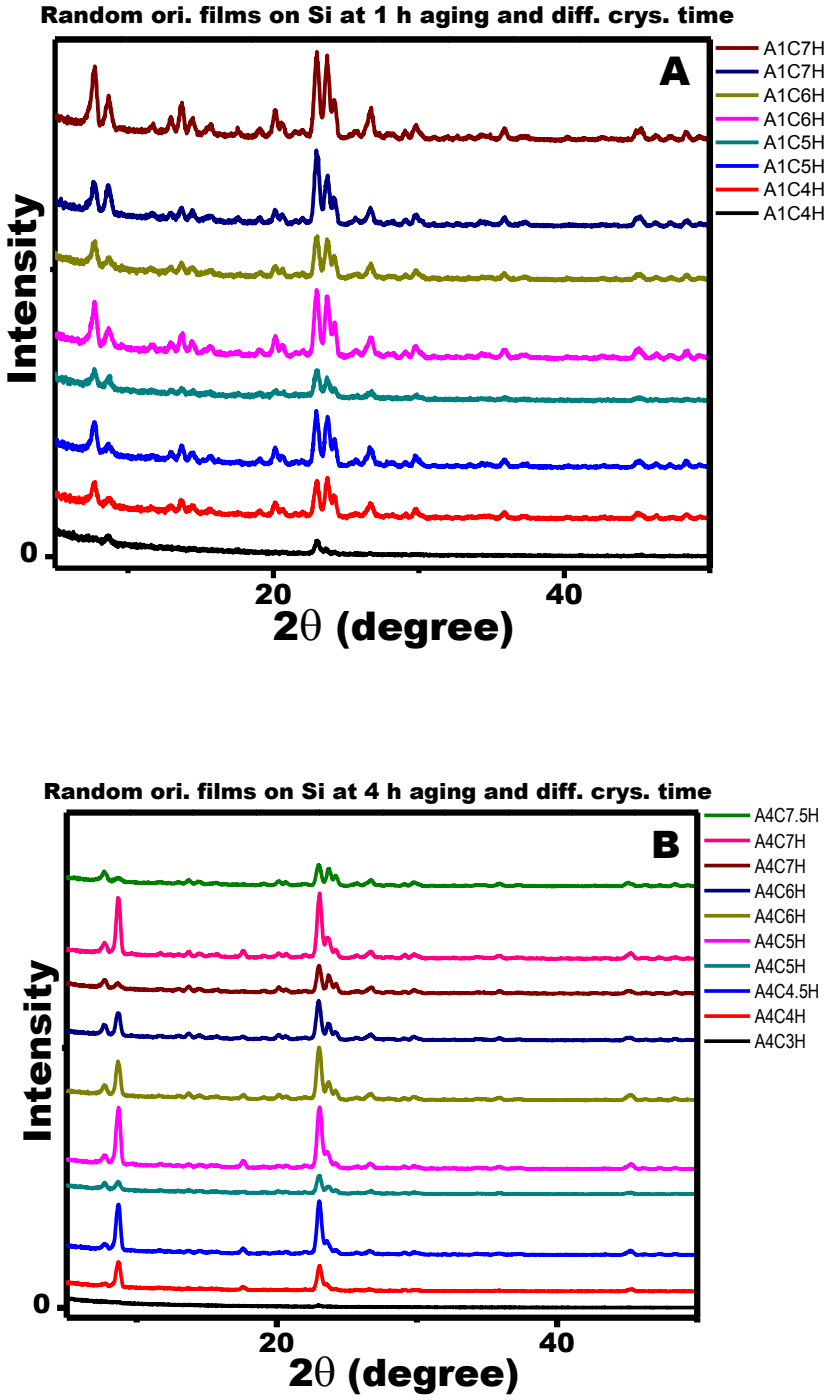

Figure 2-5: XRD of randomly oriented silicalite-1 film on Si (100) formed at (A) 1 and (B) 4 h aging and different crystallization times [A-aging, C-crystallization time, H-all substrates kept horizontal].

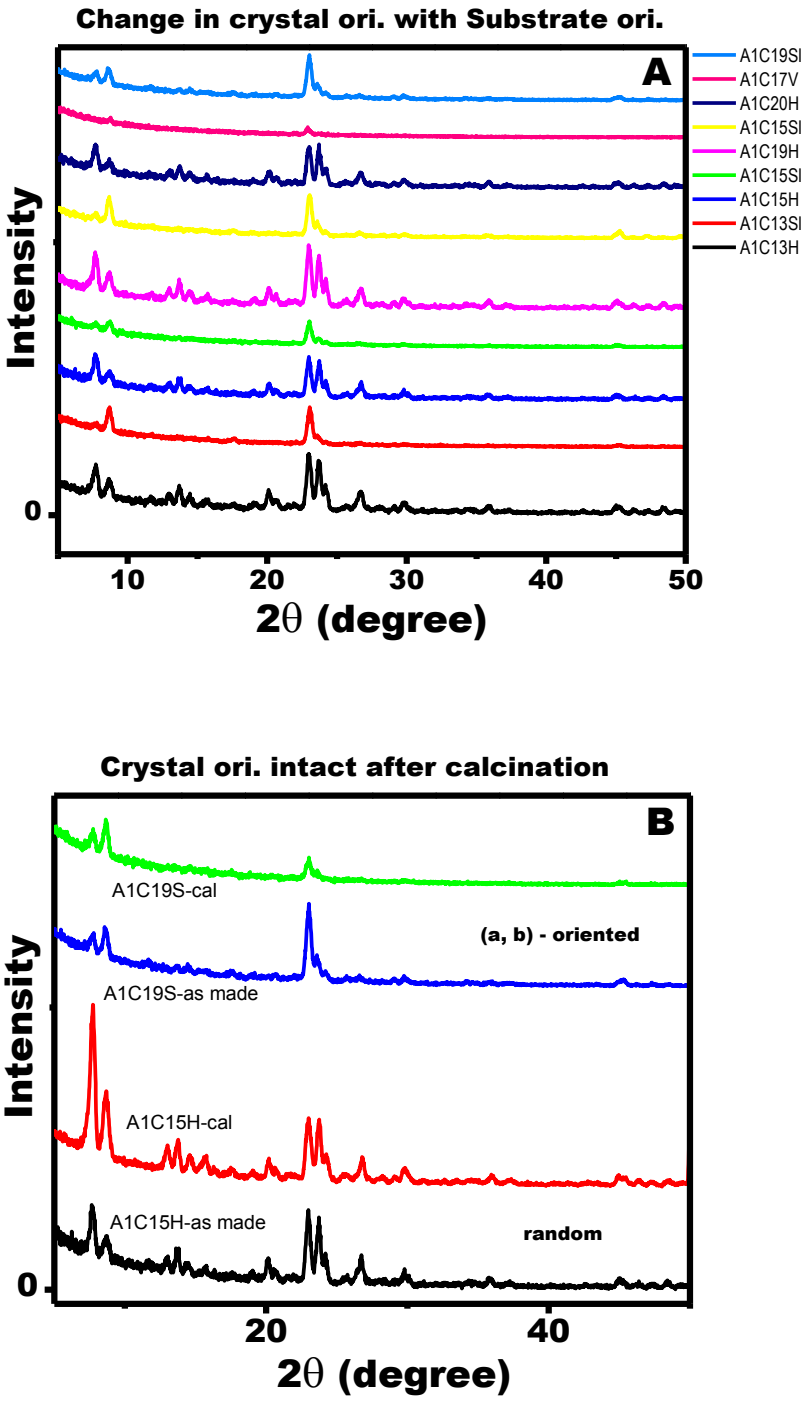

Figure 2-6: XRD of random and *(a,b)*- oriented silicalite-1 film on Si (100) formed (A) 1 h aging and different crystallization times; (B) retaining both crystal orientation after calcination [A-aging, C-crystallization time, H-horizontal, S-slant and V-vertical].

2.2.1.2 Hydrothermal Technique for Silicalite-1 Nanocrystals Synthesis and Spin-coating (Ex situ)

During synthesis of silicalite-1 nanocrystals (NC) the same steps as described in **section 2.2.2** are used, but without the substrate. However, TEOS (silica source) is added drop-wise in the reaction gel taking extra care so as to have uniform distribution and growth of silicalite-1 NC. TPA acts more like a shell of the growing silica NC; however, not imposing its structure on it. Though extensive study about the interfacial layer between silica NC and TPA have not been conducted; however, presence of a layer of water molecules strongly bonded between the positive charge of TPA cation and silanols group is likely [1]. When the reaction gel containing TPA and silica NC is heated (during crystallization) the probability of inclusion of TPA in the growing silica core rises, which is not feasible at lower temperature.

2.2.1.3 Preparation of Silicalite-1 NC and Spin-coating

At the end of crystallization the NC suspension are taken out of the autoclave and cleaned following a series of steps to isolate the NC from the reaction gel. **Figure 2-7** shows the various steps carried out in sequence.

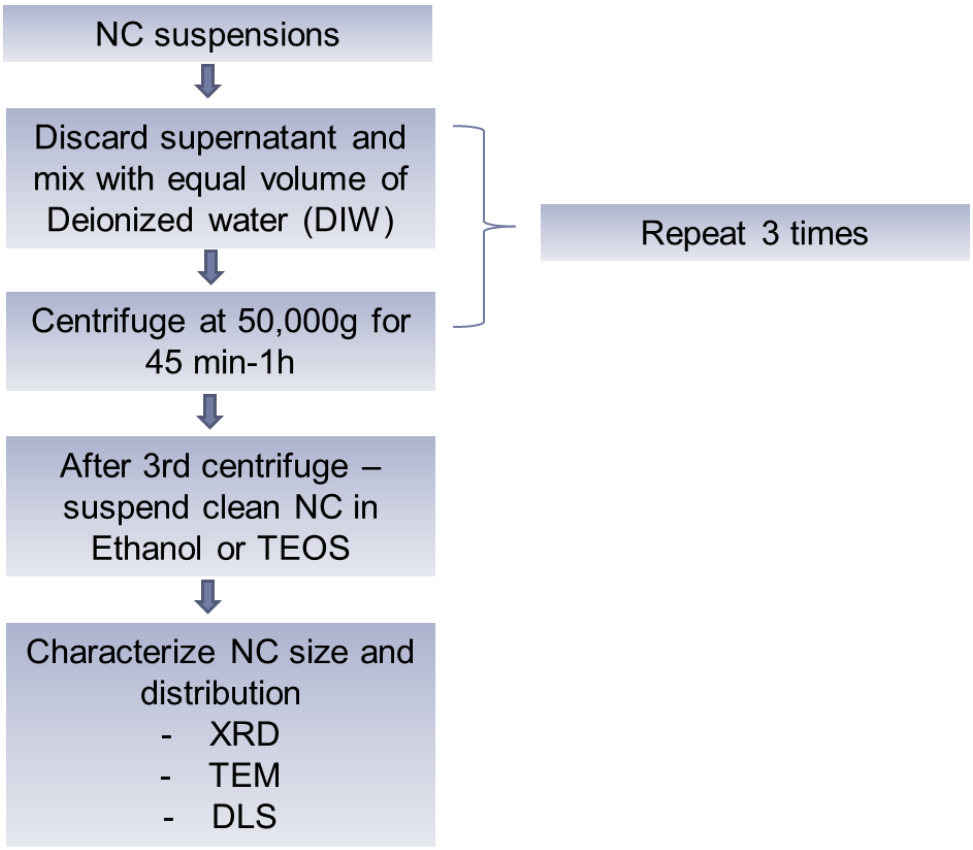

Figure 2-7: Shows the various steps performed in order to clean the NC from reaction mixture followed by their primary characterization.

After we obtain clean NC and disperse them (in suitable media) to make a stable suspension, we spin-coat on substrates (mostly Si) by following the steps shown in **Figure 2-8**. Depending on the desired film thickness the wt% of the NC in the dispersion media and the number of coating can be varied.

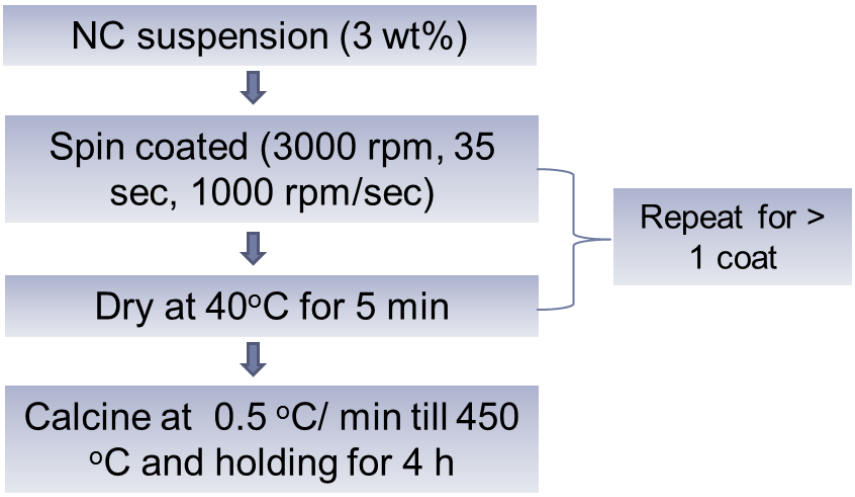

Figure 2-8: Shows the various steps performed in order to spin-coat NC on substrates.

2.2.1.4 Spin-coating with Ethanol as Dispersion Media

We use ethanol (99.5%) to make the suspension since it causes esterification of the $–CH_2$ group, which reduces the cohesive forces between silicalite-1 NC and minimizes the chances of clumping or premature aggregation hence stabilizing NC [19, 20]. Compared to other solvents ethanol also provides several advantages like; highly volatile thus can be easily removed due to evaporation from the self-assembled zeolite nanostructures formed by capillary forces, this step would be instrumental in stabilizing the nanocrystal patterned template with desired uniformity and long range structure [20, 21]. It acts by wetting both hydrophilic and hydrophobic surfaces which have dual advantages i.e. formation of patterned structures with well-defined features and applicable for different

nature of substrates [14, 19]. We further calcine the coated substrates to further cross-link the zeolite nanocrystals due to condensation of the surface silanols bonds.

However, these spin-coated (*ex situ*) films when observed under scanning electron microscope (SEM), showed that the films are not interwoven with uniformly laid crystals thus forming mesopores and increasing the overall film roughness **(Figure 2-9)**. Though there is significant coverage and uniformity in the film, in order to have uniformity in composition and fully compact, intergrown films with micropores only we use pre-hydrolyzed TEOS as dispersion media.

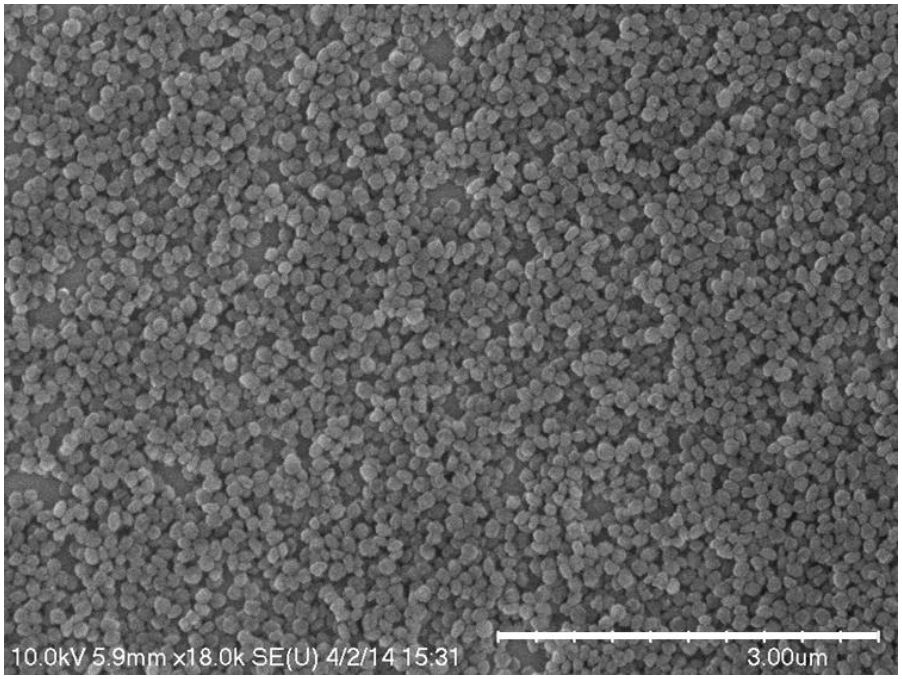

Figure 2-9: Representation of the spin-coated silicalite-1 films using ethanol as dispersion media.

2.2.1.5 Spin-coating with Pre-hydrolyzed TEOS as Dispersion Media

In order to obtain compact, uniform and smooth silicalite-1 thin film by spin-coating (*ex situ*) of silicalite-1 NC pre-hydrolyzed TEOS were also used as dispersion media. Pre-hydrolyzed TEOS is expected to have higher viscosity thus causing greater NC binding to form uniform pore along with uniformity/continuity of silica composition in the film hence, will be optimum for optical characterizations and applications [22]. **Figure 2-10A** shows that while using TEOS much compact and uniformly bind NC are formed. **Figure 2-10B** shows that the NC are bonded so well with TEOS as the binding media on forming the films that they cause distinct film curling effects. Further discussion on the requirements of coated films for optical applications can be found in **section 5.3** in **Chapter 5**:**.**

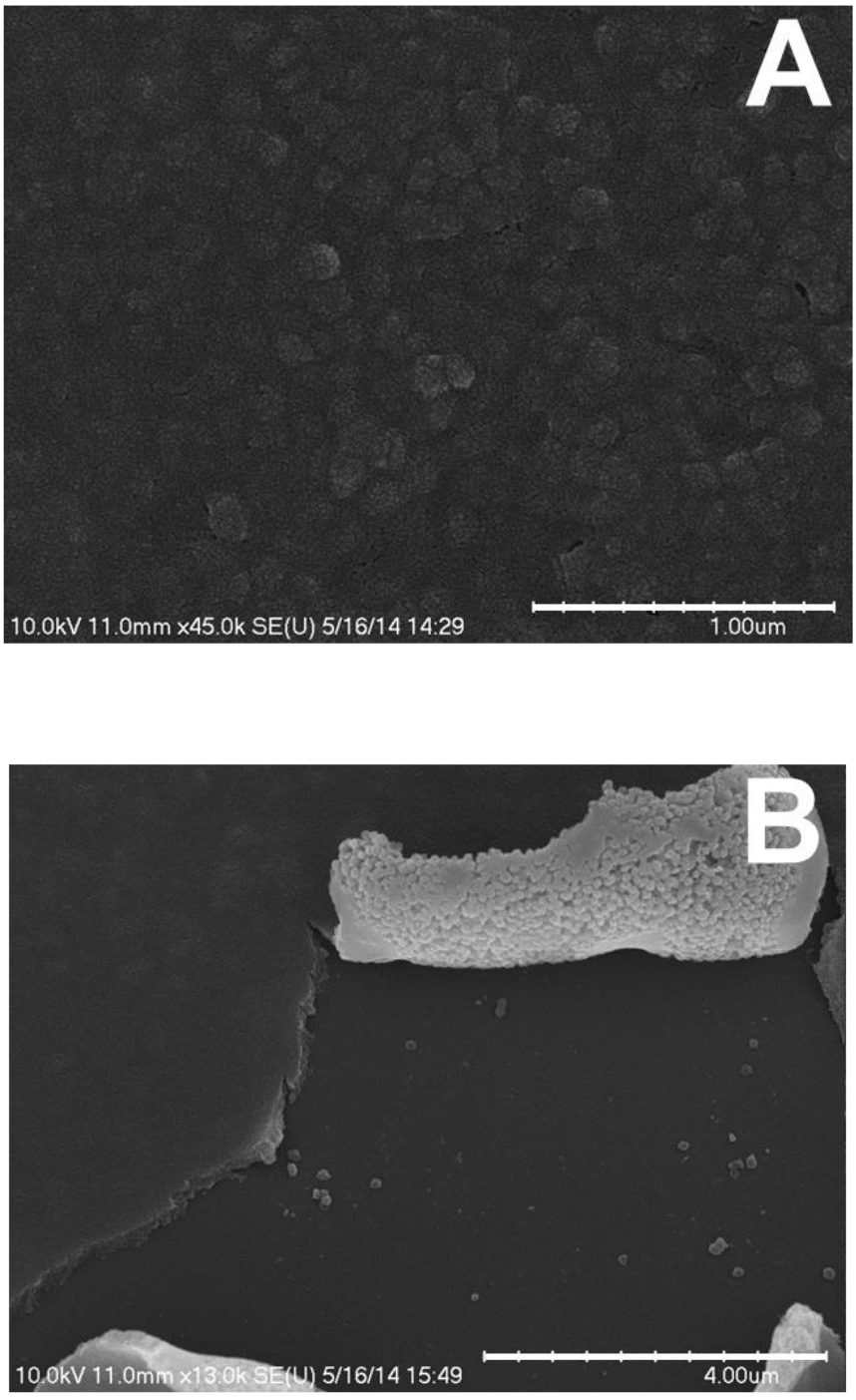

Figure 2-10:Representation of the spin-coated silicalite-1 films using pre-hydrolyzed TEOS as dispersion media which shows; (A) considerably high binding in the NC and (B) compact film curling with NC.

2.2.2 Characterization Techniques

The purity of the silicalite-1 nanocrystals (NC) and films grown on Si (100) were confirmed using X-ray diffraction (Rigaku). The particle size and distribution with dispersion media ethanol and was measured using dynamic light scattering (Horiba-LB-550). The particle size and morphology was also checked with Transmission Electron Microscope (FEI Tecnai F30 Twint). The film thickness, surface coverage, crystal size, crystal habit, degree of intergrowth, morphology, quality and nature of thin film on Si (100) substrates both at the end of coating and *in situ* growth were studied under Scanning Electron Microscope (SEM) (Hitachi S4700). Compositional analysis was accomplished via Energy Dispersive Spectroscopy (EDS) with an FEI Quanta 600 Field Emission Gun, Extended Vacuum to confirm removal of the organic template after calcinations. VASE JA Woollam ellipsometer was used to determine the film thickness and refractive index of different films. In order to determine roughness of the measured film they were observed under Optical Profilometer (Veeco -NT9100). The Raman spectra were taken with Renishaw in microscope equipped with HeNe laser (volt 115-230, 50/60 Hz), power max 50 W with grating 2400 l/mm^{-1} with Renishaw CCD camera as detector, laser 633 nm, edge exposure time 60/s, laser power 10%, objective 50 (camera at high gain, low speed). The IR spectra of the laser irradiated film were obtained using Thermo Electron Corporation, Nicolet 4700 (KBr crystal, resolution 0.5 cm^{-1}). **Table 2-2** summarizes the various characterization techniques used in this thesis to study various film and material properties of silicalite-1.

Table 2-2: Techniques used to chacracterize and study properties of silicalite-1 films and NC

Properties	Characterization Technique
Morphology	SEM
Identification Structure, Fingerprinting	XRD
Film Thickness	SEM, Ellipsometer
Nature of the Film (bond vibrations, thickness)	FTIR-ATR
Surface Roughness	Optical Profilometry
Elemental Composition	EDS
Nanocrystal size	TEM
Nanocrystal distribution	DLS
Chemical fingerprint	Raman
Optical properties	Optical Reflectance

2.2.3 Strategies for Defect Elimination in Films

The application and efficiency of the silicalite-1 films are largely determined by the quality and effectiveness of the synthesis techniques for e.g. deposition techniques where zeolite layer consists of individual crystals attached to the substrate by means of physical or chemical bonds might lead to occurrence of inter-crystalline gaps or membrane defects which adversely affect its sieving selectivity [9]. Based on the purpose of film synthesis in this research we expect to have full coverage of the films throughout the substrate upon *in situ* or *ex situ* spin-coating synthesis. Hence, we might need to optimize several

synthesis parameters (gel composition, aging/crystallization times, orientation of substrate, crystallization temperature) to ensure full coverage with intergrowth of films. The areas were care and precaution needs to be taken to minimize defects in films and optimize yield can be narrowed down to the following strategies:

- Using pure precursors which are stored at optimum conditions
- Uniformly mixing the precursors during aging
- Ensuring that clean substrates are used
- Ensuring that cleaned reaction vessel (autoclaves) are used without any deposit from earlier synthesis
- The oven temperature should be brought to equilibrium crystallization temperature before putting the reaction vessel
- Depending on the desired film thickness, the substrate orientation can be modified from being horizontally, vertically or slightly slanted
- Proper storage and handling of the films is also required to prevent flaking and peeling effects

Figure 2-11 shows some examples of defects that were seen in the silicalite-1 films synthesis and were subsequently resolved by monitoring the above stated factors.

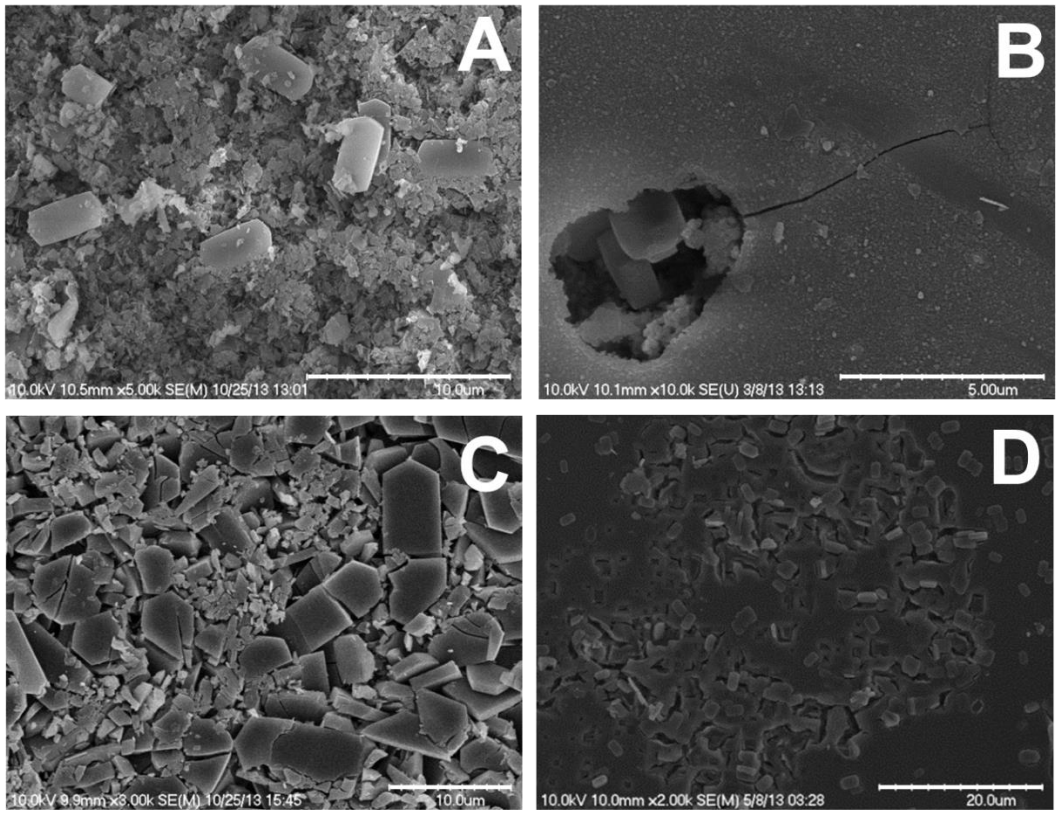

Figure 2-11: Representation of the various defects observed in hydrothermally grown silicalite-1 films. The film defects shown are most likely caused due to; (A) non-uniform mixing of reaction gel, (B) improper handling of film, (C) uneven heating and (D) improper cleaning of substrates before hydrothermal growth.

2.3 References

[1] R. Szostak, Molecular sieves, Springer1998.

[2] T. Humplik, J. Lee, S. O'Hern, B. Fellman, M. Baig, S. Hassan, M. Atieh, F. Rahman, T. Laoui, R. Karnik, Nanostructured materials for water desalination, Nanotechnology, 22 (2011) 292001.

[3] J.D. Rimer, J.M. Fedeyko, D.G. Vlachos, R.F. Lobo, Silica Self-Assembly and Synthesis of Microporous and Mesoporous Silicates, Chemistry – A European Journal, 12 (2006) 2926-2934.

[4] J.D. Wright, N.A. Sommerdijk, Sol-gel materials: chemistry and applications, CRC press2000.

[5] R. Barrer, E. White, 286. The hydrothermal chemistry of silicates. Part II. Synthetic crystalline sodium aluminosilicates, J. Chem. Soc., (1952) 1561-1571.

[6] R. Barrer, J. Baynham, 562. The hydrothermal chemistry of the silicates. Part VII. Synthetic potassium aluminosilicates, J. Chem. Soc., (1956) 2882-2891.

[7] V. Valtchev, L. Tosheva, Porous Nanosized Particles: Preparation, Properties, and Applications, Chemical Reviews, 113 (2013) 6734-6760.

[8] M.E. Davis, Ordered porous materials for emerging applications, nature, 417 (2002) 813-821.

[9] M. Pina, R. Mallada, M. Arruebo, M. Urbiztondo, N. Navascués, O. De La Iglesia, J. Santamaria, Zeolite films and membranes. Emerging applications, Microporous and Mesoporous Materials, 144 (2011) 19-27.

[10] Y.S.S. Wan, J.L.H. Chau, K.L. Yeung, A. Gavriilidis, 1-Pentene epoxidation in catalytic microfabricated reactors, Journal of Catalysis, 223 (2004) 241-249.

[11] Z. Wang, H. Wang, A. Mitra, L. Huang, Y. Yan, Pure-Silica Zeolite Low-k Dielectric Thin Films, Advanced Materials, 13 (2001) 746-749.

[12] Z. Wang, Y. Yan, Oriented zeolite MFI monolayer films on metal substrates by in situ crystallization, Microporous and Mesoporous Materials, 48 (2001) 229-238.

[13] Z. Wang, H. Wang, A. Mitra, L. Huang, Y. Yan, Pure-Silica Zeolite Low-k Dielectric Thin Films, Advanced Materials, 13 (2001) 746-749.

[14] S. Mintova, T. Bein, Microporous Films Prepared by Spin-Coating Stable Colloidal Suspensions of Zeolites, Advanced Materials, 13 (2001) 1880-1883.

[15] M.E. Davis, R.F. Lobo, Zeolite and molecular sieve synthesis, Chemistry of Materials, 4 (1992) 756-768.

[16] T. Bein, Synthesis and applications of molecular sieve layers and membranes, Chemistry of Materials, 8 (1996) 1636-1653.

[17] A. Dong, Y. Wang, Y. Tang, N. Ren, Y. Zhang, Z. Gao, Hollow Zeolite Capsules: A Novel Approach for Fabrication and Guest Encapsulation, Chemistry of Materials, 14 (2002) 3217-3219.

[18] S. Li, C. Demmelmaier, M. Itkis, Z. Liu, R.C. Haddon, Y. Yan, Micropatterned Oriented Zeolite Monolayer Films by Direct In Situ Crystallization, Chemistry of Materials, 15 (2003) 2687-2689.

[19] T. Kawai, K. Tsutsumi, Reactivity of silanol groups on zeolite surfaces, Colloid Polym Sci, 276 (1998) 992-998.

[20] L. Huang, Z. Wang, J. Sun, L. Miao, Q. Li, Y. Yan, D. Zhao, Fabrication of Ordered Porous Structures by Self-Assembly of Zeolite Nanocrystals, Journal of the American Chemical Society, 122 (2000) 3530-3531.

[21] K.T. Jung, J.H. Hyun, Y.G. Shul, D.S. Kim, Synthesis of fibrous titanium silicalite (FTS-1) zeolite, Zeolites, 19 (1997) 161-168.

[22] C.M. Lew, R. Cai, Y. Yan, Zeolite Thin Films: From Computer Chips to Space Stations, Accounts of Chemical Research, 43 (2009) 210-219.

Part I

Chapter 3: Techniques for Microscale Patterning of Zeolite-Based Thin Films

Abstract

Micro- and nano-scale devices have made a significant impact on electrical, optical, mechanical, and medicinal platforms, such as microchips, environmental sensors, and smart implants. Of particular interest for these devices is the use of nano-porous materials, such as aerogels, zeolites, and mesoporous materials, whose inherent nano- to micro-scale porosity provides potentially beneficial properties that could be harnessed for these devices, particularly when the materials are synthesized in thin film form. However, the primary challenge to utilizing these materials remains the ability to fabricate or pattern the thin film materials into appropriate micro- and nano-scale features. A number of techniques have been developed to address the issue of patterning thin films of nonporous materials, from bottom-up approaches, like chemical or mechanical assembly, to top-down approaches, such as sputtering, ablation, and lithography. However, most of the patterning techniques represented in the literature for thin film materials are typically less compatible with porous thin films, particularly microporous and mesoporous thin films. Here, we present a review of the various patterning techniques that have been either heavily investigated or proposed for microporous thin film materials, along with their advantages and potential limitations. Specifically, we focus on top-down, bottom-

up, and deposition-based approaches that have yielded micro- to nano-scale patterning abilities for zeolite-based materials. Given the unique physical, chemical, mechanical, and structural properties of zeolites and other inherently-nanostructured materials, the ability to choose and adapt an appropriate patterning technique will greatly enhance the success of their utilization in micro-scale and potentially nanoscale device fabrication.

3.1 Introduction

With advances in nanotechnology, researchers have been able to address several challenges associated with device efficiency and cost of production. In the last decade alone, we have seen remarkable progress in the ability to synthesize, functionalize, and manipulate materials at the nanometer length scale, creating such interesting materials as carbon nanotubes (CNT), graphene, quantum dots, nanowires, superlattices, and nanoshells - all of which have been used to create high functionality devices [1-8]. In many cases, the functionality of these devices derives not just from their small footprint, but also from the effects of miniaturization, such as quantum confinement, on the material's fundamental electrical, optical, and chemical properties. For instance, the development of devices capable of storing information in the form of magnetic or optical energy, such as disk drives, is possible due to their nanometer scale features [9]. Given the potential benefits of nanoscale materials, it is unsurprising that researchers have proposed a wide array of novel applications for such devices, including the development of smart drugs, efficient DNA and protein sensors, energy storage, and biological imaging, not to mention the multitude of novel coatings, such as self-cleaning, color-masking, or reflection-reducing, that are possible due to the presence of inherent or created nanofeatures [6, 10-16].

Recently, there has been growing interest in utilizing nano- and micro-structured porous materials, such as aerogels, zeolites, and mesoporous materials, in these devices [17]. This interest arises from their peculiar, and in some cases, superior, physicochemical properties in comparison to their non-porous counterparts [18]. For

example, these nano- and microporous materials have characteristically larger surface areas and uninterrupted or greater conductivity than their non-porous counterparts of similar composition [18, 19]. It is unsurprising, then, that they are capable of, for instance, more efficient and faster charge transport in comparison to nonporous materials of the same composition, and have been extensively utilized in electrical devices such as electrodes, capacitors, and Mott insulators [20-22]. Moreover, many of these materials offer the flexibility of tuning their pore sizes in the sub-nanometer regime, further enhancing their functionality for these applications [8].

Some of the most widely-used microporous materials include zeolites and zeolite-like materials [23]. These materials possess crystalline frameworks typically composed of silicon and aluminum atoms that are tetrahedrally linked with oxygen to form a three-dimensional, microporous structure made of channels (pores) and voids. This open space is often occupied by water molecules, or alkali or alkali-earth cations. By varying the ratio of Si/Al and introducing atoms like P, B, Ga, Fe, and Ti, into the tetrahedral framework, many compositions and structures of zeolites and zeolite-like materials have been synthesized [8]. These materials have pores ranging in size from 1-20 Å [26, 27]. To date, 217 different framework types of zeolites, many with multiple compositions, have been successfully created, and many more have been theoretically predicted [24]. Because of their unique porous and crystalline nanostructure, zeolites have been traditionally used in separations, catalysis, ion exchange, and heavy metal adsorption processes, primarily as powders or powder-coatings of structured materials [18, 21, 25, 26]. More recently, these materials have been produced in thin film or membrane form,

which has attracted immense interest for non-traditional applications, such as microreactors, chemical or molecular sensors, electrodes, optoelectronic devices, diffusion devices, corrosion resistant coatings, hydrophilic antimicrobial coatings [27], proton exchange membranes [28] and electrical insulators [29]. The application of zeolite and zeolite-like thin films varies based on no only their structure and composition, but also their orientation with respect to the substrate/membrane surface, which influence their molecular sieving abilities, in addition to their electronic and optical properties. **Figure 3-1** summarizes various devices that have been reported in the literature and utilize zeolite thin films on the micro-scale.

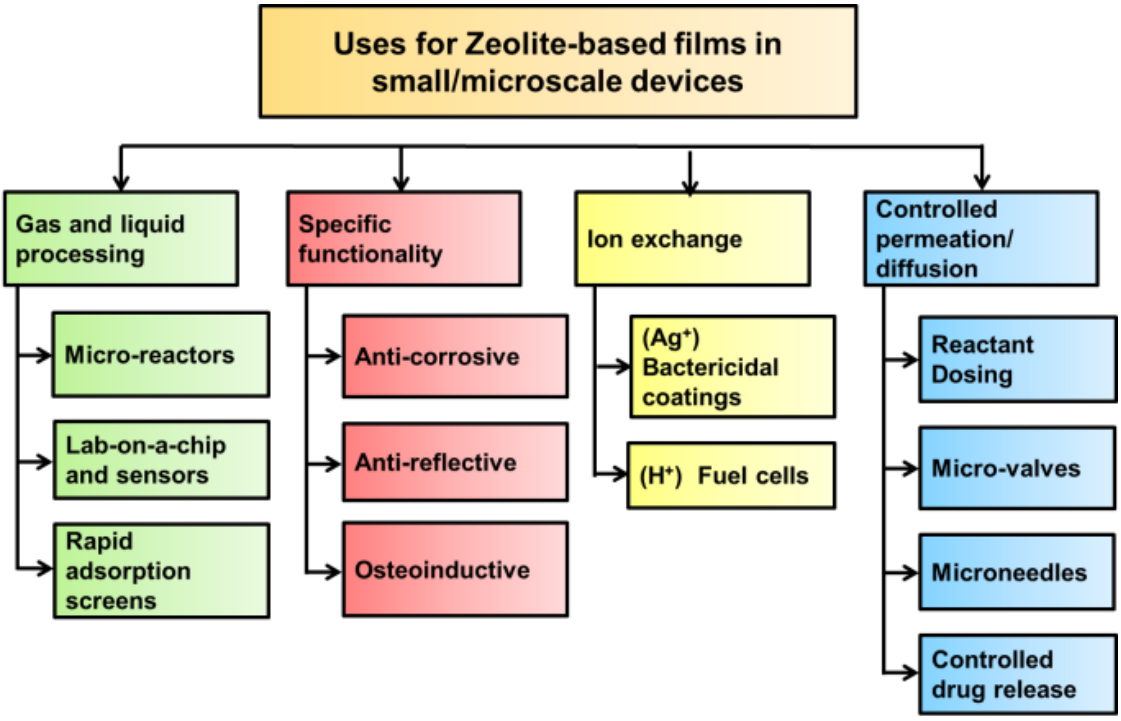

Figure 3-1: Examples of applications of zeolite-based thin films to microscale devices. (Adapted with permission from [25]).

As an example, micromixers, microseperators and microreactors are a few of the major devices that could help us realize miniaturization to the extent of 'desktop miniature factories, micropharmacies and nanomills' [30]. Microreactors and microseperators benefit from large surface area to volume ratios, which increase their rate of mass and heat transfer and make zeolite-based materials suitable candidates from which these devices could be fabricated [29, 31]. However, for these applications, the post-patterned deposition of zeolite films often tends to be rough due to indiscriminate zeolite crystal precipitation onto the patterned surface during hydrothermal synthesis. Wan *et al.* has shown that in a film of thickness 16 μm, the average roughness could be 8 μm, forcing researchers to pattern reactors by etching away the zeolite films deposited on silicon wafers in order to form clean and precise structures [30].

In order to extend the applications of zeolites into microscale and smaller devices, it is essential to be able to pattern micro– and nanoscale features on a number of different substrates. However, the number of available techniques to prepare features from such films, typically based off of existing semiconductor fabrication methods, is limited and often not well-known for these materials. Given the increasing interest in using these materials in micro- and nano-scale devices and applications, it is important that the methods that have been tried for these materials are consolidated and reviewed, particularly for their limitations and achievements. Here, we review some of the typical techniques, focusing on the patterning steps that have been utilized to create microfeatures in zeolites or zeolite-based thin films. This work represents the first review of patterning techniques used for zeolite and zeolite-like thin films, and will enable the

development of new, simple, less-expensive, and one-step processing methods that will greatly enhance our ability to apply these unique materials to a broader range of applications.

3.2 Zeolite Film Synthesis

In order to understand the impetus for the development of certain kinds of patterning, it is important to understand the standard methods of zeolite synthesis as powders or thin films. Either post-preparative (*ex-situ*) methods, where powdered zeolite is embedded in a matrix of choice, or *in-situ* methods are used for the fabrication of a thin film containing zeolites.

From a thermodynamic perspective, zeolites form through a combination of nucleation and growth processes where the smaller particles, which are energetically unstable, are deposited onto or subsumed into larger particles, minimizing the surface area to volume ratio. Essentially, the smaller crystals provide the material for the growth of the larger crystal and are consumed in the process. In some cases, pre-formed seeds of small zeolite particles can be added to the reaction gel to speed up the reaction process by decoupling the nucleation and growth phases of zeolite crystallization [32-34]. However, in concentrated solutions, the phenomenon of nucleation is governed by the reaction gel, which consists of a source of T-atoms like silicon or aluminum, the structure directing agent (SDA), the mineralizing agent, and water. The SDA molecule interacts with the T-atoms due to van der Waals forces that are produced upon loss of their hydration spheres. The mineralizing agent, typically OH^- or F^-, provides the essential pH condition for

crystallization to occur at a specific rate (which is also determined by the molar composition of the reaction gel and the temperature). OH^- is also used to solubilize silicate and aluminate species in the gel. The reaction gel is heated to hydrothermal conditions (70-200 ^oC) under autogenous pressure, which leads to the formation of highly crystalline materials after a few hours to several days. Zeolites can be synthesized as coatings, membranes, films and nanocrystalline powders, and possess the necessary qualities to act as a "Fast Sol-Gel" with applications as micro-optical elements [35, 36]. The interested reader is directed to a number of excellent resources with more information on these processes [37-39].

The rate of crystal formation and its consequent deposition on a substrate to form films can be tuned by modifying several of the synthesis parameters. Investigations have shown that regulation of the aging time and/or the crystallization under autogenous conditions of the reaction gel allows for films of various thicknesses to be deposited on various substrates. By controlling the hydrothermal reaction parameters, it is also possible to have zeolite films of deposited crystals with tunable pore sizes, structures, thickness, orientation and intergrowth. By choosing different structure directing agents and T-atoms such as Ge, Al, B, Be, Zn etc., zeolites with several different geometries have been synthesized [32].

Zeolite films and membranes have been used with various supports such as silicon, glass, quartz, ceramic, alumina, polymeric membranes, stainless steel, clay, and Teflon [18, 25, 40-42]. Zeolites can be synthesized at low temperatures while maintaining high purity, which provides a method of precise control over its composition,

properties, physical structure, pore size and distribution. Post-synthesis calcination of the crystalline product is performed to open the pore structures previously occluded by the structure directing agent, thus revealing the outstanding chemical and physical properties of the zeolite.

3.3 Patterning Techniques of Zeolite Films and Membranes

Several powerful tools have been designed and developed for making structures and devices in the micro-domain from pre-existing bulk or thin-film materials. Most of the currently available techniques have evolved from microelectronic fabrication processes[49, 50], including wet-chemical etching [43, 44], chemical vapor deposition [45, 46], XeF_2 etching [47], ion-beam etching [48], e-beam etching [49, 50], LIGA (German acronym for Lithography, Electroplating, and Molding) [51, 52], multi-lamination[61, 62], laser micromachining [53, 54] and dip-pen lithography [55]. These techniques have been successfully adapted for similar fabrications in the micromechanics and micro-optics industries [56].

Conversely, various studies have shown that inorganic silicates are capable of self-organizing in the presence of organic surfactant precursors, and can be used to make the aforementioned structures and patterns on the nanometer scale through sputtering, laser ablation, or self-organization around a template. Moreover, several reports in the literature suggest that these materials can be deposited or grown on previously-patterned substrates using hydrothermal techniques.

Here, we discuss the various techniques from both approaches to make micro-scale patterns with zeolite and zeolite-like materials. Most of the available micro-patterning methods that have been investigated so far for zeolites comprise of the deposition of zeolite as powders or patterning films post-synthesis, although recent work by Kirdeciler *et al.* have demonstrated the advantages to combining these techniques [57]. This section is organized by addressing bottom-up, then top-down, approaches to patterning.

3.3.1 Bottom-Up Approaches

For the purposes of this review, bottom-up approaches are designated as approaches where the patterning of the zeolite thin film occurs during thin film synthesis, with or without the use of a pre-patterned substrate. Pre-patterned zeolite deposition techniques use a zeolite layer consisting of individual crystals attached to the support or substrate by means of physical or chemical bonds. This might lead to the occurrence of inter-crystalline gaps or membrane defects, which could adversely affect the properties of the final device, such as the sieving selectivity. However, in other cases, this property of coated films can be beneficial, e.g. as sensors or catalytic coating [25]. The use of pre-patterned substrates simply means that the patterned support is dipped or immersed in the zeolite reaction gel, then placed in an autoclave and subjected to autogenous pressure and temperature conditions for crystallization. This process of direct, *in-situ* crystallization on supported or unsupported films requires precise control, as well as techniques for

preventing seeds or the reaction gel from penetrating areas of the support where a coating is unwanted.

It should be pointed out here that for such processes of directly synthesizing zeolites on supports, it is essential to check the compatibility of the support materials with that of the reaction gel so as to protect the integrity of the support. Some adapted techniques used to achieve such a goal involve coating the support with zeolite MFI. Jansen *et al.* has provided a comprehensive list of the various substrates that are currently used for zeolite coatings along with their properties and stabilities [58]. They also mentioned that for the direct synthesis method, the reaction gel uses a greater volume and a greater mass of reactants than required. This inadvertently causes excess precipitation of crystals with varied sizes due to uncontrolled crystallization. Under such conditions, it becomes essential that we understand the theory of nucleation and crystallization specific to the support used so as to produce films and coatings with the desired continuity, crystal orientation, and thickness.

Here, we present six examples of *in situ* zeolite crystallization approaches in the presence of pre-patterned supports.

3.3.1.1 Micromachining Pre-Patterned Supports

Example 1. Rebrov *et al.* deposited a single, well-adhered layer of ZSM–5 (MFI) on AISI 316 stainless steel plates with pre-engraved microchannels [67]. The dimensions of the channels in the final microreactor were around 1 mm (large enough for

microreactions). **Figure 3-2** shows that the microchannels were made by stacking two plates (each possessing half of the channel diameter) on top of another. This means that the thickness, orientation of deposited crystals of the coating cannot be readily studied unless the plates are disassembled.

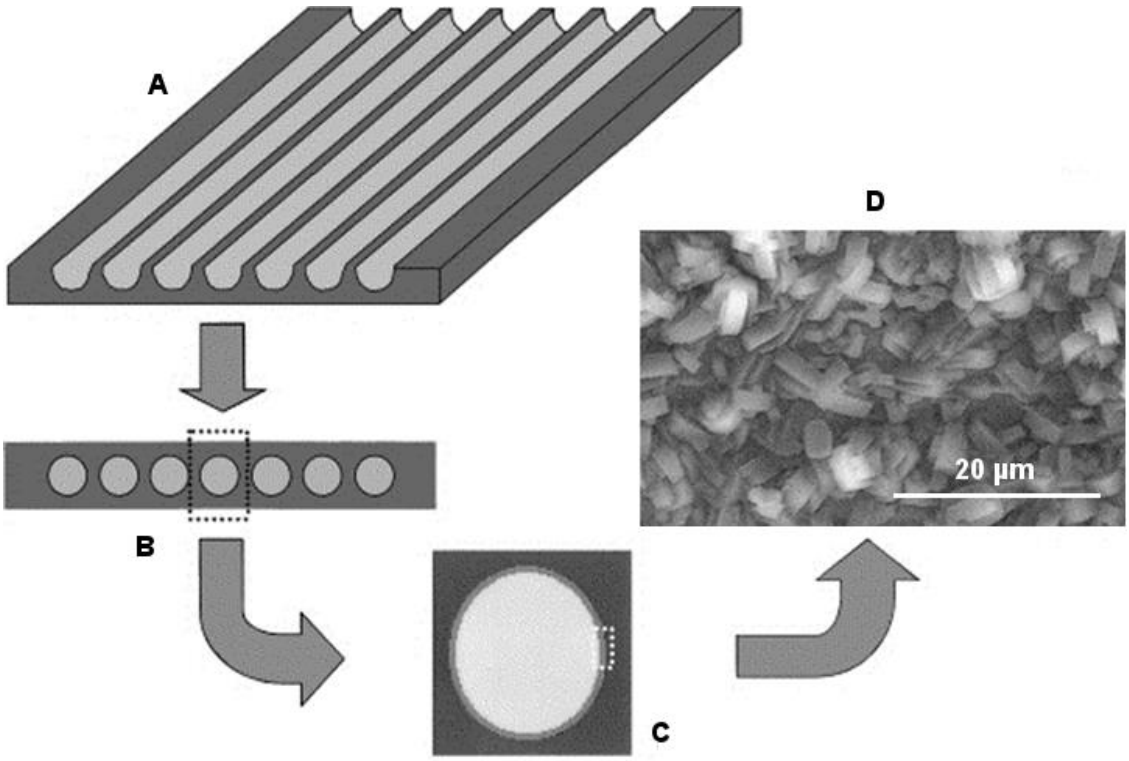

Figure 3-2: Schematic representation of (A) engraved channel of ZSM-5 (MFI) on AISI 316 steel plates, (B) front view after uniting both parts of the channels, (C) single microchannel with zeolite coating, and (D) SEM image of zeolite coating inside the channel. (Adapted with permission from [91]).

Example 2. Iglesia *et al.* prepared Na-ZSM-5 (MFI) films on stainless steel substrates for use in microreactors [59]. Microchannels of 41 mm in length and 500 μm in diameter were engraved on stainless steel plates (50 mm long, 10 mm wide). The 14 channels in each plate were further attached to wider inlet and outlet regions. Three different routes (direct liquid phase, seeded, and vapor-phase) of hydrothermal synthesis were used. In these methods, the deposition of zeolite film was allowed to occur after the channels were engraved on the plates. This was done to enhance/confine growth of film on the channel surface and minimize deposition between the channels. The channels were coated with zeolite/silicalite-1 seeds or pretreated with a sulfuric acid solution. Unfortunately, SEM images, as shown in **Figure 3-3**, revealed zeolite growth in both treated and un-treated regions. This was due to uncontrolled crystal formation in the reaction gel, which eventually deposited onto the entire substrate irrespective of the channel or the spaces in between. Although the synthesis using seeds promoted desired growth, i.e. it was homogeneous and had good coverage, the film growth outside the channels could not be eliminated [30, 56, 59, 60]. Using vapor-phase synthesis, however, allowed for deposition mostly within the channels. While the steam-assisted technique prevented zeolite deposition in undesired regions and provided good coverage over the channel, it adversely resulted in less crystallization of the zeolite films. Analysis of these channels showed the presence of non-crystallized gel embedded in between zeolite crystals. This process also required a long crystallization time, which causes a significant change in the degree of crystallinity and the structure of the zeolite films.

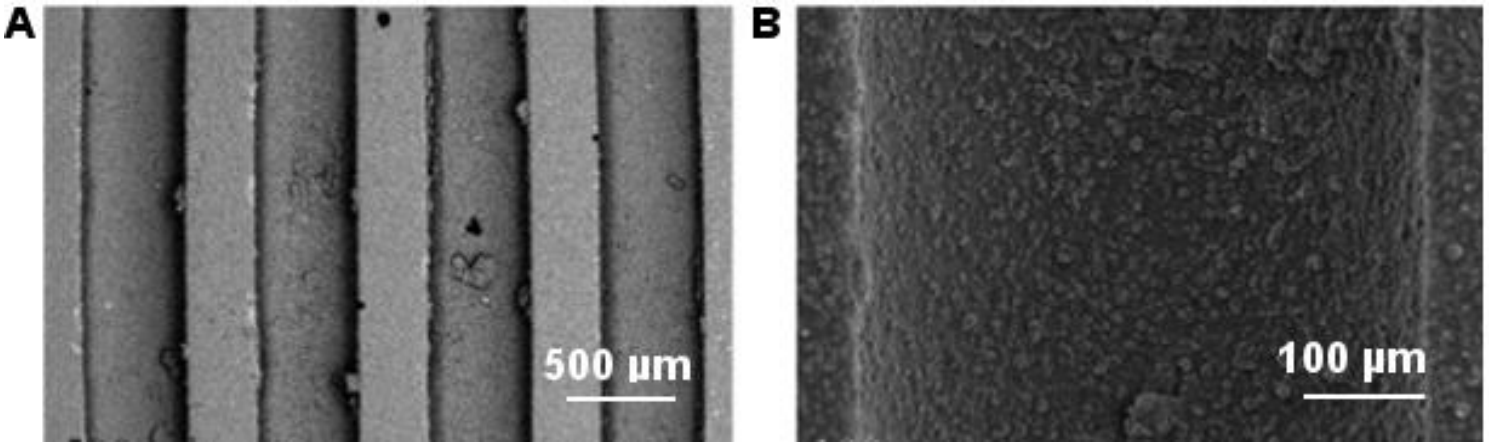

Figure 3-3: SEM micrograph of (A) Na-ZSM-5 (MFI) sample made by liquid phase hydrothermal synthesis on seeded channels, 8h synthesis time, 170^{o}C; (B) magnification of the microchannel. (Adapted with permission from [59]).

Example 3. Mateo *et al.* used both continuous and pulsed lasers to create perforations in stainless steel sheets (75 μm thick) [61]. The steel substrate was ablated (average power 4 W, pulse energy 0.80 mJ, fluence 1.3 mJ/mm^2, pulse rate 4.5 KHz, peak power 3.14 GW/mm^2) to make an array of microholes where each microhole's cross section is 60 X 90 μm . This was due to the outward flow of molten steel during laser ablation. The rough edges of these microholes had a height about 10-15 μm tall.

Hydrothermally synthesized silicalite-1 (MFI) nanocrystals (~100 nm) were used to rub the laser-perforated edges, which were typically rough (diameter 15 nm). This substrate was then placed inside a Teflon-lined autoclave filled with reaction gel and subjected to hydrothermal conditions. This step allowed the growth of silicalite-1 crystals inside both the microholes (cylindrical, 80 μm–inner diameter) and the rough edges of the substrate. At the end of hydrothermal synthesis, the entire substrate was fully covered with intergrown coffin-shaped silicalite-1 (MFI) crystals, completely filling the pores **(Figure 3-4A, B, C)**. The thickness of the deposited film was ~ 30 μm, which could be tuned by changing the synthesis time or temperature. **Figure 3-4D** shows the top view of a substrate after laser-cleaning the film and confirms that the microholes remained filled and the film remained intact.

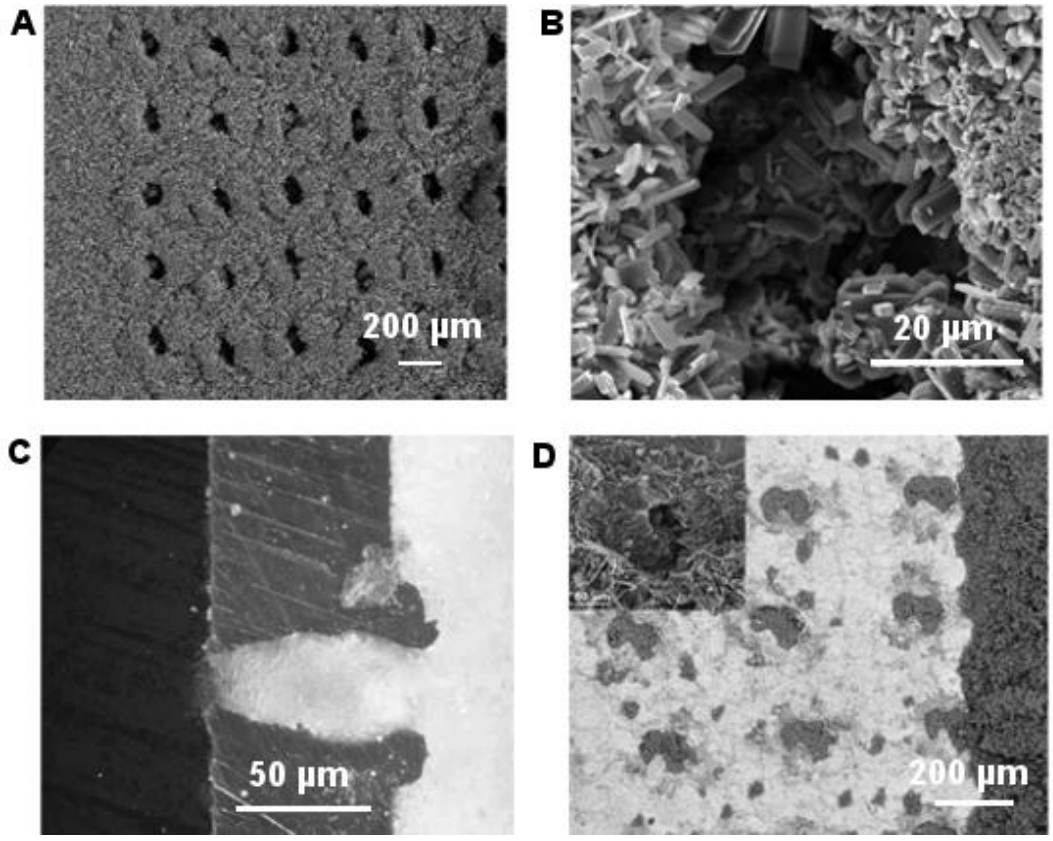

Figure 3-4: (A, B) Electronic images of substrate fully covered with silicalite-1 crystals following hydrothermal synthesis; (C) optical microscope image of cross-section of zeolite-filled holes; (d) plate surface after laser polishing with detail of the microhole in the insert. (Adapted with permission from [72]).

3.3.1.2 Photolithography for Pre-Patterning Supports

The development of one- and two-dimensional features has been carried out for quite some time with advanced nano-lithographic techniques borrowed from the semiconductor industry. These techniques include e-beam/focused-ion beam [62], proximal-probe patterning [63, 64], X-ray and extreme-UV [65, 66]. Here, we discuss some typical examples.

Example 1. Wan *et al.* made a T-shaped microreactor and separator from TS-1 (MFI) zeolites. A standard photolithography technique and a chromium mask were used to fabricate a pre- patterned support containing three channel widths (200, 500 and 1000 μm) all with depth of 250 μm, made on silicon wafers using [40]. After the excess photoresist was removed by oxygen plasma, the channels were further etched with 30 wt% potassium hydroxide (KOH), forming a trapezoidal channel cross-section (54.7 ^{o}C) due to anisotropic etching. **Figure 3-5** shows spherical TS-1 (MFI) zeolite seeds with an average particle size of 100 nm used to form intergrown films after a secondary hydrothermal synthesis. The zeolite microreactors were made using four different methods. In the first method, the powdered zeolite seeds were suspended and coated onto the channels, which were already engraved on the substrate [67]. To ensure that the suspension covered the entire surface of the channel, the substrates were carefully sonicated, dried at 333 K, and calcined in air at 823 K. Repetition of the coating step was used to obtain the desired zeolite load. In another method, seeded silicon wafers were patterned to grow zeolites by dipping the entire substrate in the zeolite reaction gel. This dipping could be done after the pattern formation on the silicon wafer or after coating.

The substrates were placed upside down in the Teflon liners for the hydrothermal synthesis to prevent the precipitation of zeolite powders and crystals randomly on the film. In a third method, the authors selectively grew zeolites by seeding. In order to confine zeolite growth within the microchannels, they coated/functionalized the channels with mercapto-3-propyltrimethoxysilane. Multiple seeding was also performed to obtain the desired density and thickness. In the last method, a 5 μm uniform layer of zeolite film was grown using hydrothermal means.

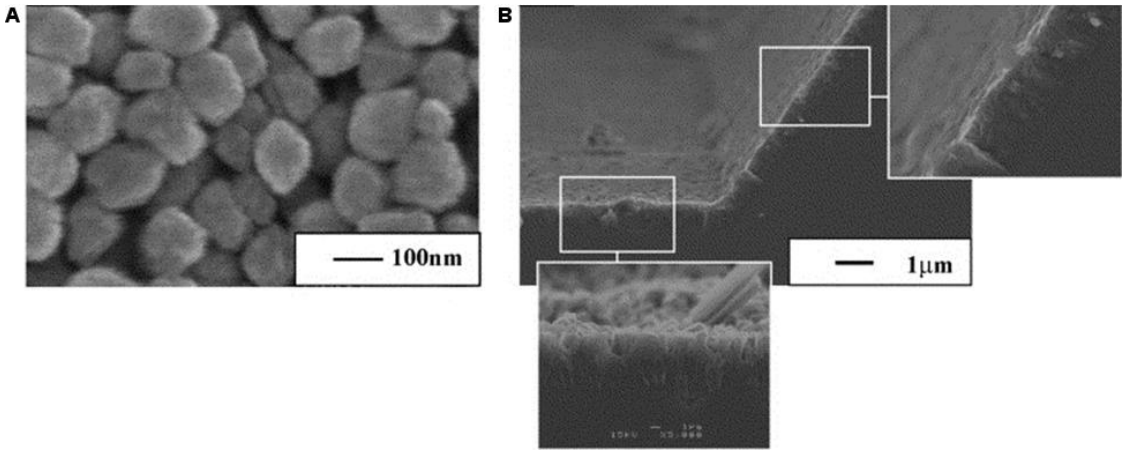

Figure 3-5: SEM of (A) TS-1 zeolite seeds with average particle size 100 nm and (B) microreactor channel after secondary hydrothermal growth of seeded channels (Note: inserts are twice the magnification of the picture). (Adapted with permission from [40]).

Example 2. Jansen *et al.* presented an alternate approach of making zeolite coatings on pre-patterned substrates fabricated via photolithography [58]. By using different gel compositions, variations in thicknesses, crystal orientations, crystal size distribution, and growth kinetics can be obtained. This allowed for the formation of continuous and monolayer zeolite coatings (films < 1 μm or layer > 1 μm) [68]. Si (100) (0.5 mm thick) was used as an underlying substrate, and coated with SiN (silicon nitride) (0.5 μm thick) by chemical vapor deposition. Si was etched by 1M NaOH at 80 ^{o}C for 5-6 h, (chosen due to the thickness of the final zeolite film/membrane desired). A thin SiN layer was obtained at the end of the etching step. This was exposed to the desired zeolite composition and kept in an autoclave at autogenous temperature and pressure conditions. A thin membrane of unsupported zeolite held on both sides by silicon ridges was finally obtained upon dissolving the SiN with 85% H_3PO_4 [58, 68]. The process is illustrated in **Figure 3-6.**

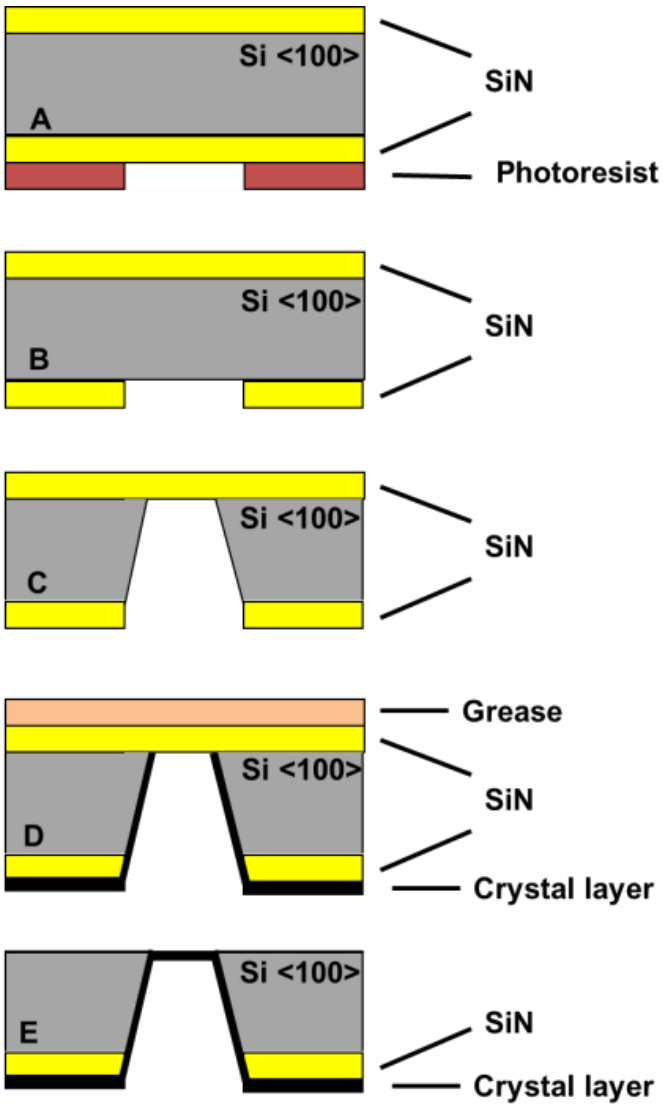

Figure 3-6: Schematic of the steps towards making thin zeolite layer through silicon-silicon nitride composites; (A) Si (100) coated with 0.5 µm SiN, (B, C) photoresist is etched and thin SiN layer is released, (D) while protecting the top of SiN layer with grease silicalite-1 is grown on the exposed SiN layer; (E) SiN layer is finally removed to release thin membrane of silicalite-1. (Adapted with permission from[58]).

3.3.1.3 Photoassisted Electrochemical Etching for Pre–Patterned Supports

Various methods of micropatterning using photo-assisted electrochemical etching (ECE) have been developed. ECE has been used to create macropores (microneedles/hollow microcapillaries) with diameters in the range of 2-5 μm [76, 78]. Using this technique, macroporous arrays with high perfections having applications as photonic crystals [69], optical filters [70], and sensors [71, 72] can be fabricated. By controlling conditions like current density, etching time, concentration of etchant, temperature and bias, n/p–type Si and its resistivity, the morphology (aspect ratio) of the pores can be controlled [67, 73, 74].

Example 1. In one such method, Urbiztondo *et al.* made nanofeatures, such as microliths and microneedles, from silicalite-1 (MFI) films [73]. To do this, macropores with diameters of 2-3 μm were made on n-type Si (100) wafers and coated with silicalite-1 (MFI). Photoassisted ECE was carried out using 2.5 wt% aq hydrogen fluoride (a low percent of the etchant makes pores with higher aspect ratio). The macropores were grown to be straight with the aid of lithographical patterns, which determined the distance between the pores. The extent/depth of etching of the substrates determined if microneedles or micromonoliths were fabricated. The microneedle structures were made by stopping the propagation of etching to the wafer edge while growing an underlying structure of SiO_2. Grown microneedles were released from the base using 25% tetramethylammonium hydroxide (TMAH) whereas the released microneedles for the Si micromonoliths were immersed in the buffered hydrogen fluoride (BHF) solution. BHF dissolved SiO_2, which resulted in straight and periodically arranged channels. By altering

the extent of etching caused by the TMAH solution, it was possible to make channels of different lengths. After making these microstructures, zeolite crystals were laid over them via seeded or unseeded hydrothermal synthesis. This process involved the typical steps of cleaning the substrates in an ultrasonic bath with acetone and DI water, treating the surface such that it was positively charged so as to deposit zeolite seeds from the colloidal suspension, drying the colloidal suspension, and repeating these steps to obtain films of the desired thickness.

According to the original source, when the reaction mixture for thin films or *b*-oriented zeolite coating was used, the surfaces between the SiO_2 microneedles were coated. **Figure 3-7C, D** shows the formation of intergrown silicalite-1 films on the microneedles. Each microneedle is isolated from one another in the array, increasing the accessible surface area.

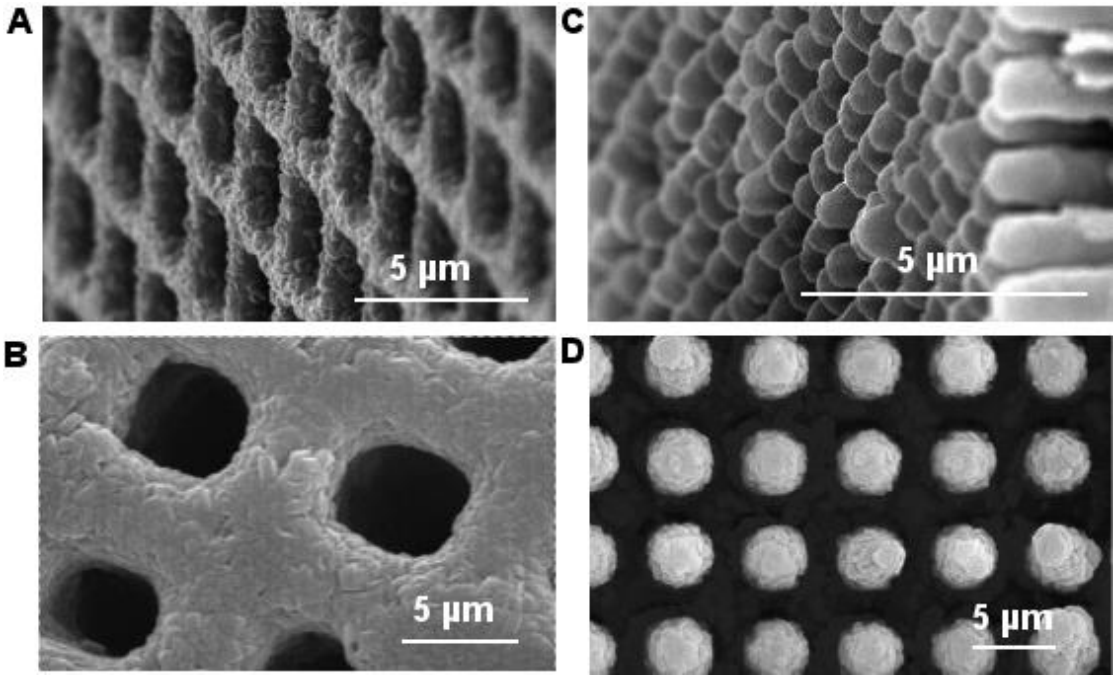

Figure 3-7: Shows (A, B) continuous silicalite-1 coatings formed by seeded growth over Si different grid (macropore) spacings, these coatings did not clog the pores;(C, D) regularly spaced microneedles are formed and are completely covered with silicalite-1 (MFI) with retained covered with are formed with retained individuality. (Adapted with permission from [73]).

3.3.1.4 Micromolding and Self–Assembly Approaches

Micropatterned zeolite films with complex pore architectures can be fabricated by using zeolite nanocrystals. Smaller nanocrystals are more likely to self-assemble than larger crystals, which have broad size distributions [23, 75]. Zeolite nanocrystals tend to self-assemble due to the combination of capillary forces, hydrogen bond formation, and reduction of cohesive forces between individual crystals.

Example 1. Huang *et al.* created nanofeatures of zeolites by combining the techniques of micromolding and self–assembly [4, 5, 75]. They used a pre-patterned polydimethylsiloxane (PDMS) stamp to apply a compression pressure of ~ 1-2x10^5 Pa on a drop of silicalite-1 (MFI) nanocrystals suspended in ethanol. Upon leaving the mold for a prolonged period (~ 12 h), the solvent evaporated and caused self-organization of the silicalite-1 nanocrystals into a continuously close-packed structure complementary to the pattern on the PDMS stamp. The solvent used is highly volatile, amphiphilic in nature and causes esterification due to the presence of terminal $–CH_2$ groups. This improved the strength of hydrogen bonding, preventing the aggregation of individual crystals. Thus, the final orientation was retained and further strengthened by calcination. The dimensions of the patterned area and smallest feature size obtained using this technique were 0.8 X 0.8 cm and 200 nm respectively [75]. **Figure 3-8** shows an SEM image of self-organized zeolite nanoparticles forming a continuously close-packed network. This formation occurred by self-assembly with polystyrene latex (9.9 wt%, 300 nm diameter) as the template at room temperature. Long cylindrical fibers (diameter, 27–33 μm; length, ~ 1.5

cm) of silicalite-1 zeolite nanocrystals were also formed due to self-assembly and evaporation of the dispersion solvent (ethanol).

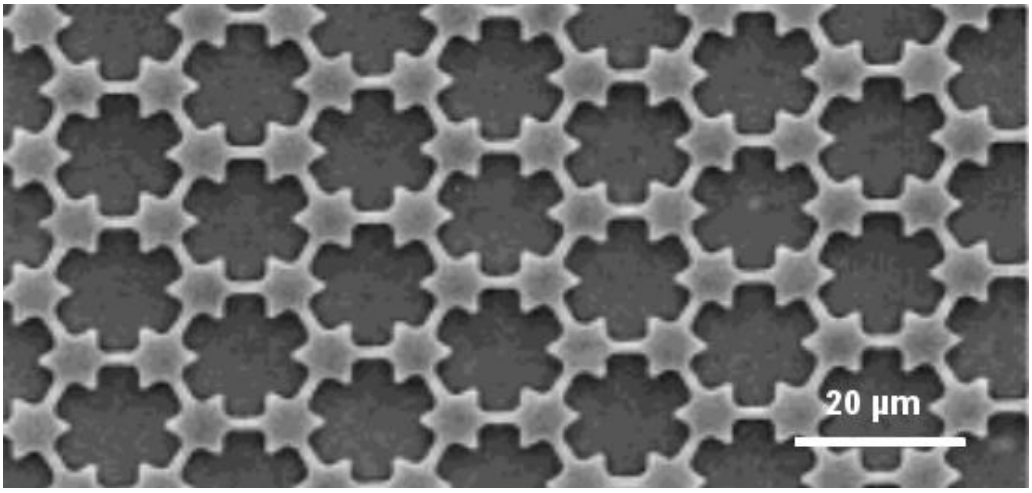

Figure 3-8: SEM images of closely-packed networks of self-organized zeolite silicalite-1 (MFI) nanoparticles formed by self-assembly and evaporation. (Adapted with permission from [75]).

3.3.1.5 Photodecomposition of Covalently Bonded Zeolite Layers

Example 1. Another way to pattern zeolite films is by the direct dipping of the supports patterned with surface-protecting organic functional groups into the reaction mixture. Ha *et al.* has illustrated the procedures for patterning covalently bonded monolayers of zeolite ZSM-5 (MFI) crystals and continuous films [76, 77]. By generation of carbon- or silicon-based hydroxyl groups from the photodecomposition of the attached groups (here it is tethered by 3-iodopropyl or IP groups), it was possible to create patterns. The attached groups, i.e. iodoalkyl compounds, were vulnerable to UV light, and therefore the zeolite crystals attached to these groups created monolayers on the substrate surface. **Figure 3-9** illustrates the different paths followed to create both patterned and continuous ZSM-5 (MFI) films on a glass substrate.

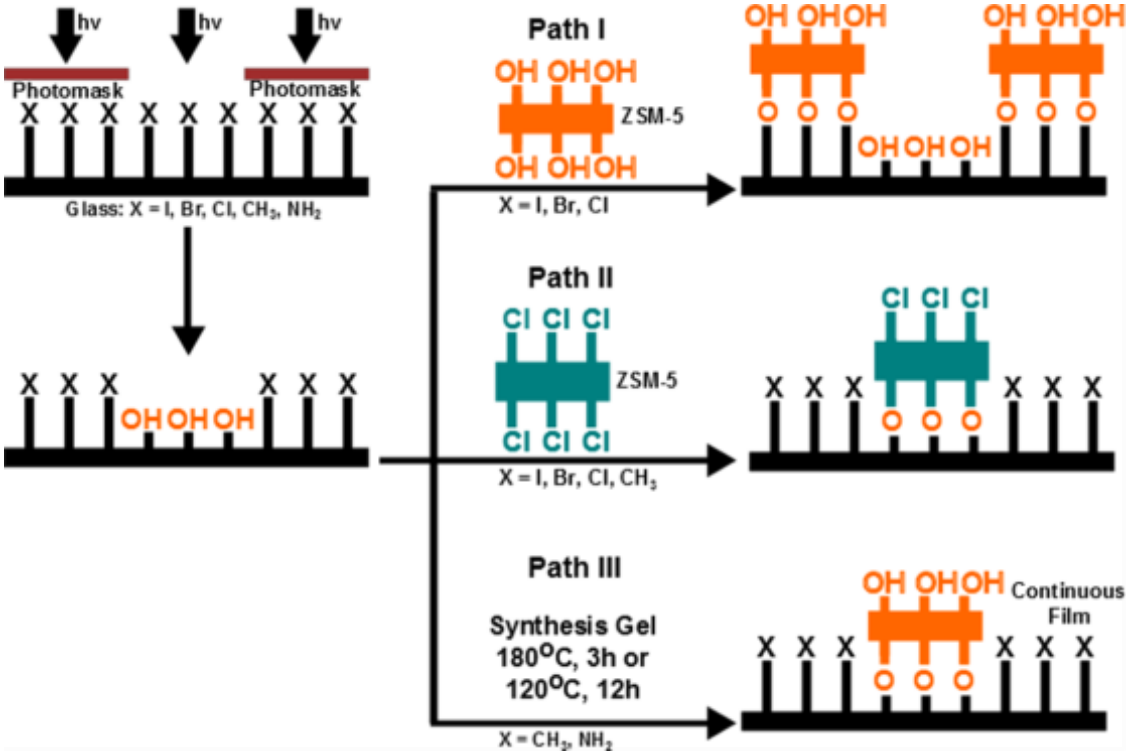

Figure 3-9: The steps of patterning bonded monolayers of ZSM-5 (MFI) crystals (path I and II) and continuous ZSM-5 (MFI) films (path III). (Adapted with permission from [76].

Figure 3-10A shows that ZSM–5 (MFI) crystals remained attached to the masked regions on the glass substrate after sonication (2 min) and formed a monolayer. **Figure 3-10B** shows that ZSM–5 (MFI) crystals formed a monolayer only in the unmasked regions when the crystals were attached with 3–chloropropyl. Calcination further strengthened the attachment between the crystals and the substrate. When the glass plate, patterned with organic functional groups, was directly dipped into synthesis gel, ZSM-5 (MFI) crystals were deposited, forming a square-patterned array (size ~ 70 μm) as dictated by the shape of the photomask grid **(Figure 3-10C)**. These features had a continuous film of intergrown crystals as compared to the previous two methods where there was monolayer formation. An interesting observation made in this work was that a longer period of UV exposure was required to obtain a similar Nature and degree of patterning of ZSM-5 (MFI) monolayers for those groups that are less photosensitive when they are attached to the glass substrate due to 'carbon-halogen bond cleavage' [76]. The direct dipping method produced patterns in continuous films of intergrown crystals. In the covalent assembly method, the patterned monolayers consisted of highly oriented, closely packed, discrete crystals. Sometimes the photo-induced decomposition would be non-uniform due to the presence of multiple layers or inaccurate time of exposure to light, causing blurring.

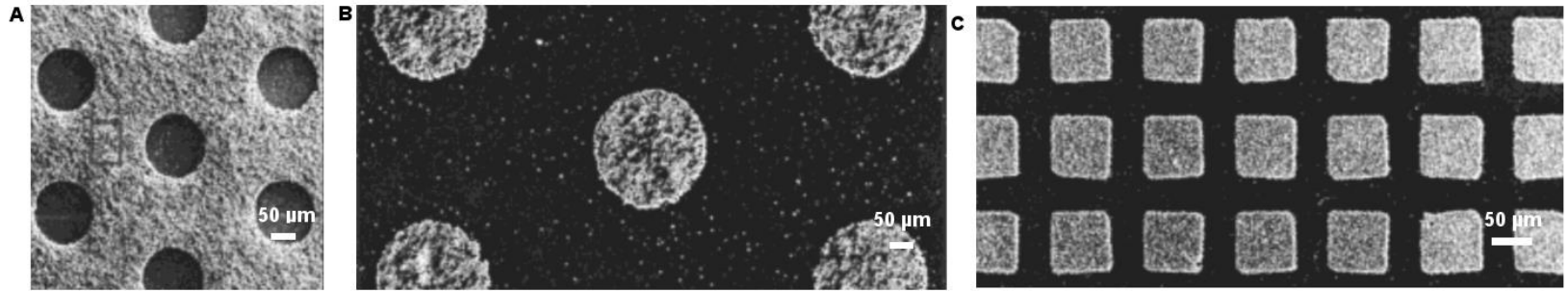

Figure 3-10: SEM images of the glass plates patterned with covalently bound ZSM-5 (MFI) monolayers according to paths I (A), II (B) and III (C). (Adapted with permission from [76]).

3.3.1.6 Selective Growth Technique

Example 1. Micropatterns of continuous and oriented zeolite films can be made by utilizing the repulsive/weak interaction between a colloidal suspension of zeolite crystals and gold surfaces [48, 88,89]. Li *et al.* has utilized this weak interaction to pattern silicalite-1 (MFI) films by selectively depositing gold in certain areas and growing zeolite crystals in the islands between them [78]. Firstly, 200 nm TEM grid was glued on top of a thoroughly washed Si (100) wafer, which was then coated with 10 nm of chromium as adhesion layer and 300 nm of gold using e-beam (CHA-vacuum deposition system) at a rate of 1.5 Å/s. Later, the TEM grid was peeled off to release a square-shaped gold patterned Si (100) wafer, which was used as the substrate for hydrothermal synthesis of *b*-oriented silicalite-1 MFI films vertically placed inside a 45 ml Teflon-lined Parr autoclave under autogenous conditions. Well-defined micropatterns were created **(Figure 3-11)** due to the tendency of colloidal zeolite crystals to repel gold, which caused zeolite crystals to be deposited between the gold surfaces and thus forming patterned zeolite regions **(Figure 3-12)**. Since gluing of the TEM grid does not provide an intact leak-proof boundary, there was diffusion of gold through the grid, as detected with EDS at different points throughout the pattern. EDS analysis reveals that the amount of gold diffusion through the TEM grid boundary decreased with distance from the edge of the grid into the film. In many cases, this factor can prove as a limitation for its applications, specifically where pure zeolite films are important and no contamination of gold can be allowed. Also, it was observed that the patterns obtained using this technique

can have dimensions limited to the TEM grid feature sizes, which are typically 1 μm between gold islands [78].

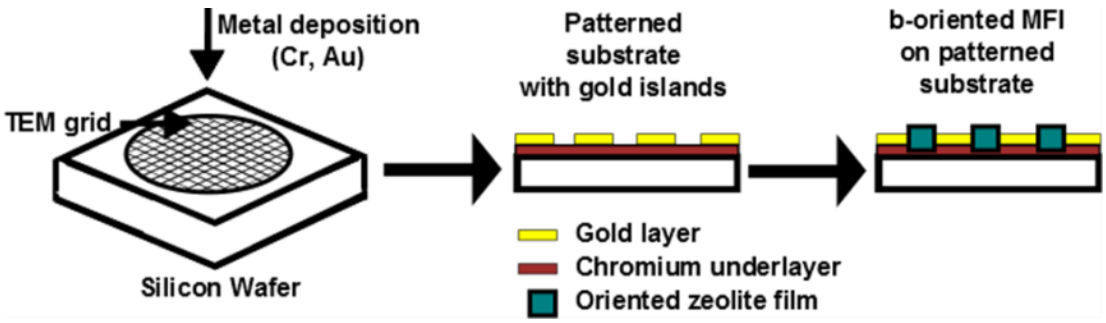

Figure 3-11: Preparation of micropatterned MFI film. (Adapted with permission from [78]).

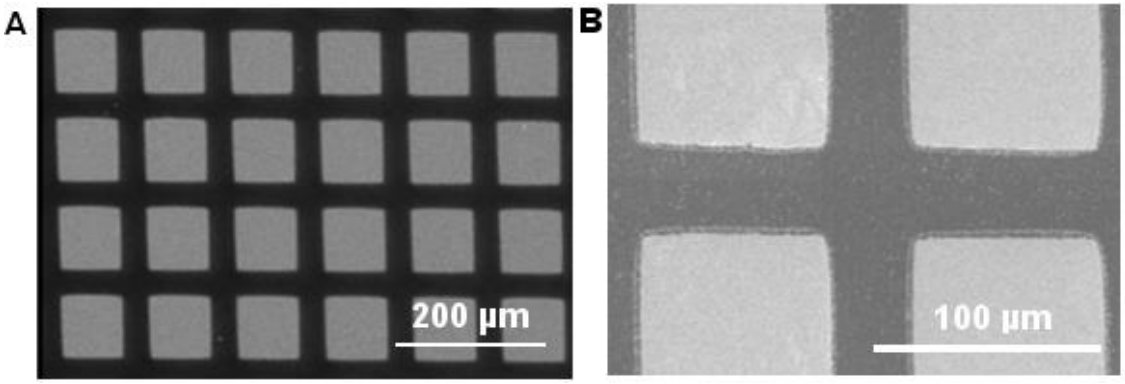

Figure 3-12: SEM images of (A) gold islands on Si (100) wafer; (B) after deposition of MFI film. (Adapted with permission from [78]).

Table 3-1: Summary of bottom-up approaches

Patterning Tech.	Substrate	Structure	Zeolite	Major applications	Limitations	Ref
Micro-machining	Stainless steel	MFI	*In situ* hydrothermal, seeded and unseeded, steam-assisted crystallization	Microreactor	Difficult to study the quality/ Nature and grow zeolites coating inside channels/patterns	[59, 61, 91]
Photo-lithography	Silicon	MFI MOR BEA	Coating with suspension of zeolite seeds and ultrasonication, dipping, surface functionalization, hydrothermal	Microreactor and separator, Catalysis, microelectrochemical	Defect formation , roughness of the channel boundary	[40] [58, 68]
Photoassisted electrochemical etching	Silicon	MFI	Hydrothermal synthesis-seeded or unseeded	Coatings	Preferential growth on Si substrate compared to the microneedles	[67] [73] [92]
Micro-molding- and Self-assembly	Si	MFI	Pre-synthesized crystals	Microelectronic Devices	Largest pattern area and smallest line feature are 0.8 X 0.8 cm and 200 nm	[4] [5] [75]
Photo-decomposition	Glass	MFI	Covalently bonded monolayers of pre-formed zeolite ZSM-5 crystals	Combinatorial catalysts, low-dielectric packing materials for integrated circuits	Non-uniform decomposition	[76] [77]
Selective Growth technique	Si	MFI	*In situ* hydrothermal growth	Molecular sieving sensor arrays, nanowires arrays Optical devices	Diffusion of gold, dimensions limited to the TEM grids (1 μm)	[42] [78]

3.3.2 Top-Down Approaches

For the purposes of this review, top-down approaches are designated as approaches where the patterning of the zeolite thin film occurs after thin film synthesis, without using a pre-patterned substrate.

3.3.2.1 Photolithography Post-Seeded/Unseeded Zeolite Film Growth

Example 1. Photolithography is a standard semiconductor microfabrication method where light is used to transfer patterns on a substrate using light-sensitive resist. Chau *et al.* grew oriented, polycrystalline zeolite films on a Si (100) wafer and then later used photolithography to create microstructure patterns for microchemical or microelectrochemical systems [56]. The zeolite films were deposited following two primary techniques. **Figure 3-13** shows the schematic of the two approaches in step-wise manner. In the first case, they deposited silicalite-1 (MFI) by the typical zeolite synthesis procedure, except that the polished surface of Si (100) was kept downwards and the backside was protected from deposited crystals using a Teflon ribbon. In the second technique, the Si (100) substrate was seeded by the process of surface functionalization and then dip-coated in a colloidal suspension followed by secondary growths for various amounts of time to obtain different film thicknesses. These zeolite-silicon films were spin-coated with a 2.5 μm thick positive photoresist. This was then soft baked for 1 min. The purpose of this step was to evaporate away the resultant solvent of the photoresist from the substrate. The micropattern on the photo-mask was then transferred onto the

zeolite film by contact printing under UV exposure. The positive resist was washed away at the UV exposed places, thus exposing the underlying zeolite film. The next step was hard baking, which hardens the photoresist and improves its adhesion. Buffered oxide etchant (BOE) was then used to etch away zeolites from the exposed areas and create the desired micropattern, which was then rinsed in deionized water and dried in nitrogen. The photoresist, which had been protecting the underlying zeolite films at selective places, was then removed with acetone. After a final rinsing in deionized water, the patterned substrate was dried at 33 K overnight and then calcined in air at 823 K for 6 h to open the micropores in the zeolite film by removing the SDA.

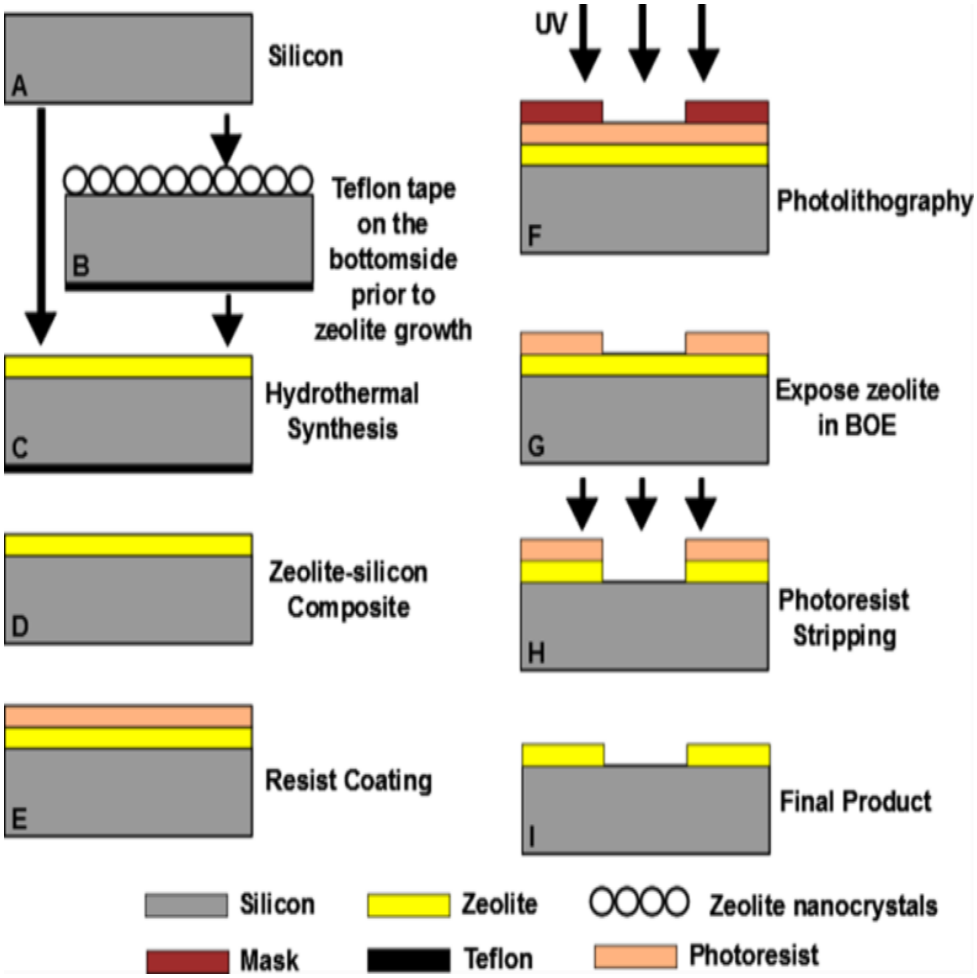

Figure 3-13: Silicalite-1 is synthesized on Si (100) using two different approaches; (A,C) hydrothermal synthesis on polished surface while backside is covered with teflon; (B, C) Si (100) is pre-seeded with zeolite nanocrystals with protective teflon on the backside; (D) zeolite-silicon composite is rinsed and dried; (E) 2.5 µm of photoresist is spin-coated; (F)Photolithography via contact printing; (G) zeolite layer is exposed by developing irradiated photoresist; (H) zeolite layer is isotropically etched using BOE; (I) Final product after rinsing with deionized water, drying and stripping off photoresist. (Adapted with permission from [56]).

Figure 3-14 shows the micro-patterned images reported by Chau *et al.* after their series of thermal cycling between 303 and 873 K for a period of 2 weeks. Points that should be noted here are that the smallest width of channel reported are 3 μm (and the silicalite-1 (MFI) film thickness is 10 μm) and that the creation of complex features required the availability of an individual mask. No damage of the pattern after thermal exposure was reported. Changes in the orientation of zeolite crystals in the film will allow for modifications in final porosity, surface roughness, etc. Chau *et al.* also explored the technique of depositing zeolite onto pre-patterned microchannels, thus creating a matrix with much greater precision in size, shape, and resolution of the final features **(Figure 3-14C)**; however, there were chances of formation defects in the zeolite lines while etching. The smallest feature size obtained in this approach was also 3 μm, whereas for photolithography and e-beam, limits were 1.25 and 0.1 μm, respectively. It is important to note that the latter was much more expensive and time-consuming.

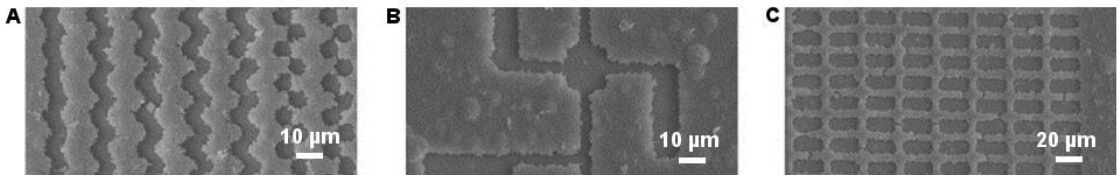

Figure 3-14: Showing different micropatterns obtained with this technique namely (A) microchannels (B) fluid distribution hub and (C) micro-fabricated grid. (Adapted with permission from [56]).

The T-shaped channel etched on a layer of (101)-oriented zeolite crystals, which were deposited on top of the Si (100) substrate by the seeded mechanism, featured a thickness of 500 μm and 20 mm length. There was considerable roughness of the channel boundary and an absence of zeolite crystals at the bottom of the channel, thus allowing reactions to occur only on the walls of the channels.

Example 2. Pellejero *et al.* prepared patterned zeolite coatings on Si (100) substrates by first creating a continuous zeolite film on the support, followed by several etching techniques used in the microfabrication industry [79]. **Figure 3-15** shows the schematic of the micropatterning steps. The authors show that this method allows for greater direct control on the thickness and degree of intergrowth of the zeolite film. Here, silicalite-1 (MFI) films in both '*c*' and '*b*' orientations were formed on Si (100), while the structural layers were made by micro-patterning via physical (ion milling) and reactive (reactive ion etching) patterning techniques. **Figure 3-16** shows SEM images of the patterned films as a result of ion milling (dry-etching at 5 X 10^{-4} mbar, acceleration voltage 300 V, current density 0.3 mA/cm^2) and ultrasonication (to remove photoresist). Analysis of the cross-sectional view of the pattern gives us an idea about the etching rate. The figure also shows that the features have rounded edges as a result of ion milling, although the mask used had vertical side walls.

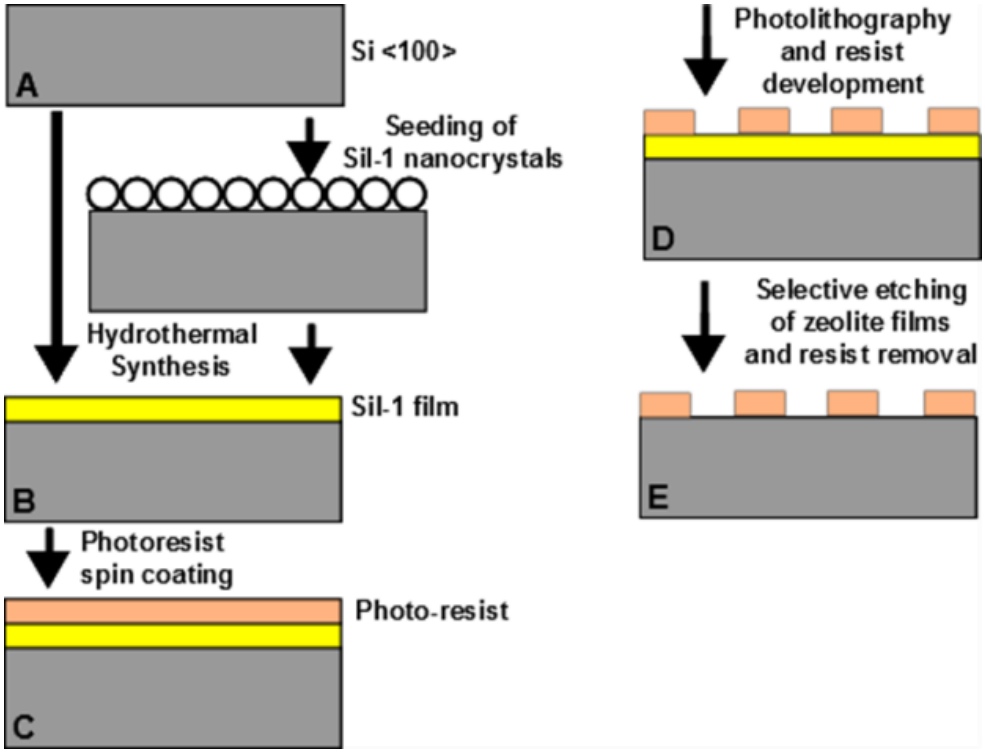

Figure 3-15: (A, B) Silicalite-1 is synthesized on Si (100) via hydrothermal synthesis or secondary growth; (C) 2-methoxy-1-methyl ethyl acetate in propylene glycol monomethyl ether acetate is spin coated to improve adhesion of photoresist to the zeolite layer, followed by 2.1 µm thick layer of positive photoresist; (D) photolithography is done using soft contact printing and developed to expose underlying zeolite film; (E) wafer+zeolite film+resist is hard baked to harden and improve adhesion of the photoresist. (Adapted with permission from [79]).

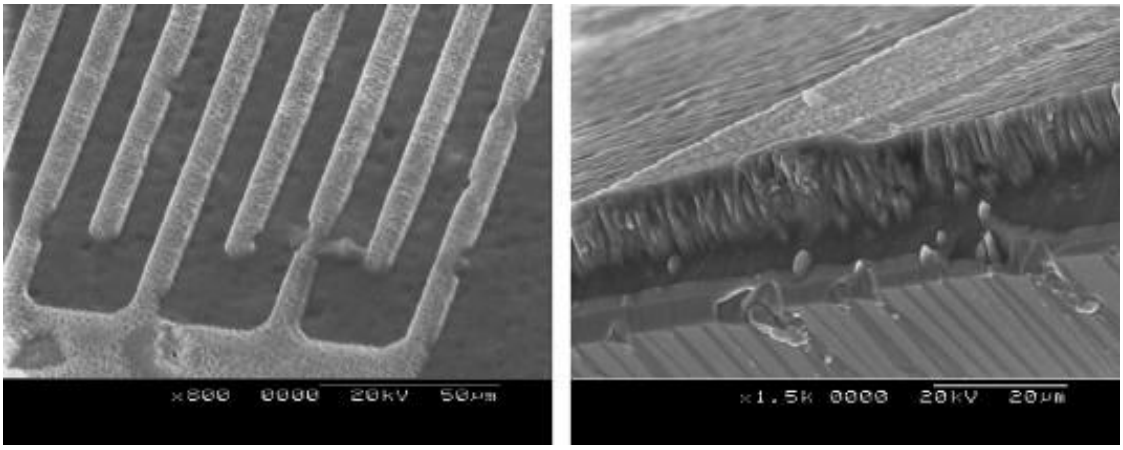

Figure 3-16: SEM of top (inter-digitated patterns) and cross section of c-oriented silicalite-1 (MFI) films after undergoing dry etching (ion milling). (Adapted with permission from [79])

Additional patterns in the films were formed using another form of dry etching, i.e. reactive ion etching (RIE), where etching occurs due to mixed physical and chemical reaction (P = 8–10 $X10^{-2}$ mbar, 10 sccm of SF_6 gas, 150 W RF power at 13.56 MHz) and the silicalite-1 (MFI) is ultrasonicated to remove the photoresist. It was observed that, due to the thickness of *b*-oriented films being less than that of the *c*-oriented films, there were etching reactions occurring in the silicon under-layer when using the reactive ion etching method. Hence, there was lateral thinning of the unprotected crystals, demonstrating that etching occurred not only in the direction of impinging or entering

ions, i.e. top to bottom, but also laterally. This caused preferential etching of the reactive edges of each individual crystal, resulting in under-etching in many cases. **Figure 3-17A** shows a cross sectional view of under-etching formed while using an interdigitated mask and 15 min RIE. Silicon pillars supporting silicalite-1 (MFI) film were formed under the mask due to under-etching. It is evident that the lateral spatial resolution varied for different etching techniques, i.e. wet and dry (ion milling, reactive ion etching). Another important observation made in this work was that the etching rates were significantly different for calcined and uncalcined crystals.

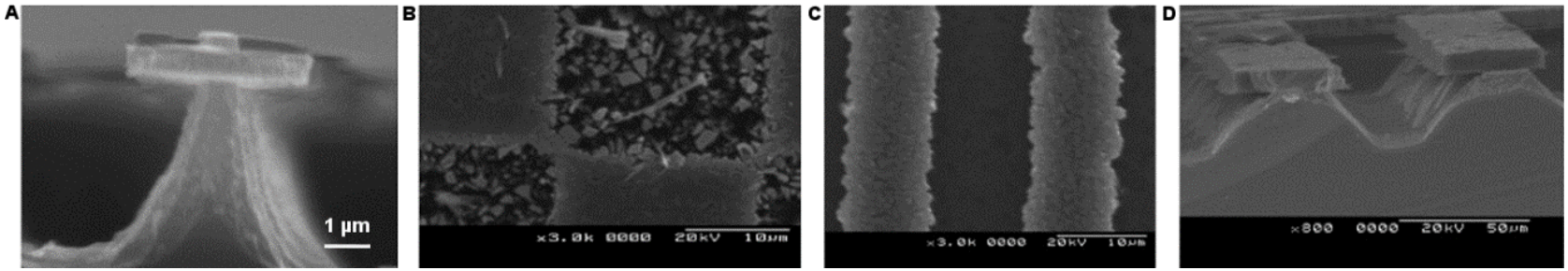

Figure 3-17: SEM of cross-section view of a *b*-oriented silicalite-1 film after reactive ion etching at reference conditions under an interdigital type mask with (A) 5 µm wide lines, (B) partially wet-etched (5 min) *c*-oriented silicalite-1 films with checkered pattern, (C) top view of interdigital patterns created by partially wet-etching *c*-oriented silicalite-1 of thickness 10 µm grown onto Si (100) wafers, (D) cross-sectional views of partially calcined *c*-oriented silicalite-1 (MFI) structures. (Adapted with permission from [79]).

Silicalite-1 (MFI) microstructures were also formed with wet-etching processes using etchants like HF solution (20 wt%) or buffered oxide etching mixtures at room temperature. Etching of *c*-oriented silicalite-1 films were completed for different time intervals. Initially the etchant dissolves the side walls of the wedge-shaped crystals and consequently penetrates and etches each crystal inwardly. **Figure 3-17B** shows that after 5 minutes of etching, silicalite-1 microneedles with increasing microporosity (due to etchant diffusion) were formed. However, after 10 minutes of etching, the microneedles between the interdigitated sheets were completely etched away. Pellejero *et al.* also created free-standing structures of *c*-oriented silicalite-1 by following the steps of fabrication shown in **Figure 3-18**. As a result of wet etching and the removal of the underlying silicon (7 wt% Tetramethylammonium hydroxide(TMAOH) solution, 70 ^{o}C, 3h) due to anisotropic etching, trapezoidal cross-sections of the channels were formed **(Figure 3-17D)**. Upon further etching, the silicalite-1 (MFI) structure were released (length 100 μm, width 20 μm, thickness 8 μm) and further strengthened by calcination.

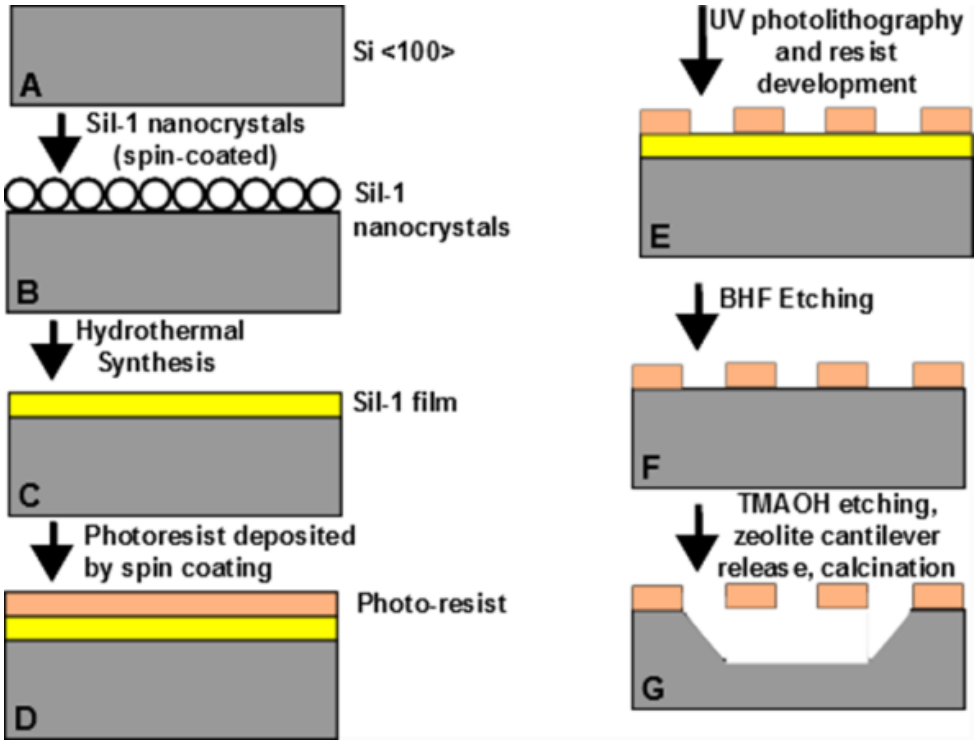

Figure 3-18: (A, B) Si (100) is seeded using silicalite-1 nanocrystals; (C) 8 µm thick zeolite layer is formed by secondary growth; (D) positive photoresist is spin coated; (E) photolithography via contact printing and resist development; (F) BHF etching for 10 minutes to pattern the zeolite layer, washed with deionized water and dried with inert gas; (G) anisotropic etching using TMAOH solution (7 wt%). (Adapted with permission from [79]).

Example 3. Chau *et al.* reported the fabrication of zeolite-based microtunnels and microchannels [80]. Microtunnels refer to channels that are enclosed by a zeolite film on top, and formed by removing photoresist as a sacrificial layer on silicon substrates. Conversely, microchannels are formed by etching the silicon substrate penetrating through the zeolite film. In order to create the microtunnels, an array of 100 parallel lines (width 100 μm, spacing 100 μm, length 20 mm), was formed by photolithography with photoresist (AZ4620) [81]. These patterns were coated with poly-(diallylmethylammonium chloride) (PDMAC), which were used to adsorb TPA-silicalite-1 (MFI) seeds (120 nm). These had grown into a continuously intergrown film after hydrothermal synthesis inside a Teflon-lined stainless steel autoclave. The structure directing agents were removed under oxygen plasma (RF=400 W, 473 K). This step was important for further etching of the underlying photoresist. It is important to note that the product of resist etching escaped through the micropores of zeolite film. Hence, it was crucial to control the rate of plasma etch of the resist so as to prevent damaging the integrity of the zeolite film and microtunnel.

Figure 3-19A shows that the microtunnels are equally spaced with an arch of zeolite film on top (height 25 μm, width 80 μm, thickness 20 μm) **(Figure 3-19B)**. The reason for the tunnel's arch shape has been attributed to swelling of the resist during hydrothermal growth of film.

Fabrication of the microchannels started with synthesis of silicalite-1 (MFI) film on silicon substrate and a top coat of metal (TiW-Au) as a protective layer, which was then micropatterned again following standard techniques [77]. Later, the metal layer was

etched and the top layer of zeolite was treated under oxygen plasma to remove the structure directing agent/template. In order to create the microchannels, wet etchant (25% tetramethylammonium hydroxide-water solution) was used to etch away silicon underneath the patterned zeolite pattern. Since the etchant had to diffuse through the zeolite film (1 μm), the rate of etching was slowed. Thus, microtunnels shown in **Figure 3-19C, D** was formed due to anisotropic etching of Si (100) wafer. **Figure 3-19E, F** show different dimensions (250 μm and 50 μm) of the microchannels that can be obtained by wet etching the silicon substrate under a 4 μm thick (101)-oriented silicalite-1 film.

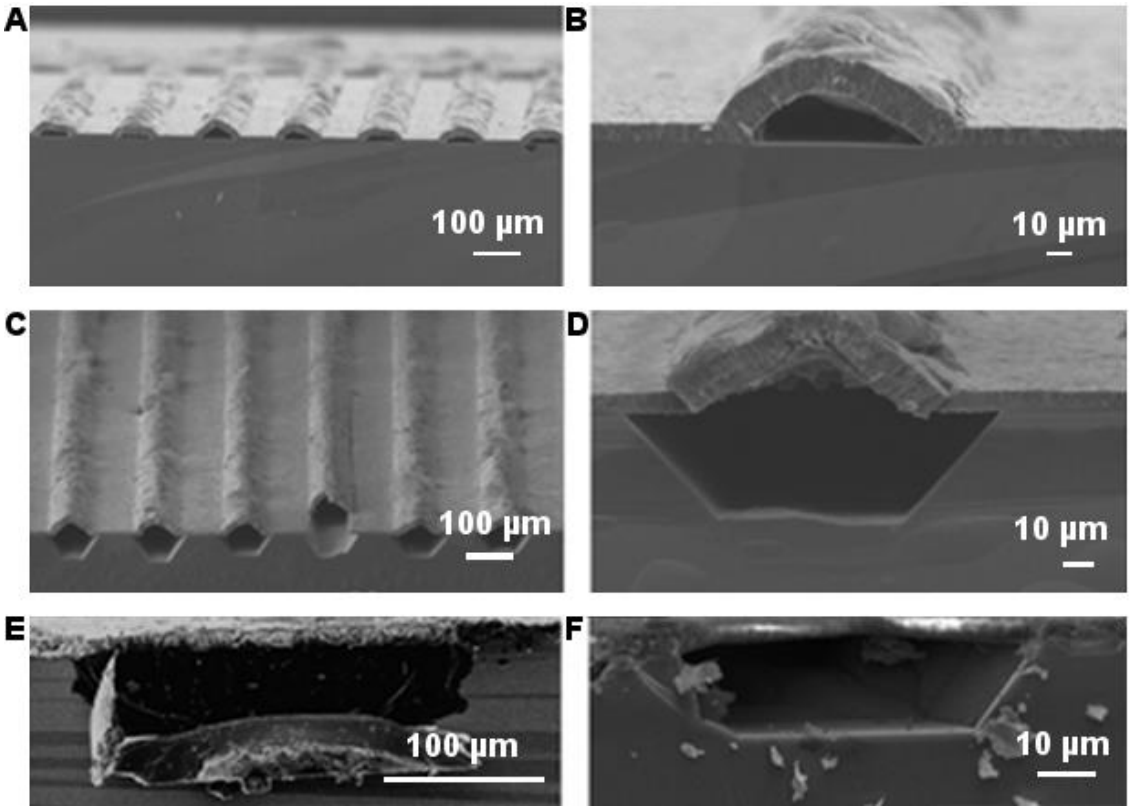

Figure 3-19: (A,B) Evenly spaced zeolite microtunnels with MFI wall supported on silicon (A, B), zeolite microtunnels created by anisotropic etching (C, D) with widths of 200 µm (E) and 40 µm (F). (Adapted with permission from [80]).

Table 3-2: Summary of top-down approaches

Patter-ning technique	Substrate	Structure	Synthesis	Major applications	Limitations	Ref
Photo-lithography	Silicon	MFI LTA	Seeded unseeded hydrothermal	Microreactors, membrane microseparators microelectrochemical, Delivery system for microdevices, Chemical and Biological storage, Biochemical sensors	Defect formation , roughness of the channel boundary, Difficult to control etch rate	[26] [56] [57] [79] [80]

3.3.3 Deposition Approaches

For the purposes of this review, deposition approaches are designated as approaches where pre-formed zeolite crystals are deposited in a patterned fashion on a substrate. Spray deposition techniques like ink-jet printing can be used to create micropatterns that are highly processable, scalable, and suitable for area printing. However, this technique is limited to materials with good solubility and is not compatible with polymeric or highly viscous solutions. This is significant given that zeolites are usually synthesized in highly viscous colloidal suspensions when not in the form of thin films, and therefore cannot utilize this method [19]. Other deposition methods, such as molecular linkers, mechanical vibration, or optical tweezers, are capable of imposing greater control and reproducible features in micro- or nano- domain.

3.3.3.1 Arranging Zeolite Crystals through Molecular Linkers

One of several ways to establish strong bonds between zeolite monolayers and a substrate (specifically glass or mica) is by using covalent linkers or surface charges [82]. By thermal annealing of block co-polymers above the glass transition temperature, different morphologies can be formed at the surface due to preferential interactions between the polymer and substrate at the bottom and the free surface at the top. It is important to note that when we intend to establish strong linkages among micrometer-sized crystals and their solid substrates, a large number (e.g. ~600,000 linkages for cubic zeolite-A (LTA) of interconnecting linkages must be formed [83]. The presence of microscopic roughness decreases the number of interconnecting covalent linkages. For example, linkage groups, consisting of epoxy and amino groups, were attached to zeolite A (LTA) crystals and the substrate to determine the extent of adherence [84]. Results show that there is a considerable increase in the strength of adhesion between zeolite crystals and the substrate and an even greater increase when polyethylenimine is used as a linker as compared to dendritic polyamine (amongst the two polyamines used in this study). It is stated that the extent of bonding strength of the zeolite crystals to the substrate can be enhanced considerably by calcination (at 450 ^{o}C) due to the formation of 'direct siloxane linkages' [84]. By using polyethylenimine, the adhesion of zeolite-A (LTA) monolayers on curved surfaces of glass have also increased considerably, as tested by ultrasonicating them for prolonged periods of time and then observing the amount of crystals that remain adhered [84].

3.3.3.2 Alignment by Mechanical Vibration

Example 1. Breaking away from the various methods of depositing zeolite crystals, coating with zeolite powders, or *in situ* film synthesis on pre-patterned substrates, Scandella *et al.* introduced a method of mechanically aligning zeolite crystals to produce a desired crystal orientation [85]. The direction in which the zeolite crystals are laid on the surface of the substrate can promote changes in the effectiveness and properties (optical, physical) that can be explored to expand the applications of zeolite thin films and membranes. The substrate that was used here was Si (110). By using the typical etching techniques of the electronic industry, grids were etched anisotropically, creating structures on the substrate. The authors proposed mechanically aligning single crystals of zeolites on grids, which increased the area of coverage because three-dimensional area coverage was utilized instead of just individual zeolite dimensional coverage. They used ZSM-5 (MFI) single crystals of two different dimensions, 30 μm X 25 μm X 120 μm and 30 μm X 25 μm X 120 μm. The frequency and intensity of the vibration of the grid were both kept at low levels to allow the crystals to fall inside the grooves. The percent coverage of the structures obtained using this technique was about 50%, which is suitable for the applications in sensing, catalytic reactors, and other applications where the properties of the material, and its specific composition are utilized. However, 50% surface coverage means that a considerable part of substrate surface remains uncovered. Scandella *et al.* used zeolite crystals all oriented in the same way such that they would have the same order of implanted molecules. These implanted

molecules were able to polarize incident rays based on their specific orientation inside the three-dimensional pore of the zeolite. The authors used this technique to analyze the embedded molecules inside the zeolite pore structure. In applications where the interaction of light with zeolite crystals and its orientation occur, the presence of gaps and space in the overall films and membrane are detrimental. Moreover, the way crystals react to vibrations varies with changes in the size and the mass in the crystal. Therefore, small crystals are not as stable on the grid as large crystals and eventually the small crystals fall off the grid. This renders less surface coverage of 35%, thus making this technique ineffective for the entire range of crystal dimensions and morphologies [85].

3.3.3.3 Alignment Using Optical Tweezers

Example 1. Woerdemann *et al.* used an interesting technique called 'holographic optical tweezers' (HOT) to control the placement of zeolite L (LTL) at the level of a single crystal [86-88]. An important point made here is that most top-down or bottom-up methods are limited in that they are carried out with an entire film or membrane and there is no control over an individual host. Here, the specific method of holographic optical tweezers was used to transfer momentum from the laser light to the contents of the film. The benefits of zeolite L (LTL) are (1) that these materials can be synthesized in a broad size and aspect ratio range, (2) the geometrical constraints promote 'extremely high concentration of supra-molecularly organized guest molecules' when doped with organic dye, and (3) the metal clusters or complexes of these materials have interesting optical properties [87].

The authors showed that zeolite L crystals can be trapped using optical tweezers. Zeolite L (LTL) crystals of length 1 μm and 3 μm were trapped stably with their cylindrical axes along the propagating beam. They were successful in creating three-dimensional rectangular arrays of 4 X 4 with 1 μm long zeolite L (LTL) crystals. According to the authors, HOT is capable of creating further interactive, dynamic, and reversible patterns using such crystals. This technique also allows control over the orientation of each zeolite crystal (along with its position) with the 'two-trap' mode [87]. This means that the force of trap is applied on the opposite poles of the cylindrical zeolite L (LTL) crystals (thus acting as handles), which helps in fine-tuning its final position. This allows zeolite crystals to be positioned in a multitude of three-dimensional orientations. Complex geometries and positioning of multiple crystals can be achieved simultaneously by controlling both the individual zeolite crystals and their translational position **(Figure 3-20)**.

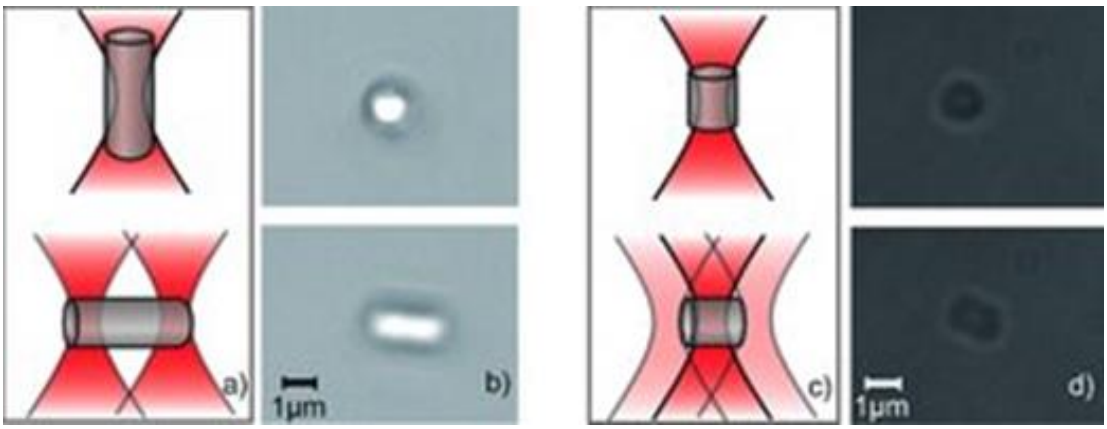

Figure 3-20: Shows the (A) mechanism and geometry to trap zeolite L (LTL) crystals (B) experimental image; (C, D) more sophisticated rotational control and its experimental image. (Adapted with permission from [88]).

3.3.3.4 Pulsed Laser Deposition

Xiong *et al.* introduced the concept of using pulsed, laser-based deposition (PLD) for the formation of zeolite films [89]. This technique involves irradiating a zeolite target with an excimer laser (248 nm, KrF, 10 Hz). The fragments of laser ablation of the zeolite target coat the substrate. In order to ensure even distribution of the crystal on the substrate, the authors carefully used a vibrating plume [90]. Here, the authors used mesoporous (acronyms: DAM-1 and SBA-15) spheres as substrates on which the zeolite was deposited with the aid of a vibrating pan. The evenly covered substrate acted as seeds for crystal growth when subjected to hydrothermal treatment. When these composites

were treated under vapor (at a specific temperature for a specific amount of time) the core materials were dissolved while the coated zeolite nanoparticles were crystallized to form hollow spheres of ZSM-5 (MFI). Conversion of PLD coated DAM-1 and SBA-15 spheres to hollow spheres of ZSM-5 (MFI) was confirmed by using a control experiment where PLD coating of ZSM-5 (MFI) was made on Si wafers (due to the difficulty associated with imaging cross-section of hollow ZSM-5 (MFI) microspheres) at two different laser energies (120 mJ and 70 mJ) for 45 min. Measured film thicknesses of ~600 nm (at 120 mJ) and ~300 nm (at 70 mJ) revealed a film growth rate of ~13 nm/min and ~6.5 nm/min at laser powers of 120 mJ and 70 mJ, respectively. The deposited fragments increased the surface roughness of the original DAM-1 spherical substrates due to its range of sizes (20 to 50 nm) (Figure 3.21A). XRD analysis confirmed formation of zeolites with the MFI structure for samples made at different energies for PLD deposition and consequent crystallization time for hydrothermal synthesis. As we would expect, increased crystallinity was observed with an increase in crystallization time. However, it was stated that the rate of crystallization was also governed by the thickness of the film formed by PLD, which in turn could be modulated by tuning the laser energy. The films made by ablation at higher laser energy showed higher crystallinity compared to the ones made at lower energy after same the duration. The SEM images reveal that the zeolite crystals grew by consuming silica from the DAM-1 sphere lying in the core, which later gave rise to the hollow ZSM-5 (MFI) spheres. Evidently after 5 days of crystallization ZSM–5 (MFI) spheres of dimension ~1.0 μm were obtained **(Figure 3-21B)**. The authors attribute the consumption of the DAM–1 core to one of the following two processes, (1) solution mediated transport,

wherein the amorphous gel gets consumed by replenishing reactants for nucleation and their growth into crystals, and (2) solid phase transformation, where there is direct conversion of the gel from amorphous to crystalline in Nature. The authors consider the first option to be more likely. This technique allows flexibility over the composition of the ZSM–5 (MFI) by either tuning the thickness of the film during laser ablation or by changing the target to the desired composition. This method is also suitable where precise control over the proto-zeolite film (zeolite fragment) is desired, which can be achieved by controlling laser energy and time of ablation [87].

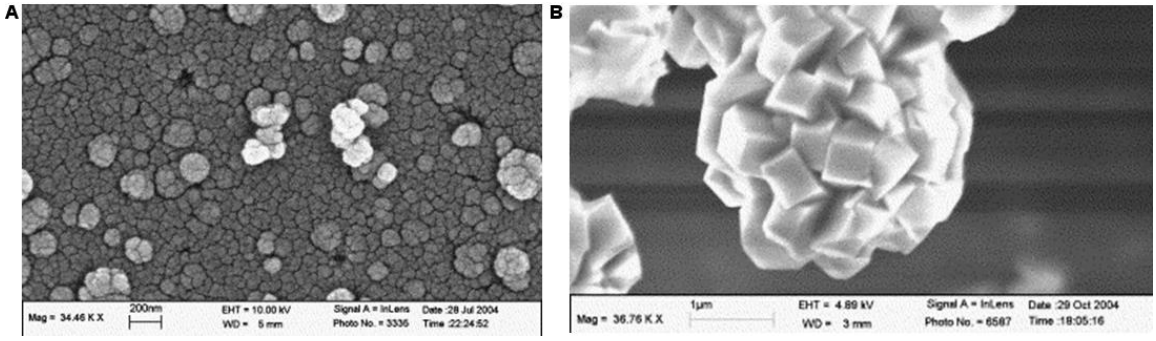

Figure 3-21: PLD coating layer on DAM 1 spheres (A), ~1.0 µm ZSM-5 (MFI) spheres after a 5 day crystallization (B). (Adapted with permission from [89]).

Table 3-3: Summary of deposition approaches

Patterning technique	Substrate	Structure	Form of zeolite	Major applications	Limitations	Ref.
Molecular linkers	Glass	MFI	Pre-formed zeolite crystals	Catalyst, molecular sieves, chemical sensors, optical fibers	Interzeolitic spaces, non-uniform film	[82] [83] [84]
Mechanical aligning	Silicon	LTA, FAU	Zeolite crystals grown hydrothermally	Physical/Chemical/humidity sensors, micromechanical cantilever	-	[85] [93] [94]
Optically	-	LTL	Pre-synthesized crystals	Antenna material, imaging, bio-medical	-	[87] [88] [95]
Pulse-Laser Deposition	Spherical mesoporous DAM-1 /SBA-15	MFI	Protozeolites and hydrothermal	Encapsulation, Catalysis and Drug delivery	Difficult to control thickness of seeded film by ablation	[89] [96] [97] [98] [99] [100]

3.4 Conclusions

The objective of this article was to compare various techniques of patterning zeolites and zeolite-like thin films with micro- to nano-scale features in order to create a variety of usable small- scale devices. Our discussion of the variety of techniques was organized into three main categories: bottom-up approaches, top-down approaches, and deposition approaches. This review serves to provide a convenient means by which to access and analyze the current knowledge regarding zeolites and nano-featured materials.

Optimization of the synthesis parameters has allowed us to consistently achieve zeolite films that are polycrystalline, inter-grown, continuous, and well-adhered to their substrate. However, much still remains to be done to create better patterning techniques that can be widely used for a variety of zeolite film structures, compositions, and orientations before these materials will see consistent application in micro- and nano-scale devices. In particular, the creation of new, simple, less-expensive, and one-step processing methods, will greatly enhance our ability to apply these unique materials to a broader range of applications.

3.5 References

[1] H. Gao, C. Mu, F. Wang, D. Xu, K. Wu, Y. Xie, S. Liu, E. Wang, J. Xu, D. Yu, J. Appl. Phys., 93 (2003) 5602-5605.

[2] Z.R. Dai, Z.W. Pan, Z.L. Wang, Adv. Funct. Mater., 13 (2003) 9-24.

[3] Z. Wang, H. Wang, A. Mitra, L. Huang, Y. Yan, Adv. Mater., 13 (2001) 746-749.

[4] M. Trau, N. Yao, E. Kim, Y. Xia, G. Whitesides, I. Aksay, Nature, 390 (1997) 674-676.

[5] P. Yang, T. Deng, D. Zhao, P. Feng, D. Pine, B.F. Chmelka, G.M. Whitesides, G.D. Stucky, Science, 282 (1998) 2244-2246.

[6] S. Iijima, Nature, 354 (1991) 56-58.

[7] E. Steven, J.G. Park, A. Paravastu, E.B. Lopes, J.S. Brooks, O. Englander, T. Siegrist, P. Kaner, R.G. Alamo, Sci. Technol. Adv. Mater., 12 (2011) 055002.

[8] V. Valtchev, L. Tosheva, Chem. Rev., 113 (2013) 6734-6760.

[9] Y. Xia, P. Yang, Y. Sun, Y. Wu, B. Mayers, B. Gates, Y. Yin, F. Kim, H. Yan, Adv. Mater., 15 (2003) 353-389.

[10] D. Wouters, U.S. Schubert, Angew. Chem. Int. Ed., 43 (2004) 2480-2495.

[11] A.M. Morales, C.M. Lieber, Science, 279 (1998) 208-211.

[12] L. Li, J. Mater. Sci. Lett., 20 (2001) 1459-1461.

[13] M.G. Hale, R. Little, M.A. Salem, J.H. Hedley, B.R. Horrocks, L. Siller, Thin Solid Films, (2012) 7044-7048.

[14] E. Shapira, A. Holtzman, D. Marchak, Y. Selzer, Nano Lett., (2012) 808-812.

[15] A. Holtzman, E. Shapira, Y. Selzer, Nanotechnology, 23 (2012) 495711.

[16] P.G. Globa, S.P. Sidel'nikova, N.I. Tsyntsaru, A.I. Dikusar, Russ. J. Electrochem., 47 (2011) 357-360.

[17] M. Zaarour, B. Dong, I. Naydenova, R. Retoux, S. Mintova, Microporous Mesoporous Mater., 189 (2014) 11-21.

[18] M.E. Davis, Nature, 417 (2002) 813-821.

[19] Y. Zhao, B. Liu, L. Pan, G. Yu, Energy Environ. Sci., 6 (2013) 2856-2870.

[20] F. Keller, M. Hunter, D. Robinson, J. Electrochem. Soc., 100 (1953) 411-419.

[21] G.E. Thompson, R.C. Furneaux, G.C. Wood, J.A. Richardson, J.S. Goode, Nature, 272 (1978) 433-435.

[22] S. Shingubara, J. Nanopart. Res., 5 (2003) 17-30.

[23] K.T. Jung, J.H. Hyun, Y.G. Shul, D.S. Kim, Zeolites, 19 (1997) 161-168.

[24] International Zeolite Association (http://www.iza-online.org/)

[25] M. Pina, R. Mallada, M. Arruebo, M. Urbiztondo, N. Navascués, O. De La Iglesia, J. Santamaria, Microporous Mesoporous Mater., 144 (2011) 19-27.

[26] I. Pellejero, J. Agustí, M.A. Urbiztondo, J. Sesé, M.P. Pina, J. Santamaría, G. Abadal, Sensors Actuators B: Chem., 168 (2012) 74-82.

[27] A.M. McDonnell, D. Beving, A. Wang, W. Chen, Y. Yan, Adv. Funct. Mater., 15 (2005) 336-340.

[28] B.A. Holmberg, S.-J. Hwang, M.E. Davis, Y. Yan, Microporous Mesoporous Mater., 80 (2005) 347-356.

[29] J. Caro, M. Noack, P. Kölsch, R. Schäfer, Microporous Mesoporous Mater., 38 (2000) 3-24.

[30] Y.S.S. Wan, J.L.H. Chau, A. Gavriilidis, K.L. Yeung, Microporous Mesoporous Mater., 42 (2001) 157-175.

[31] G. Meindersma, A. De Haan, Desalination, 149 (2002) 29-34.

[32] J.D. Rimer, J.M. Fedeyko, D.G. Vlachos, R.F. Lobo, Chem. Eur. J., 12 (2006) 2926-2934.

[33] B.J. Schoeman, O. Regev, Zeolites, 17 (1996) 447-456.

[34] B.J. Schoeman, Microporous Mater., 9 (1997) 267-271.

[35] Y. Haruvy, S. Webber, Chem. Mater., 3 (1991) 501-507.

[36] Y. Haruvy, S.E. Webber, Fast sol-gel preparation of glasses, US Patent No. 5272240 A.

[37] M.E. Davis, R.F. Lobo, Chem. Mater., 4 (1992) 756-768.

[38] M.E. Davis, A. Katz, W.R. Ahmad, Chem. Mater., 8 (1996) 1820-1839.

[39] R. Szostak, Molecular sieves, Springer1998.

[40] Y.S.S. Wan, J.L.H. Chau, K.L. Yeung, A. Gavriilidis, J. Catal., 223 (2004) 241-249.

[41] Z. Wang, H. Wang, A. Mitra, L. Huang, Y. Yan, Adv. Mater., 13 (2001) 746-749.

[42] Z. Wang, Y. Yan, Microporous Mesoporous Mater., 48 (2001) 229-238.

[43] S.C. Jacobson, R. Hergenroder, L.B. Koutny, R.J. Warmack, J.M. Ramsey, Anal. Chem., 66 (1994) 1107-1113.

[44] S.C. Jacobson, R. Hergenroder, L.B. Koutny, J.M. Ramsey, Anal. Chem., 66 (1994) 1114-1118.

[45] S. Fan, M.G. Chapline, N.R. Franklin, T.W. Tombler, A.M. Cassell, H. Dai, Science, 283 (1999) 512-514.

[46] C. Burda, X. Chen, R. Narayanan, M.A. El-Sayed, Chem. Rev., 105 (2005) 1025-1102.

[47] H.F. Winters, J.W. Coburn, Appl. Phys. Lett., 34 (1979) 70-73.

[48] J.W. Coburn, H.F. Winters, J. Appl. Phys., 50 (1979) 3189-3196.

[49] Y. Xia, X.-M. Zhao, G.M. Whitesides, Microelectron. Eng., 32 (1996) 255-268.

[50] M. Kahl, E. Voges, S. Kostrewa, C. Viets, W. Hill, Sensors Actuators B: Chem., 51 (1998) 285-291.

[51] H. Lehr, W. Ehrfeld, J. Phys. IV, 4 (1994) C9-229-C229-236.

[52] W. Ehrfeld, V. Hessel, H. Löwe, C. Schulz, L. Weber, Microsys. Technol., 5 (1999) 105-112.

[53] S. Johansson, J.A. Schweitz, H. Westberg, M. Boman, J. Appl. Phys., 72 (1992) 5956-5963.

[54] J. Arnold, U. Dasbach, W. Ehrfeld, K. Hesch, H. Löwe, Appl. Surf. Sci., 86 (1995) 251-258.

[55] R.D. Piner, J. Zhu, F. Xu, S. Hong, C.A. Mirkin, Science, 283 (1999) 661-663.

[56] J.L.H. Chau, Y.S.S. Wan, A. Gavriilidis, K.L. Yeung, Chem. Eng. J., 88 (2002) 187.

[57] S.K. Kirdeciler, C. Ozen, B. Akata, Microporous Mesoporous Mater., 191 (2014) 59-66.

[58] J.C. Jansen, J.H. Koegler, H. van Bekkum, H.P.A. Calis, C.M. van den Bleek, F. Kapteijn, J.A. Moulijn, E.R. Geus, N. van der Puil, Microporous Mesoporous Mater., 21 (1998) 213-226.

[59] O. de la Iglesia, V. Sebastián, R. Mallada, G. Nikolaidis, J. Coronas, G. Kolb, R. Zapf, V. Hessel, J. Santamaría, Catal. Today, 125 (2007) 2-10.

[60] J. Coronas, J. Santamaria, Chem. Eng. Sci., 59 (2004) 4879-4885.

[61] E. Mateo, R. Lahoz, G.F. de la Fuente, A. Paniagua, J. Coronas, J. Santamaría, Chem. Mater., 16 (2004) 4847-4850.

[62] S. Matsui, Y. Ochiai, Nanotechnology, 7 (1996) 247-258.

[63] S. Hong, J. Zhu, C.A. Mirkin, Science, 286 (1999) 523-525.

[64] J.A. Dagata, Science, 270 (1995) 1625.

[65] P.N. Dunn, Solid State Technol., 37 (1994).

[66] M. Levenson, Solid State Technol., (1994).

[67] A. Rodriguez, D. Molinero, E. Valera, T. Trifonov, L. Marsal, J. Pallares, R. Alcubilla, Sensors Actuators B: Chem., 109 (2005) 135-140.

[68] J. Jansen, D. Kashchiev, A. Erdem-Senatalar, Stud. Surf. Sci. Catal., 85 (1994) 215-250.

[69] R.B. Wehrspohn, J. Schilling, Physica Stat. Sol. A, 197 (2003) 673-687.

[70] V. Lehmann, R. Stengl, H. Reisinger, R. Detemple, W. Theiss, Appl. Phys. Lett., 78 (2001) 589-591.

[71] C.A. Betty, R. Lal, D.K. Sharma, J.V. Yakhmi, J.P. Mittal, Sensors Actuators B: Chem., 97 (2004) 334-343.

[72] A. Kurowski, J.W. Schultze, H. Lüth, M.J. Schöning, Sensors Actuators B: Chem., 83 (2002) 123-128.

[73] M.A. Urbiztondo, E. Valera, T. Trifonov, R. Alcubilla, S. Irusta, M.P. Pina, A. Rodríguez, J. Santamaría, J. Catal., 250 (2007) 190-194.

[74] V. Lehmann, U. Grüning, Thin Solid Films, 297 (1997) 13-17.

[75] L. Huang, Z. Wang, J. Sun, L. Miao, Q. Li, Y. Yan, D. Zhao, J. Am. Chem. Soc., 122 (2000) 3530-3531.

[76] K. Ha, Y.-J. Lee, Y.S. Chun, Y.S. Park, G.S. Lee, K.B. Yoon, Adv. Mater., 13 (2001) 594-596.

[77] K. Ha, Y.-J. Lee, D.-Y. Jung, J.H. Lee, K.B. Yoon, Adv. Mater., 12 (2000) 1614-1617.

[78] S. Li, C. Demmelmaier, M. Itkis, Z. Liu, R.C. Haddon, Y. Yan, Chem. Mater., 15 (2003) 2687-2689.

[79] I. Pellejero, M. Urbiztondo, M. Villarroya, J. Sesé, M.P. Pina, J. Santamaría, Microporous Mesoporous Mater., 114 (2008) 110-120.

[80] J.L.H. Chau, K.L. Yeung, Chem. Comm., (2002) 960-961.

[81] M. Madou, Fundam. Microfab., CRC Press, New York, 1997.

[82] A. Kulak, Y.-J. Lee, Y.S. Park, H.S. Kim, G.S. Lee, K.B. Yoon, Adv. Mater., 14 (2002) 526.

[83] J.R. Agger, N. Pervaiz, A.K. Cheetham, M.W. Anderson, J. Am. Chem. Soc., 120 (1998) 10754-10759.

[84] A. Kulak, Y.S. Park, Y.-J. Lee, Y.S. Chun, K. Ha, K.B. Yoon, J. Am. Chem. Soc., 122 (2000) 9308-9309.

[85] L. Scandella, G. Binder, T. Mezzacasa, J. Gobrecht, R. Berger, H. Lang, C. Gerber, J. Gimzewski, J. Koegler, J. Jansen, Microporous Mesoporous Mater., 21 (1998) 403-409.

[86] G. Calzaferri, A. Devaux, V. Ramamurthy, Y. Inoue, Manipulation of Energy Transfer Processes within the Channels of L-Zeolite, John Wiley & Sons, Hoboken, NJ2011.

[87] M. Woerdemann, C. Alpmann, F. Hörner, A. Devaux, L. De Cola, C. Denz, SPIE Proc. (2010) 77622E-77622E.

[88] M. Woerdemann, S. Gläsener, F. Hörner, A. Devaux, L. De Cola, C. Denz, Adv. Mater., 22 (2010) 4176-4179.

[89] C. Xiong, D. Coutinho, K.J. Balkus Jr, Microporous Mesoporous Mater., 86 (2005) 14-22.

[90] K.J. Balkus Jr, M.E. Kinsel, A.S. Scott, Method of coating three dimensional objects with molecular sieves, Google Patents2002.

[91] E.V. Rebrov, G.B.F. Seijger, H.P.A. Calis, M.H.J.M. de Croon, C.M. van den Bleek, J.C. Schouten, Appl. Catal., A, 206 (2001) 125-143.

[92] V. Lehmann, H. Foell, J. Electrochem. Soc., 137 (1990) 653-659.

[93] L. Scandella, G. Binder, J. Gobrecht, J.C. Jansen, Adv. Mater., 8 (1996) 137-139.

[94] G. Binder, L. Scandella, J. Kritzenberger, J. Gobrecht, J.H. Koegler, R. Prins, J. Phys. Chem. B, 101 (1997) 483-490.

[95] M. Veiga-Gutiérrez, M. Woerdemann, E. Prasetyanto, C. Denz, L. De Cola, Adv. Mater., 24 (2012) 5199-5204.

[96] A. Dong, Y. Wang, D. Wang, W. Yang, Y. Zhang, N. Ren, Z. Gao, Y. Tang, Microporous Mesoporous Mater., 64 (2003) 69-81.

[97] K.J. Balkus Jr, A.S. Scott, M.E. Gimon-Kinsel, J.H. Blanco, Microporous Mesoporous Mater., 38 (2000) 97-105.

[98] K.J. Balkus Jr, G. Gbery, Z. Deng, Microporous Mesoporous Mater., 52 (2002) 141-150.

[99] Z. Deng, K.J. Balkus Jr, Microporous Mesoporous Mater., 56 (2002) 47-53.

[100] K.J. Balkus Jr., E.M. Kinsel, S.A. Scott, US Patent No. 6,423,411

Chapter 4: Patterning Silicalite-1 Films using Carbon Dioxide Laser Ablation

Abstract

Nanostructured materials represent an intriguing foundation on which to build new devices for applications in electronics, photonics, energy storage, and biological/chemical analysis. For example, porous, nanostructured materials, such as pure-silica zeolite films, have been used to form 2D and 3D structures for building intricate micro-scale assemblies for light-harvesting, sensing, and microreactor applications. The standard methods used to pattern such devices and features from nanostructured materials are based on either typical microfabrication techniques, which involve either several complex and time-consuming steps, and can result in pore clogging, or the organization of pre-formed seeds/crystals uniformly arranged on the substrate by chemical or physical linkages, which requires precise control and positioning. Here, we present a simple, flexible alternative to both techniques: CO_2 laser ablation. We demonstrate the effects of this technique on a model zeolite thin film system, pure-silica MFI (silicalite-1), to evaluate its potential for patterning complex, multicrystalline, nanostructured materials. We use SEM and XRD to determine the crystallinity, film thickness, surface coverage, crystal size, and crystal habit of the films pre- and post- patterning. Using this technique, we demonstrate that it is possible to make 3D structures in these films, such as channels of varying width (82-611.98 μm), depth (2.58-7.13 μm), separation distance (minimum 25 μm), and edge effects, by varying laser

power, spot size, and raster speed. This work introduces a one-step, rapid technique to pattern materials with specific framework structures and subnanometer pore sizes, thus broadening their potential usage in areas that require patterned, micro-scale features.

4.1 Introduction

Zeolites and zeolite-like materials have been widely used for gas separation and catalysis due to their unique, three-dimensional, nano-porous, crystalline structure. This structure is enhanced by their ability to host different ions, atoms, molecules and clusters within their channels and cages [1-5]. Increasingly, these nanostructured materials are being suggested as material systems from which small-scale devices, such as microreactors, micro-scale membrane separators, or components for electrical or optical devices, may be fabricated [6-9]. These applications rely on the production of well-controlled zeolite thin films or coatings that are patterned either pre- or post-synthesis to yield an appropriately scaled component or device of interest [10-13].

Based on specific application of zeolite films or membranes, the optimum/desired quality and thickness of the final film may vary [14]. Fortuitously, there has been a concomitant advancement in our ability to control the crystal orientation, composition, properties, morphology and film or membrane thickness of zeolite thin films or coatings. Pre-synthesized zeolite crystals have been used to form closely-packed layers consisting of mono-grains of zeolite for obtaining specific functionality, and to further form oriented and mono-directional microporous materials [14-17]. Assembled monolayers of zeolites have been made using various types of linkages, such as covalent, ionic, and physical linkages, as well as hydrogen-bonding and micro-contact printing. This has led to the preparation of dense assemblies of zeolite crystals in the nanometer to micrometer crystal size regime with different types of zeolite crystals and on different substrates [15, 18-27]. Furthermore, 2D and 3D structures of zeolites with varied geometrical complexity also

have been made using techniques like holographic optical tweezers (HOT) and combination of HOT, microfluidics and colloidal interactions [21, 28, 29].

Lastly, zeolites have been synthesized, via *in situ* or *ex situ* crystallization, in the form of free standing films as well as films on planar surfaces, spheres, and fibers [30-32]. The advantage of using in situ crystallization technique for synthesis of zeolite films is that it is a one-step method, involving direct crystallization of the aligned zeolite crystals on the substrate forming monolayer transformed into intergrown, continuous films under hydrothermal conditions [33]. This provides the additional benefit of having excellent adhesion of the crystals with the substrate, alleviating the need to prepare seeds. It is well-understood that using zeolite crystals to create dense and controlled monolayer with unidirectional channels is dependent on the ability to make nanocrystals with narrow size-distribution [16]. This technique acts as a straightforward method to form high quality monolayer on different substrates. It is unsurprising, then, that zeolite films have been prepared on several substrate families, including metals or metal oxides, like silicon wafers, polished or fused quartz, porous alpha-alumina, and zirconia plates, among others [8, 24, 34-36].

Historically, the pre- or post-synthetic, one- and two-dimensional patterning of features onto material surfaces has been carried out via lithographic techniques borrowed from the semiconductor industry, such as e-beam lithography, focused-ion beam lithography, proximal-probe patterning, X-ray and extreme-UV ablation, micromolding and self–assembly [7, 10, 33, 37-41]. However, their cost, material specificity, throughput requirements, and limited-scale production have limited their wide-spread

adoption to new materials, particularly porous, nanostructured materials. Thus, despite improvements in both synthetic techniques and patterning techniques, patterning large-to-small scale features into nanostructured, porous films, like zeolites and other materials, remains challenging. Moreover, each technique tends to have a limited range of patterning effects, such as size range or edge effects that can be produced for a given material system. This has limited the development and application of porous, nanostructured materials in micro- and nano-scale devices. In order to fully utilize these materials, patterning techniques that are simple, flexible, inexpensive, and broadly applicable to many types of porous, nanostructured materials must be created. To successfully pattern features onto porous, nanostructured materials, these techniques must (1) minimize pore-clogging from deposition of other materials onto the surface, (2) allow the retention of the surrounding materials' porous network and crystallinity, (3) be compatible with potentially high roughness, polycrystalline film materials, (4) be able to pattern at multiple length scales, and (5) be able to selectively "tune" the feature effects, such as edge shape, whether in an x-y plane or in terms of patterning depth. Preferably it should also be a one-step process, without the need for masking or the deposition of a sacrificial patterning material (e.g. photoresist). Although many options are available that meet one or two of the stated constraints, few meet all five [37-40, 42-44]. Of these few, laser patterning, i.e. making patterns or features using laser ablation, represents an intriguing solution to the challenge of patterning porous, nanostructured materials.

Laser ablation has been used for micromachining or etching silicon for over two decades [45, 46]. This technique creates 3D patterns, and has the advantage of being a

direct writing, one-step method with a resolution limit comparable to other multi-step techniques e.g. projection printing or photolithography [47, 48]. Previously, laser ablation via CO_2, Nd:YAG, and Ar^+ lasers has been used to make micro-holes and other patterns in metals, glass, or silicon substrates, and has been used for the heating and densification of coatings of TiO_2, SiO_2, TiO_2-SiO_2, Ta_2O_5 and WO_3 [49-53]. The structural and physical effects of laser densification have been studied on tetraethylorthosilicate (TEOS) coatings (dry, porous films with thicknesses in the range of 200-250 nm) on fused silica substrates as sol-gel films where pattern widths of 100-150 μm were obtained using a 1.06 μm line from Nd:YAG laser in indirect-writing mode. Moreover, the damage caused to dielectric coatings/films by laser ablation has also been studied, and it was shown that the resulting laser irradiated regions developed altered optical properties that could be used for storage and device purposes [54].

Of the aforementioned laser ablation techniques available, CO_2 laser ablation is the most widely used. This technique has been used for various aspects of silicon-based device creation for optical communications, optical fiber-based sensing [55], frequency metrology, and optical coherence tomography [56, 57]. CO_2 laser ablation processes typically involve heating the material of interest to the point that the material softens. Due to its point-to-point ablating abilities, intricate and complicated profiles can also be without the need for expensive masks. For instance, CO_2 lasers have been used to achieve variation in the refractive index of photonic crystal fibers by creating long period gratings via the local release of mechanical stress in the fiber when the fiber is irradiated and the temperature of the exposed regions exceeds the glass-transition temperature of the

material [58-60]. CO_2 laser processing of sol-gel films has been studied for various applications in optics, including electro-chromic films, channels and slab-waveguides [49, 51, 61, 62]. Widespread application of patterned sol-gel films, as optical interconnects, channel waveguides, optical switches, etc. has propelled our study towards the use of CO_2 laser ablation in patterning zeolite and zeolite-like materials. We hypothesize that this could be a simple, flexible, cost-effective, one-step, maskless, and fast process, in comparison to current lithographic techniques.

In order to determine if CO_2 laser ablation on zeolite films could meet the aforementioned patterning requirements, we determine if simple channels or lines, which are commonly fabricated features in optical applications of sol-gel films, could be created via a CO_2 laser-based, serial writing process. In this paper, we explore the idea of creating features in pure-silica zeolite MFI (otherwise known as silicalite-1) films using CO_2 laser ablation as a primary 3D micropatterning tool, analogous to a 2D e-beam lithography machine or projection printing. The fabrication process is based on the heating effect (thermal shock) of focused, high-frequency (100 Hz), continuous CO_2 laser irradiation. The reasoning behind the use of a high-frequency laser, as compared to a low-frequency CO_2 laser, is that the higher frequency provides a higher fluence/laser energy density to the surface of the films, which in turn cause greater release of the internal stress of the film, thus making it a more effective serial writing technique [59]. Therefore, using thin films of the well-understood, pure-silica zeolite MFI (silicalite-1) as a proof of concept zeolite material, we examine the effects of film thickness, laser power and exposure length on the patternability of these films. The rough, polycrystalline films are

characterized pre- and post- patterning to determine the impact of the method on their composition and crystallinity.

4.2 Experimental

4.2.1 Synthesis of Pure-Silica (MFI) Films

Silicon wafers (100) (University Wafers, 0.008-0.02 Ω-cm, 600-700 μm thick) were used for *in situ* synthesis of pure-silica (MFI) films. They were first washed using Piranha Solution [volume ratio; 1Hydrogen Peroxide (H_2O_2, 40 wt%): 4Sulphuric Acid (H_2SO_4, 98 wt%)] and drying under N_2. The reaction gel was prepared by first mixing DI H_2O and Tetrapropylammonium Hydroxide (1.0 M in H_2O, TPAOH, Aldrich) in a plastic container, followed by slowly adding Tetraethylorthosilicate (98%, TEOS, Aldrich) while stirring. Two different molar ratios of the reaction gel were used- 99.0H_2O: 0.14TPAOH: 0.84TEOS (Scheme 1) and 165H_2O: 0.32TPAOH: TEOS (Scheme 2). The mixture was aged for 1 h under stirring at room temperature. The two different gel composition used in this work provided different aspect ratios of the silicalite-1 crystals that formed the film **(Figure 4-3)**. The synthesis solution was then charged into 23 ml Teflon-lined Parr autoclaves with silicon substrates placed either horizontally or slightly slanted in the liners, with their polished surface facing upwards. Crystallization was carried out at 165 ^oC for times ranging from 2 to 19 h. At the end of crystallization, the samples were recovered and washed with DI water and air dried. The films were then calcined in air at 400 ^oC for 4 h at a 0.5 ^oC/min ramp rate.

4.2.2 CO_2 Laser Patterning

The CO_2 laser used (SYNRAD, USA) has average power output ~29.31 W (calculated over 5 minutes, 30 seconds warm up at 30 V), power stability ± 4.14%, peak power 40.80 W (measured with a 100 Hz, gating signal with 10% positive duty cycle), and respective rise and fall times of 86 and 88 μs (measured at 1000 Hz at 50% duty cycle). A ZeSe plano-convex focusing lens with a 5 in focal length was used to focus the emitted laser beam (diameter ~3.5 mm, divergence 4.0 mR). A ZnSe beam combiner with 1 in diameter for 10.6 μm wavelength laser, optimized for 0.633 μm was used to combine the beam with the light source coming from an optical microscope, which was used to view the surface. The power of the laser was controlled using a controller (Intelligent PC control), which acts by modulating the RF drive circuit that excites the plasma tube that causes the lasing at power density of 8.8 W/cu-in (PS-2 DC Power Supply-Emersion iMP4-3S0-00-A). The sample was held using an XYZ stage, fixed for translational movement in one direction only during experiments, which was controlled using a DC-motor (2-phase stepper) stage with 25 mm travel-stepper actuator with ¼ in-80 threads, lead screw pitch 0.5 mm **(Figure 4-1)**. Patterns are created by moving the samples past a stationary beam i.e. horizontally and vertically with respect to the laser beam using a motorized actuator (Thorlabs Inc. ZST series). **Table 4-1** summarizes the different parameters evaluated in this work to create features on silicalite-1 films.

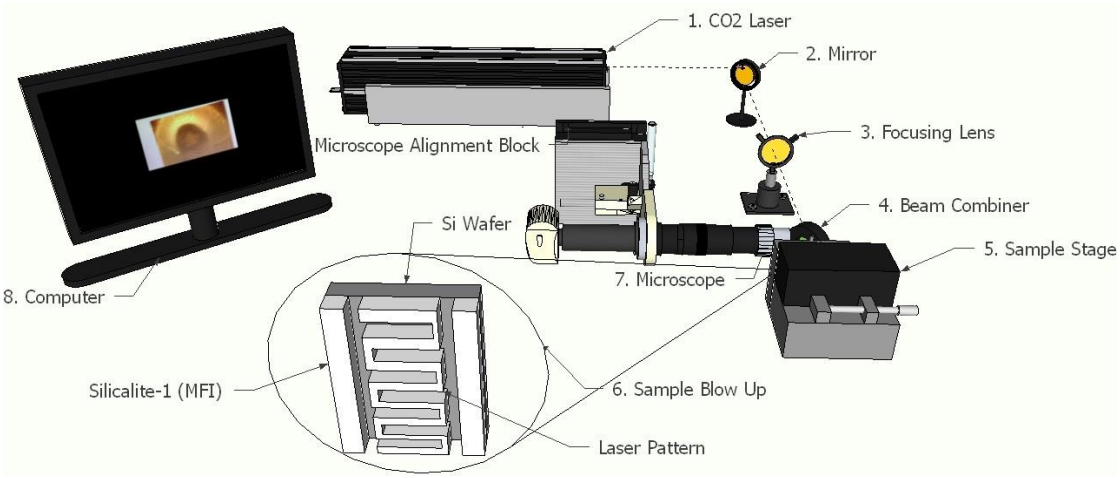

Figure 4-1: Experimental set-up for CO_2 laser irradiation used in the experiments described. The set-up shown here includes a CO_2 laser (Synrad model, 30W) with a lens that focusses the beam to a diameter 13.49 μm (Gaussian focal spot) and a CCD camera attached at 90^o to the plane of the sample to capture the image, which is displayed on the monitor of a computer.

Table 4-1: Summary of different parameters used for making patterns on silicalite-1 films.

Experimental parameter	Parameter values
CO_2 laser power (%)	5, 10, 12, 15, 20, 25, 30, 35
Film thickness (μm)	0.25, 1.2, 2.2, 3, 5, 7.5, 8, 10, ~24
Translation rate (mm/s)	0.5, 1
Time (s)	20, 30
Repetitions	Single/double scan at each power on each film thickness

4.2.3 Characterization

All characterization was done pre- and post-ablation. Surface characterization of the samples was accomplished using both Optical Microscopy and Scanning Electron Microscopy (SEM) (Hitachi S4700). Compositional analysis was accomplished via Energy Dispersive Spectroscopy (EDS) with an FEI Quanta 600 Field Emission Gun, Extended Vacuum to confirm removal, after calcinations, of the organic template also known as the structure directing agent (SDA). X-ray Diffraction (XRD) (Rigaku, 40 kV, 44 mA, 5-50 ^{o}, step size-0.02, 2 ^{o}/min) was used to determine the crystallinity and orientation of the as-made, calcined, and patterned samples. FTIR (Thermo Electron Corporation, Nicolet 4700) was used to confirm the integrity of the patterned films and their compositional stability. The widths and depths of the engraved channels were measured using SEM images (top view and cross-sectional) and optical microscope images (top view and cross-sectional) at 3/5 different points along the length of the channel. The depths of the channels were also confirmed using a step profilometer (Alpha-Step-200, Tencor Instruments).

4.3 Results and Discussion

4.3.1 As-Prepared Film Characteristics

XRD plots of hydrothermally grown, silicalite-1 (MFI) films on silicon (100) substrates were first obtained to confirm the framework structure, degree of crystallinity, and crystal orientation of the as-made films. The XRD plots confirmed the formation of

silicalite-1 (MFI) films with different crystal orientations (typical plots shown in **Figure 4-2**): randomly-oriented and *b*-oriented. XRD plots of the films were also obtained on samples irradiated with the CO_2 laser (at 10, 15, 20 % power) by rastering an area of 1 cm^2 (1 mm/s translation rate) across the surfaces of films of various thicknesses **(Table 4-1)**. This was done to ensure that the film structure remained intact and there was no structure collapse post-irradiation. The XRD plot **(Figure 4-2)** is a representation of the different films, crystal orientation and irradiated laser power on as-made and patterned silicalite-1 films. For the irradiated films, the local high temperatures, caused by laser exposure, extends from the center of the laser spot to ~1400 μm diameter, and 150 μm depth (much greater than the actual thickness of the films used) with the greatest impact extending to ~300 μm diameter and ~10 μm depth [63]. This suggests that the XRD patterns of the irradiated films arise from the exposed regions and not from any underlying, unexposed crystals. Hence, although the laser ablation can create areas of densification, as discussed later, it is clear from this initial analysis that at low powers (< 20%) where densification does not occur, the crystal structure of the film remains intact. In some cases, shown later in this work, it is possible to create much localized densification around the incident laser spot during complete removal of the film from the surface; however, the surrounding crystal structure remains intact. FTIR spectrum of the laser irradiated films also confirmed the integrity of the silica framework for the MFI type zeolites **(Figure 4-3)**.

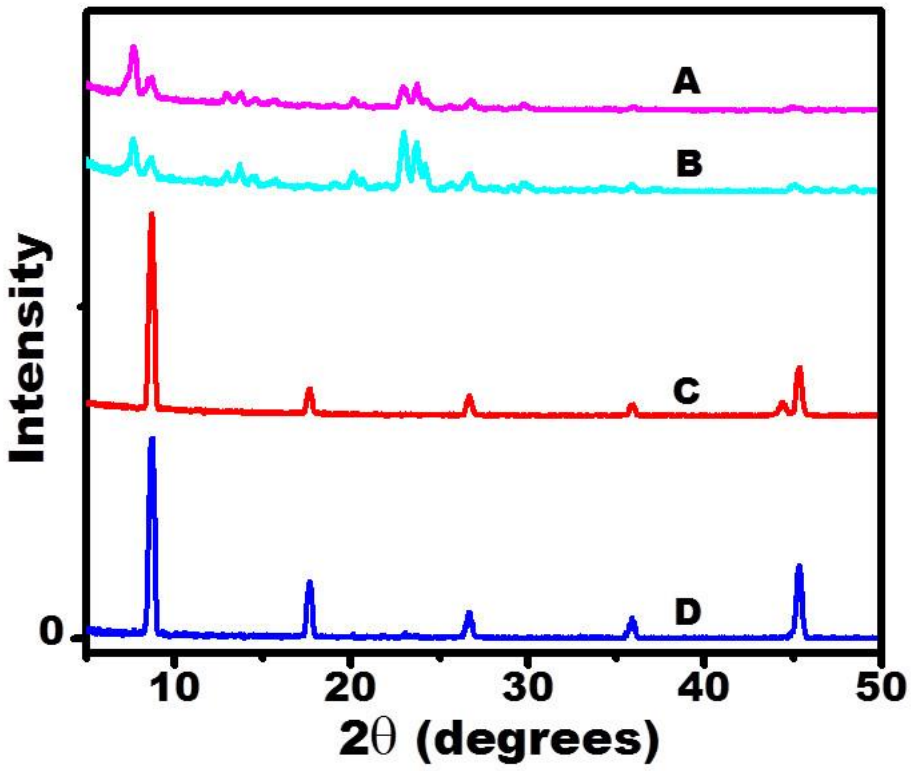

Figure 4-2: Representative X-ray diffraction patterns of silicalite-1 (MFI) (A, B) randomly-oriented films after and before patterning, respectively, and (C, D) b-oriented films after and before patterning, respectively, for laser powers less than or equal to 20%.

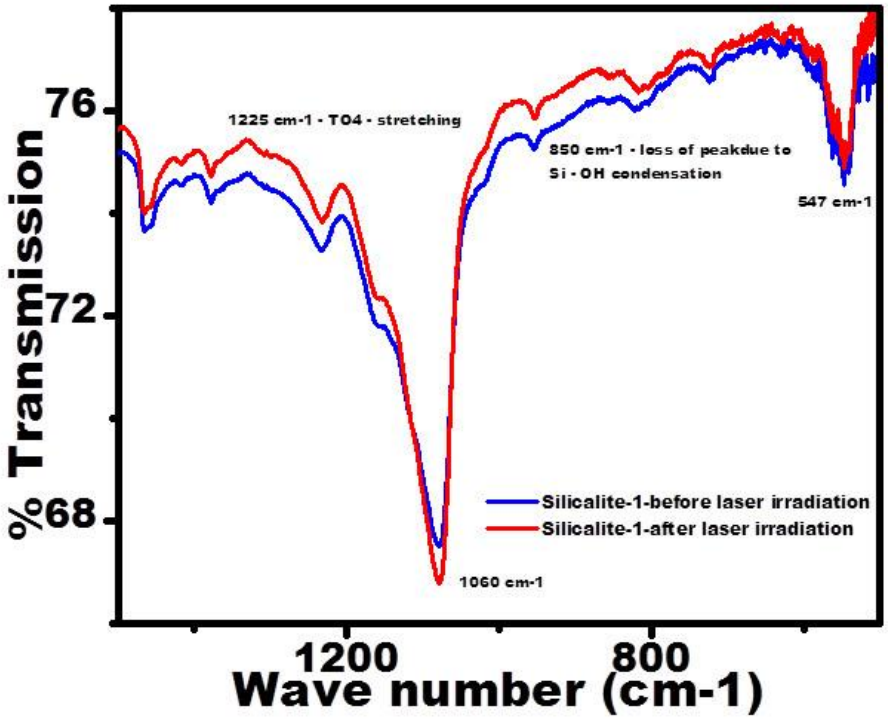

Figure 4-3: FTIR on the laser irradiated samples show that the peak at 547 cm-1 for the pentasil group in the MFI framework remains intact for films where no complete densification is seen. The plot below shows that the FTIR spectrums of the silicalite-1 films before and after laser irradiation are similar. Hence, the combination of XRD and FTIR show good support for the structure remaining intact (section 4. 3.1).

SEM micrographs of the as-made films confirmed that they were polycrystalline and inter-grown **(Figure 4-4)**. This is crucial for the purposes of our study, because a non-inter-grown film will create additional sources of energy loss into the Si (100) substrate, which has high thermal conductivity (1.3 W $cm^{-1}°C^{-1}$). This would result in the inability to create precise channels in the film and a lack of repeatability in the resulting patterns. **Figure 4-4** shows the morphology of the films and their crystal orientations. By using two different reaction gel compositions **(section 4.2.1)**, crystals with different aspect ratios (film orientations) were obtained **(Figure 4-4A, B)**. **Figure 4-4C, D** shows the SEM micrographs of the cross-sectional images of films with thicknesses ranging from 0.25-3 μm prepared to perform the patterning study (**Table 4-1** lists all the film thickness values used in this study). EDS analysis, carried out prior to patterning, confirms the complete removal of the SDA and the opening of the micropores at the end of calcination, depicted by absence of carbon atoms in the calcined films as compared to the as-made films **(Table 4-2)**. Patterning of the silicalite-1 films were carried out in calcined films as compared to as-made films since the heat created and conducted through the films during laser ablation causes burning/charring of the organic SDA (TPAOH) thus depositing carbon in the features and adjoining film.

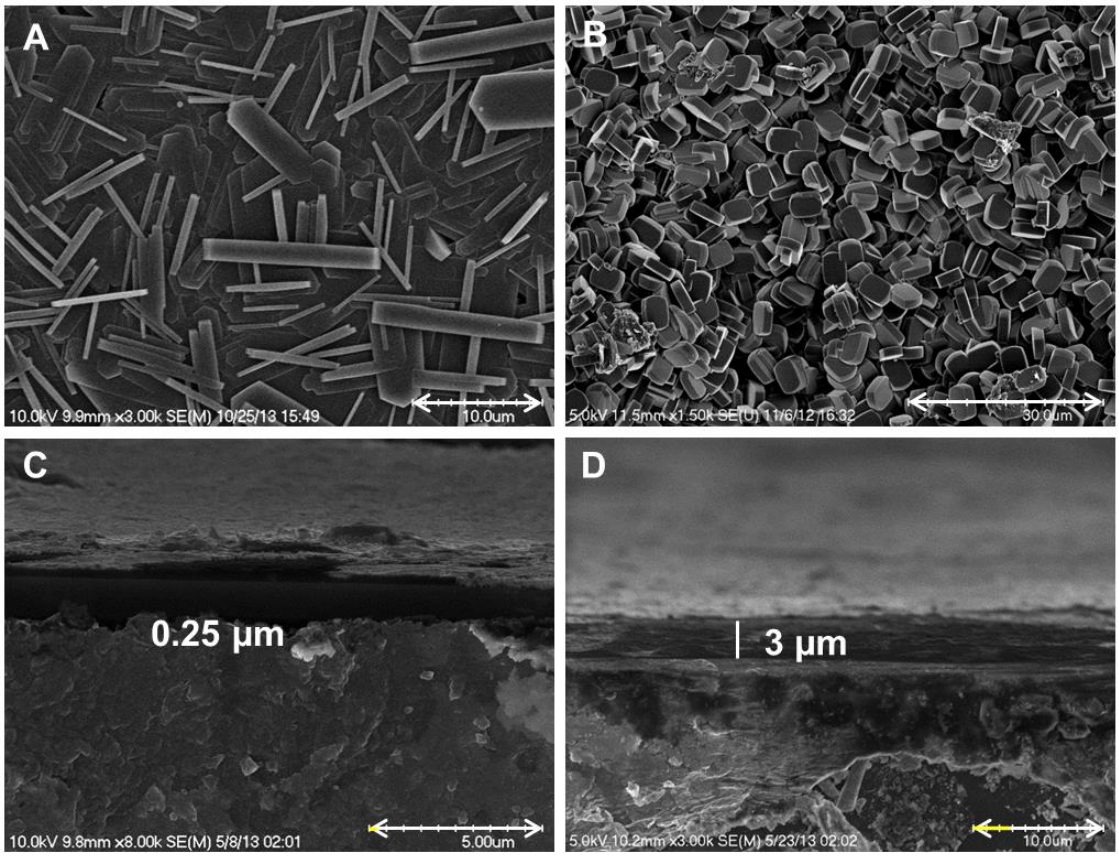

Figure 4-4: The SEM images of the pre-patterned films were taken to confirm that they are intergrown and with desirable crystal orientation (A) *b*-oriented films formed by following Scheme 2; (B) randomly-oriented crystals on films formed by following Scheme 1; (C) 0.25 µm thick film did not show any marked pattern formation; however, patterning study was carried out using films with thicknesses D and higher.

Table 4-2: Energy dispersive spectrometry (EDS) data of the zeolite MFI films on (100) Si demonstrates that the film is pure-silica, with the carbon content appearing due to the SDA in the precursor gel. EDS data for the thermally calcined sample indicates that the carbon content has been completely removed and the pore space has been successfully opened after calcination, thus leaving nanopores in the zeolite structures (Section 4.3.1). Note that the samples were coated with Pt for SEM imaging.

	As-made Films				**Calcined Films**		
	Si	O	C	Pt	Si	O	Pt
Wt.%	35.33	37.42	20.58	6.67	45.11	9.63	45.26
Wt. % σ	0.68	0.75	1.71	0.77	0.71	0.68	2.47
At. %	48.69	34.67	15.74	0.91	65.82	24.67	9.51

4.3.2 Impact of Film Thickness on Production of Patterns

In previous reports, excimer lasers have been used in conjunction with bulk materials (defined as materials whose thicknesses were much greater than the depth of ablation that can occur per laser pulse) [54]. With thin films (defined as materials whose thicknesses are < 1 μm), the process of ablation is different than that for bulk materials, owing to differences in the extent of heat conducted, the effects of the underlying substrate, the propagation of the thermal shock wave, etc. [54, 64-68]. Moreover, the ways in which the rates of heating and cooling act to create patterns in sol-gel films, and their resulting morphology, with regard to the diffusion of heat through the film upon laser irradiation has been studied [62]. These studies showed that the diffusion of the irradiated heat used to create defined patterns or regions of densification is determined primarily by the film thickness (quality, degree of intergrowth, etc.) and is not affected by the differences in heat diffusion/thermal properties caused by differences in crystal sizes. Following a similar trend, we have also used films of different thickness (by changing the crystallization times) and studied the nature of patterns created (depth, roughness, ridge formation etc.) in response to changes in films thickness and laser operating parameters (laser power, spot size, diffraction properties, and translation rate). It has been seen that for absorptive films, relatively thicker films (> 1 μm) are required in order to form arrays of visible patterns or densification [29]. Similarly, we observed that *b*-oriented silicalite-1 (MFI) films with thicknesses in the range of ~200-500 nm produced no visible, well-defined patterns or film densification upon irradiation, possibly due to absorption of the laser-induced film heating by the substrate, which acts as a heat sink, as well as the small fraction of the irradiated energy being absorbed by the material itself and not the

substrate. **Figure 4-4** is a representation of the film thicknesses prepared to validate the observations of the study.

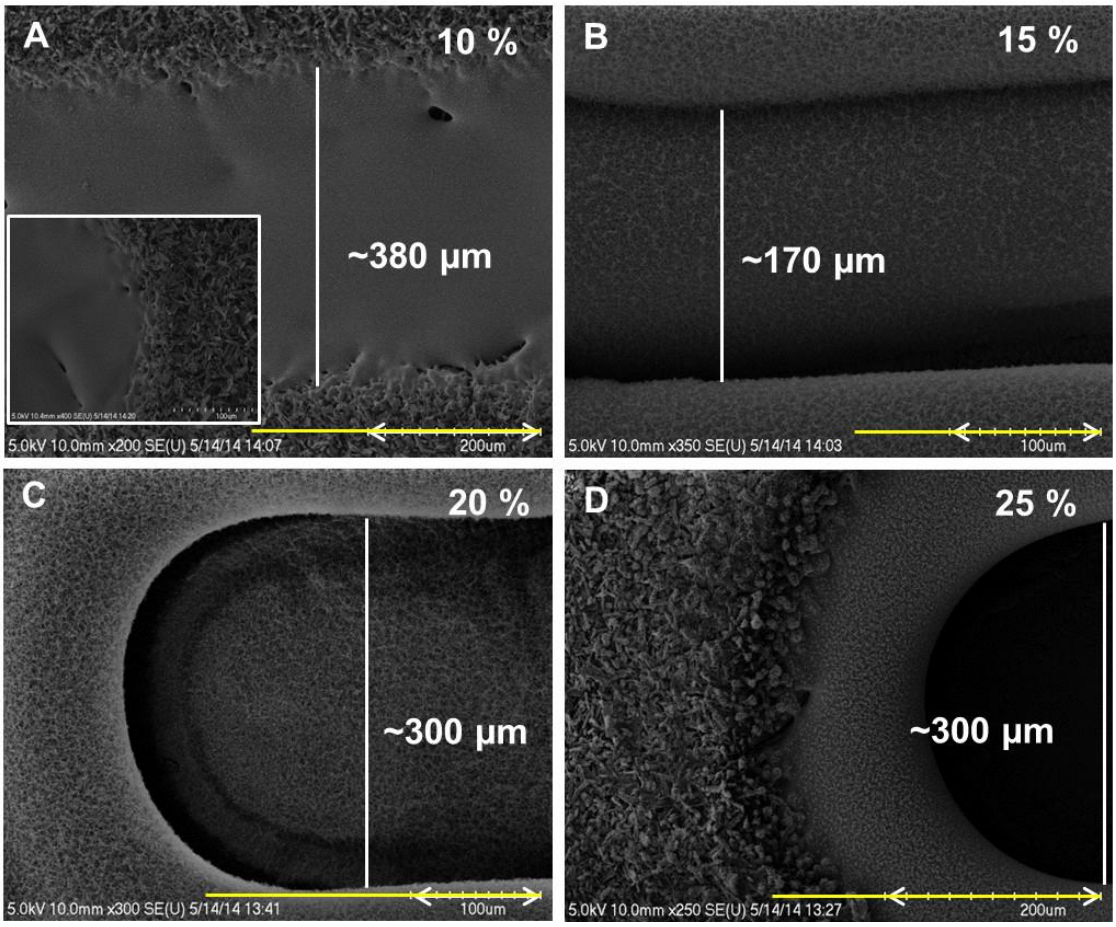

Figure 4-5: Patterns formed on silicalite-1 films on Si (100) at different laser powers (A) 10% (the inset showing clear distinction between the densified region and intact crystals); (B) 15%; (C) 20% and (D) 25%, shows increase in channel width and film removal however, decrease in edge roughness with increase in laser power. (Film thickness ~5 µm, randomly-oriented crystals, translation rate 1 mm/s, time 30 s).

4.3.3 Impact of Laser Properties on Patterning Characteristics and Pattern Morphology

4.3.3.1 Diffraction-Limited Spot Size

The direct-writing mode used here for making patterns, though having the advantage of being simple and not requiring an over-layer, unlike the indirect-heating method; has the disadvantage of reducing the preciseness of the features, thus limiting the details according to the spot size of the laser beam (its diffraction-limited spot size). Along with the constraints provided by the laser spot size, the minimum feature size/line width is further affected / broadened owing to lateral diffusion and dissipation of heat through the films, which is again determined by the properties of the film (specific heat, conductivity, thickness, etc.). The diffraction-limited spot size ($2\omega_o$ = 13.497 μm) can be obtained using **equation 4.1**, and the laser parameters included in the experimental section.

$$\omega_{\circ} = \frac{2f\lambda}{\pi a} \qquad \textbf{4.1}$$

The resolution of the ablated patterns and their boundaries can be improved by employing objectives with high NA (numerical aperture) for focusing thus reducing the spot size; however, this increases the power density and resolution.

4.3.3.2 Laser Energy/Power

In order to obtain good repeatability in the nature, dimension, and quality of features from patterning via CO_2 laser ablation is dependent on the laser energy stability. Precise channels were created on silicalite-1 films due to the stability of energy used over time (laser power) which is inherent to CO_2 lasers When a film is irradiated, the heat is transmitted through the sample until it reaches the interface between the film and the substrate, which can act as a heat sink. Moreover, due to the rapid heating and cooling and the short ablation time, any possible migration of elements from the substrates (e.g. glass, quartz etc.) to the surrounding film is minimized. Therefore, the depth of ablation changes with the amount of laser energy absorbed, which in turn is determined by the impinging laser power, by the diffusion of laser energy from the surface, and by the direct absorption into the sample at various points. At lower laser energies, there is loss/dissipation of the irradiated laser energy, on the film's substrate (Si) (thermal diffusivity, 0.86 cm^2/s at 300 K), which causes irregular patterns and does not result in the clean ablation of the film. However, at higher laser power, there is much faster heat diffusion and clean/precise ablation. These effects can be seen in **Figure 4-5**. For instance, at low laser powers, the patterns formed have non-uniform, high roughness boundaries both along the edges of the pattern and at the base parallel to the substrate. As the laser power increases, more prominent channels with sharp, distinct edges and reduced surface roughness are formed. As expected, higher powers lead to diffusion of more energy through the film and therefore, greater channel widths and depths are created. What is particularly interesting about this process is that these variations demonstrate the flexibility of the patterning process. By simple, small changes in laser

power and film thickness, it is easy to control channel depth and width, as well as the channel edge shape (sharp, curved, and slanted).

Figure 4-5 also shows the morphology of the patterns obtained at different laser powers. It is evident that at 10% laser power, there is only surface densification of the film; however, at 15, 20, and 25% laser powers, channels are formed that have more distinct boundaries and an increased amount of film ablation. The width of the channel formed increases from 170 μm (15%) to 300 (20%) μm due to the increase in the amount of laser energy that is transmitted to the sample; however, the width of the channel formed does not change markedly from 20 to 25%. This is most likely due to the limitation in the amount of heat that can be transferred laterally at a fixed scan rate (1 mm/s in **Figure 4-5**). It is interesting to note that at both lower (~10%) and higher (~25%) powers, multiple scans across the same region do not create marked changes in terms of either the channel aspect ratio or morphology. Also, depending on the power and film thickness used to make the patterns, it can produce trenches with central maxima (for thicker films) or maxima on either side of the channels. Lastly, the nature, morphology, width, and roughness of the channels thus formed are not governed or affected by the direction of scanning. **Table 4-3** summarizes the dimensions of the channels that were obtained in this work at different ranges of laser power.

Table 4-3: Summary of the channel dimensions formed at different laser power ranges on films with random and *b*- oriented silicalite-1 films with a thickness range of 5-10 µm.*

Laser power	Depth (µm)	Width (µm)	Minimum distance between channels (µm)
10-15%	(2.577 ± 0.118)-(4.76 ± 0.035)**	(170 ± 0.896)-(403.243 ± 2.374)	~65 ± 1.340
15-20%	(2.857 ± 0.067)-(6.683 ± 0.040)	(300 ± 0.346)-(540.04 ± 2.956)	~170 ± 2.382
20-25%	(3.397 ± 0.068)-(7.133 ± 0.006)	(300 ± 0.896)-(611.98 ± 1.28)	~180 ± 2.139

* Each measurement was done 3-5 times across different channels and along the length of individual channels.

** Lowest value ± SD-Highest value ± SD (SD- standard deviation).

The relationships among film thickness, laser power, and channel width and depth **(Figure 4-6)** show the formation of shallow and deeper channels/patterns depending upon the laser power, as per our expectations. Here, we label the axes with relative power instead of actual laser power. This is because, for each thickness, material removal starts at a different laser power, usually varying by ± 3%. Relative power refers to the amount of laser power after the initial ablation power level occurred on particular film. In these plots, it is clear that there is a positive linear relationship between the depth / width of the channels and the laser power for each film thickness. In terms of the widths of the channels formed, it can be seen from the graph that the value of widths increases with increase in film thickness (owing to greater diffusion of the heat energy $10 > 8 > 5$ μm) **(Figure 4-6B)**. The results of the linear fitting of the depth and width curve are shown in the supplemental information file. It must be mentioned here that the depth and width of these channels have been found to vary depending on the film properties like; roughness (causes uneven material removal from the film), degree of intergrowth of the crystals (non-uniform film results in loss of irradiated energy to the substrate), and quality of the film (poorly adhered film again causes loss of irradiated energy or it can come off completely post patterning).

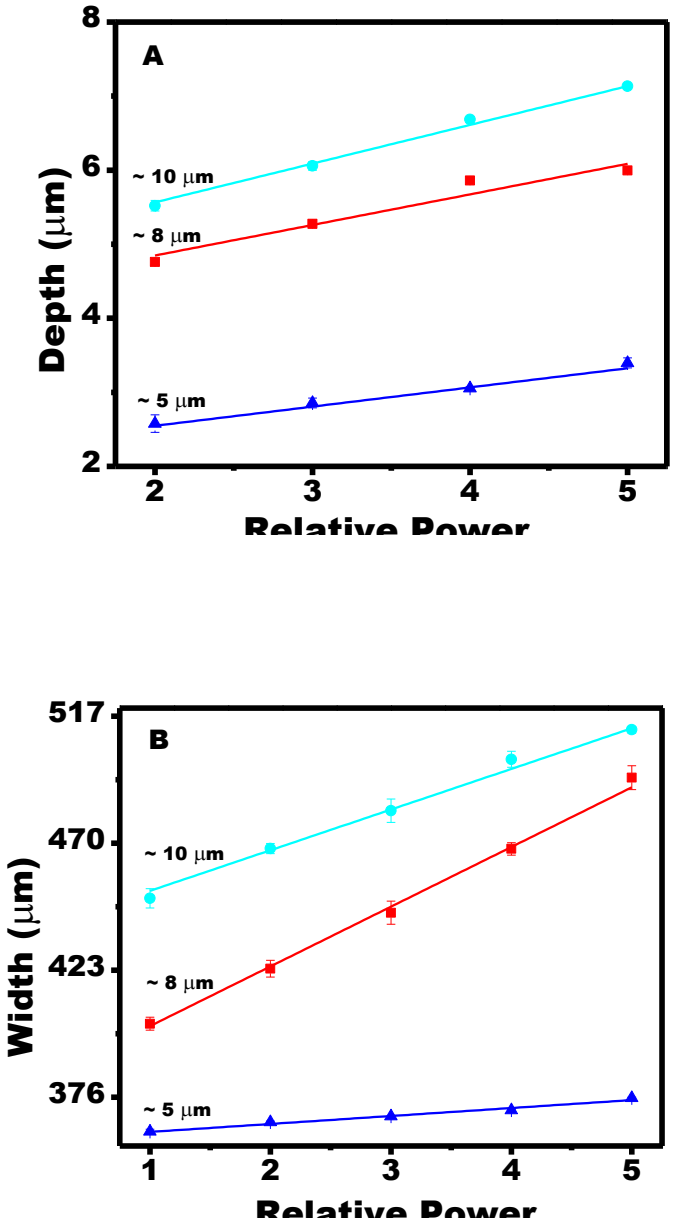

Figure 4-6: The depth (A) and width (B) of the patterned channels, measured repeatedly at each laser power, shows a strong positive, linear correlation to relative laser power for each film thickness evaluated (~ 5, 8 and 10 μm). The exact depth and width dimensions may vary depending on the film properties. Table 4-4 lists the intercepts for both the depth and width curves.

Table 4-4: Results of linear fitting of depth and width curve at different relative laser powers (Section 4.3.3.2).

Film thickness	**Depth curve**					**Width curve**				
	Intercept	SE	Slope	SE	R^2	Intercept	SE	Slope	SE	R^2
5 µm	2.029	0.148	0.259	0.037	0.938	360.247	0.446	2.948	0.129	0.956
8 µm	4.021	0.056	0.413	0.014	0.908	380.255	2.840	22.087	0.927	0.997
10 µm	4.519	0.085	0.523	0.017	0.994	437.330	2.589	15.041	0.639	0.994

SE: standard error; R^2: coefficient of determination

4.3.3.3 Laser Raster or Translation Rate

To understand these relationships, we evaluate the trends of pattern formation at constant raster or translation rates. We observe that changes in the translation rate of laser scanning result in different ablation trends in the same film, likely due to the resulting heating/cooling rate, and diffusion of heat into the film [62, 69]. At a constant translation rate (*r),* however, the variation in depths and widths of the channels can be represented by **equations 4.2** and **4.3**.

$$d\,(P) \propto t \qquad \textbf{4.2}$$

$$w\,(P) \propto t \qquad \textbf{4.3}$$

Where, t is the thickness of the film, d and w are the dimension of the depth and width respectively, both of which are functions of laser power, P.

We have also patterned using a slower scan rate (0.5 mm/s), which resulted in the production of channels with less distinct boundaries. This slow translation rate/scan is associated with less precise pattern morphologies due to reasons like thermal shock of the film, trapping of unwanted disintegration species, or water in the micropores of zeolites (silicalite-1). **Figure 4-7** shows that the pattern width changes along the channel as we change the laser energy from 15% to 10% for a relatively thicker film (~24 μm). It is important to mention here that these data are dependent on the nature and properties of

the films e.g. thickness, intergrowth, crystal habit, quality etc. and the observations made in this work are discussed based on the premises of the properties of the films used.

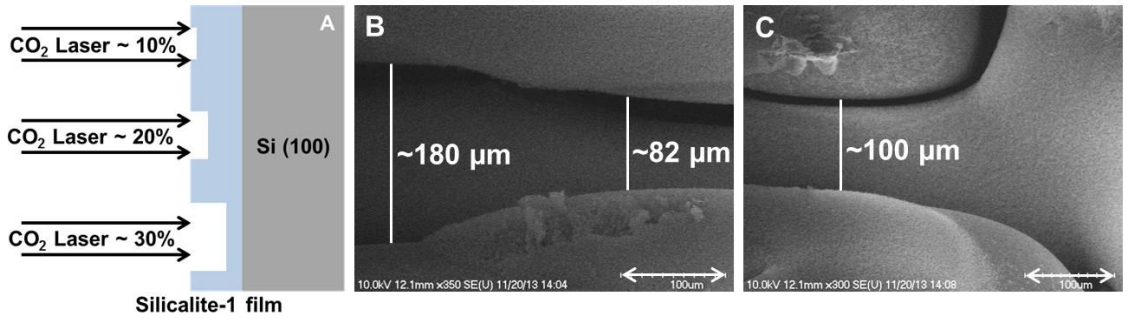

Figure 4-7: Shows (A) Schematic representation of material removal depending on laser power; SEM micrograph showing that (B) the width of the channel narrows when the laser power is changed from high to low; (C) the channel wall transient from slanted to vertical with increase in irradiated laser power.

4.3.3.4 Beam Shadowing

During patterning, we observed differences in sidewall formation. The geometrical variation in the sidewalls formed due to constraints imposed by beam shadowing. For a laser beam normally incident on the film surface and with a Gaussian beam profile, the wall angle ϕ deviation from vertical is given by **equation 4.4** [70].

$$\phi \approx (\lambda/\pi\omega_{\circ})[\left(\frac{P}{P_{\circ}}\right) - 1]^{-1/2} \qquad \textbf{4.4}$$

Here, λ is the wavelength (10.6 μm), P is the beam power and $P_{\circ}$ is the threshold melting power of silicalite-1. Thus with a spot size ($\omega_{\circ}$) of ~ 13.5 μm, the greater the $P/P_{\circ}$, the side wall inclines towards vertical as we can see in **Figure 4-7B**. **Figure 4-7C** shows the inclined/slanted walls formed on the same film at < 10% laser power and the clear transition towards vertical wall formation as the laser power is increased to ≥ 10%.

4.3.3.5 Resulting Surface Roughness

Figure 4-8 shows the flexibility of the resulting patterns: fine edges and straight pattern profiles either with or without complete ablation of underlying film. The roughness of the features formed is of the order of tens of nm in the areas which have plastic densification; however, the roughness of the boundaries may extend to hundreds of nm in the partially densified regions, as we can see from the SEM micrographs of the channel boundaries in **Figure 4-8**. Note that the densification can be clearly seen in the SEM micrographs. Also, by tuning the laser power, it is possible to modulate the presence or absence of zeolite film at the base of channel (i.e. it is possible to create

channels where the base is either still zeolite film, or where the material has been completely removed and the base is the underlying substrate). The ability to keep a film at the base of the features to various degrees will broaden the applications for this technique, particularly for optoelectronics.

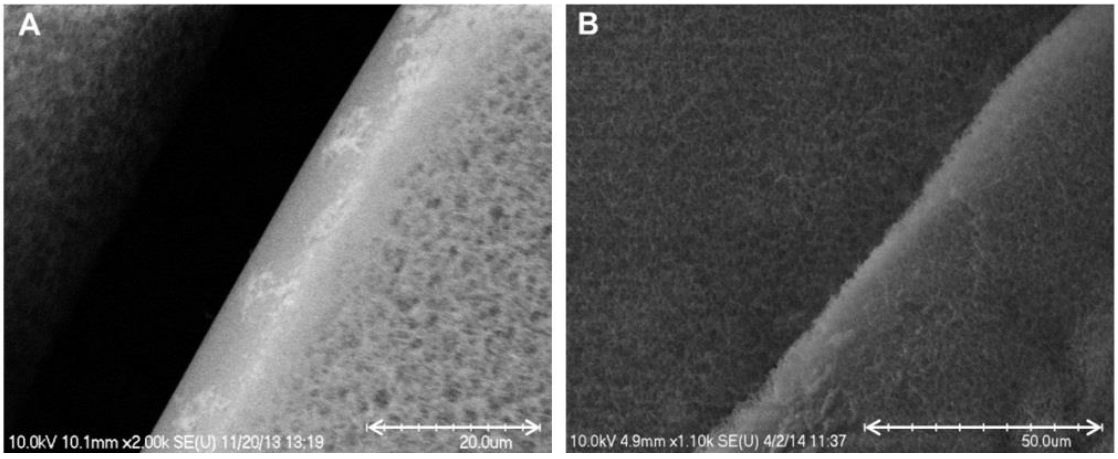

Figure 4-8: SEM images of patterns with (A) complete and (B) partial removal of film beneath.

4.3.4 Pattern Feature Size

Lithography is one of the most widely used techniques for patterning. This top-down approach typically provides structural resolution of 80 nm; however, other commonly used lithographic techniques like time-, particle-, ion- and e-beam lithography have structural resolutions of 50 nm. Though these techniques have very good resolution, the cost and time requirements are large, and they limit substrate sizes that can be patterned. In comparison, using CO_2 laser ablation, the minimum distance between adjacent features that has been achieved are 25 µm without film beneath the feature **(Figure 4-9A)** and about 65 µm with remaining film underneath **(Figure 4-9B)**. Also, depending upon the laser power used, the minimum distance between consequent features can be tuned. Features in the form of silicalite-1 rods/needles with minimum channel width of ~90 µm have been obtained in this work **(Figure 4-9C)**.

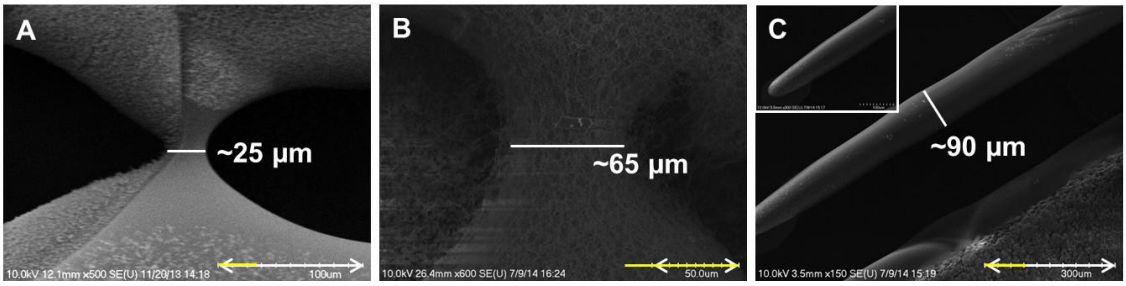

Figure 4-9: SEM images of minimum distance between adjacent features (A) without underlying films; (B) with underlying film; (C) silicalite-1 rod the inset shows the uniform and blunt tip of the rod.

With the reduction in laser power to a value just above the melting threshold of the film (>10%), it is possible to fabricate arrays of channels with minimum spacing of ~170 µm and channel width of ~190 µm **(Figure 4-10A)** with partial ablation of the underlying film; however, the minimum width between adjacent channels is ~ 180 µm and their widths are ~120 µm when the underlying film is completely ablated **(Figure 4-10B)**. The spacing's between each channel as well as the minimum widths are governed by the order of the wavelength of energy used to patterns them, which in this case is 10.6 µm. The entire film thickness is ablated with > 20% laser at 1 mm/s rate of translation.

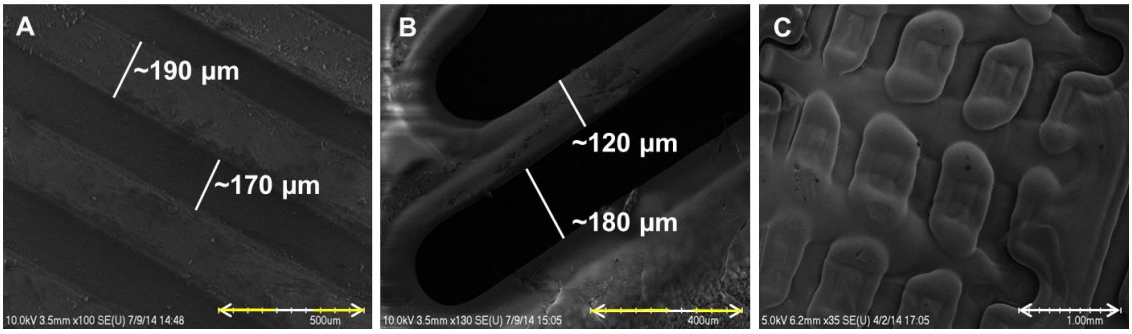

Figure 4-10: SEM images showing in an array of channels the average distance between each channel is about (A) ~170 µm.with silicalite-1 film beneath; (B) 180 µm with complete removal of underlying film; (C) representation of patterns that can be formed by raster ablation of the film.

We note that these results in patterns with features much larger than those generated through a lithographic technique, but for many micro-scale applications, it is not necessary to form features at such small scales [37, 38, 71, 72]. Moreover, the ability to directly write onto the film, without a mask, makes this technique valuable in terms of cost and speed of processing. Lastly, it is important to note that this technique may be accomplished in normal laboratory environments.

4.3.5 Densification of Films During Irradiation

Densification owing to the presence of thermal gradients in Type VI gel silica glass due to laser irradiation has been studied [69]. Those studies report that, depending on the extent of heating and heat diffusion at different laser powers, different regions of densification are observed in pure-silica films with respect to the distance from the point of laser irradiation. These three distinct regions are the: (1) Elastic, (2) Viscoelastic and, (3) Plastic regions, named for their behavior [70]. It is well understood that these regions possess different degrees of porosity and density owing to the difference in the amount of internal stress that is relaxed during their heating and cooling steps. These regions could possibly give rise to refractive index profiles, i.e. gradient index changes, which could be achieved reproducibly using this simple, single-step laser writing method on zeolite films of any other composition **(Figure 4-11)**.

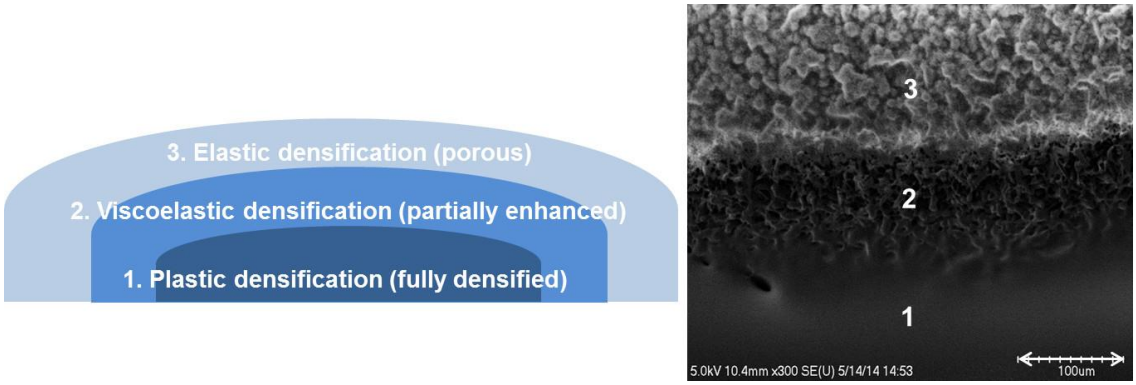

Figure 4-11: Image shows that regions with varying extent of densification/porosity are formed surrounding the channels, in line with observation made in reference [70].

Using lower laser powers (< 10%) we were not able to see complete removal of the underlying film. Similarly, at very high laser powers (> 30%), we were not able to form structures with clean surfaces due to the very high energy density impinging on the film. For the latter case, the molten material flows inward into the engraved channel, due to its surface tension governed transport **(Figure 4-12)**. Thus no distinct regions of densification to different degrees are visible owing to the formation of a quasi-equilibrium thermal profile in the irradiated film (acting as semi-infinite solid) region in time scale less than 1 μm.

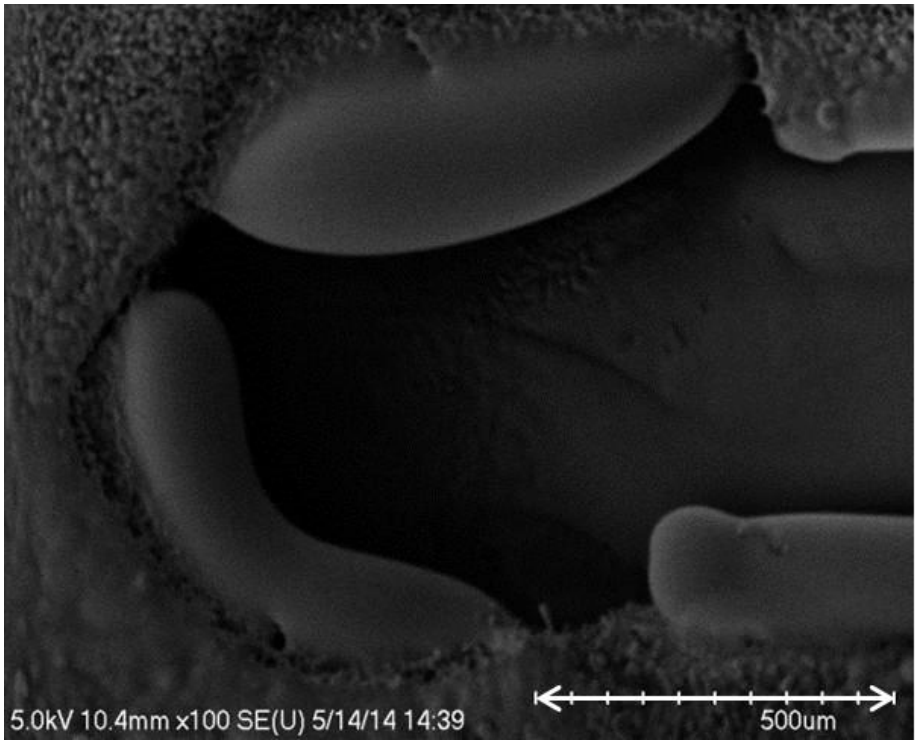

Figure 4-12: When irradiated at laser power > 30%, the molten material flows inward to partially cover the engraved channel (section 4.3.5).

At lower laser powers (~10-15% and 15-20%) the densification to form regions of different density is not very distinct; however, very distinct regions of different porosity/density are speculated with an increase in laser power to > 20%, based on the observations made in this work. The intact MFI crystals can be seen in the regions away from where laser densification occurred in patterns created with higher laser powers (~20-25%) **(Figure 4-13)**.

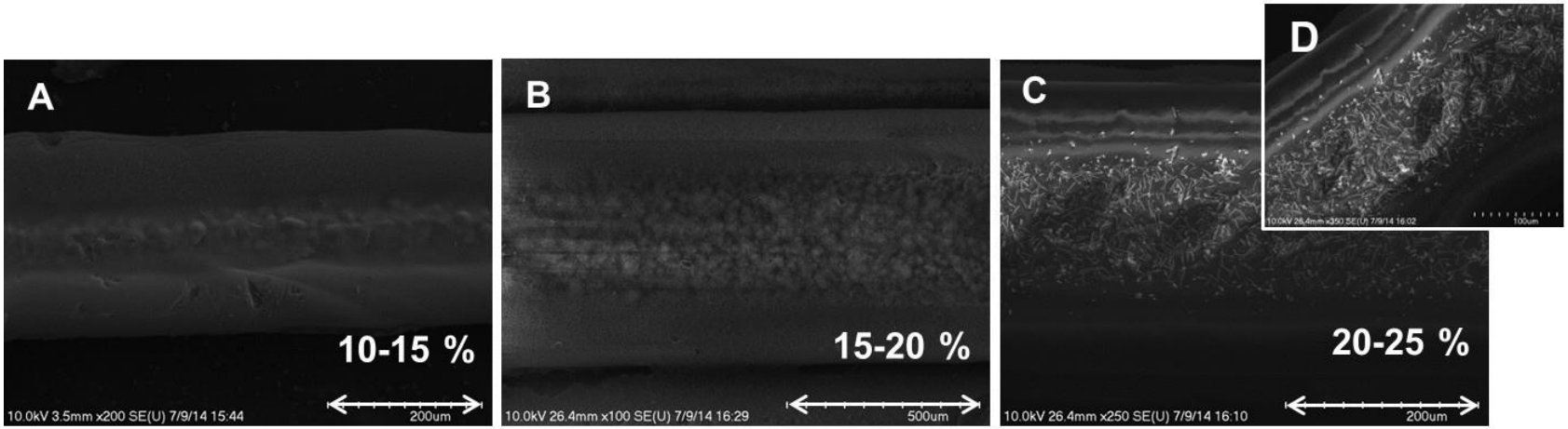

Figure 4-13: Increased laser power results in densification of silicalite-1 (MFI) films, thus forming distinct regions of materials with different degrees of porosity i.e. properties formed which could be equivalent to gradient refractive index (GRIN) characteristics; regions formed by irradiation at laser powers (A) 10-15%; (B) 15-20% and (C) 20-25% with inset showing distinct crystals in the farthest, porous zone.

Similar to other sol-gel films, it is possible that zeolite (silicalite-1) films can be converted into films of new structures and morphology, and hence properties, including such potentially useful things as variations in adsorption capacity, catalytic behavior, and refractive index. Zeolites (silicalite-1), formed by sol-gel processing steps are calcined at high temperatures (~500 ^{o}C) to open the micropores by removing the templates (SDA's) i.e. organic species by converting them into volatile component; however, when exposed to CO_2 laser the remnants of the templates or water can be trapped in the laser densified regions, which again varies with extent of densification away from the ablated region. Thus, when zeolites of other compositions with different framework atoms (Ti, Fe, Al, Ge, B etc.) are ablated/densified following the same technique, different properties and their respective variations can be expected. When different ions, molecules or metal clusters are trapped within the framework, the variation of the properties on account of densification, inter-diffusion of the entities or their decomposition (extent and ratio) could give rise to novel properties that are useful and interesting for various applications like optical interconnects, coatings etc. [18, 21, 73].

4.4 Conclusions

The impetus for studying new patterning technique porous, nanostructured materials arises because of the limitations imposed by the existing patterning methods. For instance, bottom-up approaches, where a pre-patterned substrate is coated with zeolites often requires several slow deposition steps, promotes uneven surface coverage or inclusion of a linker group [42, 43]. Moreover, limitations associated with top-down

approaches (e.g. lithography) such as expense, time requirements, and the inflexibility of feature dimensions without different masks has further fostered the development of an alternative technique. Fortunately, there has been extensive literature on bottom-up approaches that show that the aforementioned issues can be overcome by careful synthesis and alignment to form assembled zeolite monolayers with controlled orientation organized into desired 2D and 3D geometries [5, 15, 18, 21]. However, many of the limitations of the top-down approaches remain, patterning through photolithography being the premier top-down technique. This laser ablation method adds to the toolkit available to researchers for top-down patterning.

This study represents the first time CO_2 laser ablation has been used in conjunction with zeolite films. Here, we demonstrated the synthesis of pure-silica zeolite MFI on silicon (100) wafers. The resulting films were either *b*-oriented or randomly oriented, and varied in thickness (0.25-24 μm). When subjected to laser irradiation, except in cases of complete ablation or in regions of densification, the structure remained intact. By varying the film thickness (5-24 μm) and laser power (10-25%), we were able to create 3D features, such as channels of various widths (82-611.98 μm) and depths (2.58-7.13 μm). These channels also show regions of complete densification, closest to the incident laser spot, when very high laser powers are used **(Figure 4.10)**. The roughness of channels boundaries and the channel bases is in the order of tens of nm, however, the roughness of the film surface is typically hundreds of nanometers in regions where partial or elastic densification (increasingly distant from the fully densified regions) occurs. Features of these dimensions have potential applications as waveguides

(channel and slab), gratings and in integrated optics (linear and non-linear). The decrease in optical thickness cased due to laser irradiation of the silicalite-1 films can also impart applications towards multi-layer interference filters, which typically requires densification of alternating areas thus forming multilayer stacks [63].

This technique is a simple and flexible patterning method that does not require multiple steps, or extensive and precise equipment set-up. It allows us to patterns zeolite films with control over feature dimension, location, morphology, aspect ratio, roughness, etc. without the need for any specific mask design. The benefits of this technique includes; (1) simple serial writing, (2) cost-effective patterning since, aside from the laser itself, expensive equipment is not needed, (3) fast patterning, (4) mask-less patterning, and (5) the ability to tailor feature dimensions to a wide range depending on specific applications.

The resolution and preciseness of the features achieved through this technique is not considered to be limited by the fundamental properties of the film or its thickness, rather by the instrumental limitation. To extend the preciseness and variety of features that can be made using this technique we envision using advanced computer-aided design/computer-aided manufacturing (CAD/CAM) software and interfacing with laser ablation for making 3D patterns converted to stage movement by coupling with a LabView program, which can be further dissected into layers (segmenting structures into x, y planes and integrating drivers to control the stage in x, y, z directions) starting from and parallel to the surface of the film, which will also determine the rate and control that can be imparted on the rate of film ablation. The resolution of the features can be also

improved by using a different laser (pulsed laser, such as a femtosecond laser) or an objective with higher NA for reducing the diffraction limit of the spot size.

4.5 References

[1] M.E. Davis, Nature, 417 (2002) 813-821.

[2] J. Caro, M. Noack, P. Kölsch, R. Schäfer, Microporous Mesoporous Mater., 38 (2000) 3-24.

[3] J.H. Koegler, H.W. Zandbergen, J.L.N. Harteveld, M.S. Nieuwenhuizen, J.C. Jansen, H. van Bekkum, Stud. Surf. Sci. Catal., Elsevier, 1994, pp. 307-314.

[4] G. Schulz-Ekloff, Stud. Surf. Sci. Catal., 85 (1994) 145-175.

[5] G. Calzaferri, Langmuir, 28 (2012) 6216-6231.

[6] M.E. Davis, A. Katz, W.R. Ahmad, Chem. Mater., 8 (1996) 1820-1839.

[7] J.C. Jansen, J.H. Koegler, H. van Bekkum, H.P.A. Calis, C.M. van den Bleek, F. Kapteijn, J.A. Moulijn, E.R. Geus, N. van der Puil, Microporous Mesoporous Mater., 21 (1998) 213-226.

[8] M. Pina, R. Mallada, M. Arruebo, M. Urbiztondo, N. Navascués, O. De La Iglesia, J. Santamaria, Microporous Mesoporous Mater., 144 (2011) 19-27.

[9] G. Kolb, V. Hessel, Chem. Eng. J., 98 (2004) 1-38.

[10] L. Huang, Z. Wang, J. Sun, L. Miao, Q. Li, Y. Yan, D. Zhao, J. Am. Chem. Soc., 122 (2000) 3530-3531.

[11] X. Li, Y. Yan, Z. Wang, Ind. Eng. Chem. Res., 49 (2010) 5933-5938.

[12] Z. Li, C.M. Lew, S. Li, D.I. Medina, Yan, J. Phys. Chem. B, 109 (2005) 8652-8658.

[13] Y. Yan, S.R. Chaudhuri, A. Sarkar, Chem. Mater., 8 (1996) 473-479.

[14] P. Lainé, R. Seifert, R. Giovanoli, G. Calzaferri, N. J Chem., 21 (1997) 453-460J

[15] K.B. Yoon, Acc. Chem. Res., 40 (2007) 29-40.

[16] A. Zabala Ruiz, H. Li, G. Calzaferri, Angew. Chemie, 118 (2006) 5408-5413.

[17] J.-w. Li, K. Pfanner, G. Calzaferri, J. Phys. Chem., 99 (1995) 2119-2126.

[18] F. Cucinotta, Z. Popović, E.A. Weiss, G.M. Whitesides, L. De Cola, Adv. Mater., 21 (2009) 1142-1145.

[19] V. Reddy, A. Currao, G. Calzaferri, J. of Mater. Chem., 17 (2007) 3603-3609.

[20] K. Ha, J. Seon Park, K. Sun Oh, Y.-S. Zhou, Y. Sung Chun, Y.-J. Lee, K.B. Yoon, Microporous Mesoporous Mater., 72 (2004) 91-98.

[21] Y. Wang, H. Li, Y. Feng, H. Zhang, G. Calzaferri, T. Ren, Angew. Chem. Int. Ed., 49 (2010) 1434-1438.

[22] Z. Li, C. Lai, T.E. Mallouk, Inor. Chem., 28 (1989) 178-182.

[23] Y. Yan, T. Bein, J. Phys. Chem., 96 (1992) 9387-9393.

[24] J.S. Lee, H. Lim, K. Ha, H. Cheong, K.B. Yoon, Angew. Chem. Int. Ed, 45 (2006) 5288-5292.

[25] A. Kumar, H.A. Biebuyck, G.M. Whitesides, Langmuir, 10 (1994) 1498-1511.

[26] J.-H. Ahn, H.-S. Kim, K.J. Lee, S. Jeon, S.J. Kang, Y. Sun, R.G. Nuzzo, J.A. Rogers, Science, 314 (2006) 1754-1757.

[27] M.A. Meitl, Z.-T. Zhu, V. Kumar, K.J. Lee, X. Feng, Y.Y. Huang, I. Adesida, R.G. Nuzzo, J.A. Rogers, Nature Mat., 5 (2005) 33-38.

[28] M. Veiga-Gutiérrez, M. Woerdemann, E. Prasetyanto, C. Denz, L. De Cola, Adv. Mater., 24 (2012) 5199-5204.

[29] M. Woerdemann, S. Gläsener, F. Hörner, A. Devaux, L. De Cola, C. Denz, Adv. Mater., 22 (2010) 4176-4179.

[30] E.E. McLeary, J.C. Jansen, F. Kapteijn, Microporous Mesoporous Mater., 90 (2006) 198-220.

[31] X.D. Wang, W.L. Yang, Y. Tang, Y.J. Wang, S.K. Fu, Z. Gao, Chem. Comm., (2000) 2161-2162.

[32] B. Zhang, S.A. Davis, N.H. Mendelson, S. Mann, Chem. Comm., (2000) 781-782.

[33] S. Li, C. Demmelmaier, M. Itkis, Z. Liu, R.C. Haddon, Y. Yan, Chem. Mater., 15 (2003) 2687-2689.

[34] R. Lai, Y. Yan, G.R. Gavalas, Microporous Mesoporous Mater., 37 (2000) 9-19.

[35] R. Szostak, Molecular sieves, Springer, 1998.

[36] K. Ha, Y.J. Lee, H.J. Lee, K.B. Yoon, Adv. Mater., 12 (2000) 1114-1117.

[37] E.V. Rebrov, G.B.F. Seijger, H.P.A. Calis, M.H.J.M. de Croon, C.M. van den Bleek, J.C. Schouten, Appl. Catal. A: Gen., 206 (2001) 125-143.

[38] O. de la Iglesia, V. Sebastián, R. Mallada, G. Nikolaidis, J. Coronas, G. Kolb, R. Zapf, V. Hessel, J. Santamaría, Catal. Today, 125 (2007) 2-10.

[39] Y.S.S. Wan, J.L.H. Chau, K.L. Yeung, A. Gavriilidis, J. Catal., 223 (2004) 241-249.

[40] M.A. Urbiztondo, E. Valera, T. Trifonov, R. Alcubilla, S. Irusta, M.P. Pina, A. Rodríguez, J. Santamaría, J. Catal., 250 (2007) 190-194.

[41] I. Pellejero, J. Agustí, M.A. Urbiztondo, J. Sesé, M.P. Pina, J. Santamaría, G. Abadal, Sensors Actuators B: Chem., 168 (2012) 74-82.

[42] A. Kulak, Y.-J. Lee, Y.S. Park, H.S. Kim, G.S. Lee, K.B. Yoon, Adv. Mater., 14 (2002) 526.

[43] A. Kulak, Y.S. Park, Y.-J. Lee, Y.S. Chun, K. Ha, K.B. Yoon, J. Am. Chem. Soc., 122 (2000) 9308-9309.

[44] I. Pellejero, M. Urbiztondo, M. Villarroya, J. Sesé, M.P. Pina, J. Santamaría, Microporous Mesoporous Mater., 114 (2008) 110-120.

[45] D. Ehrlich, R. Osgood Jr, T. Deutsch, Appl. Phys. Lett., 38 (1981) 946-948.

[46] G. Treyz, R. Beach, R. Osgood Jr, J. Vacu. Sci. Tech. B, 6 (1988) 37-44.

[47] M. Müllenborn, H. Dirac, J.W. Petersen, Appl. Surf. Sci., 86 (1995) 568-576.

[48] D. Ehrlich, J. Tsao, Appl. Phys. Lett., 44 (1984) 267-269.

[49] B.D. Fabes, D.J. Taylor, L. Weisenbach, M. Stuppi, D. Klein, L.J. Raymond, B.J. Zelinski, D.P. Birnie, Int. Soc. Optics Photo., 1990, pp. 319-328.

[50] M. Guglielmi, P. Colombo, L.M. Degli Esposti, G.C. Righini, S. Pelli, V. Rigato, J. N. Cryst. Solids, 147–148 (1992) 641-645.

[51] D. Taylor, B. Fabes, J. N. Cryst. Solids, 147 (1992) 457-462.

[52] R.R. Krchnavek, H.H. Gilgen, R.M. Osgood, J. Vacc. Sci. Tech. B, 2 (1984) 641-644.

[53] B.D. Fabes, B.J. Zelinski, D.J. Taylor, L. Weisenbach, S. Boggavarapu, D.Z. Dent, Int. Soc. Optics Photo., 1992, pp. 227-234.

[54] J. Ihlemann, B. Wolff-Rottke, Appl. Surf. Sci., 86 (1995) 228-233.

[55] T.M. Monro, W. Belardi, K. Furusawa, J.C. Baggett, N.G. Broderick, D.J. Richardson, Mea. Sci. Tech., 12 (2001) 854.

[56] R. Holzwarth, M. Zimmermann, T. Udem, T. Hansch, P. Russbüldt, K. Gäbel, R. Poprawe, J. Knight, W. Wadsworth, P.S.J. Russell, Optics Lett., 26 (2001) 1376-1378.

[57] J. Knight, T. Birks, P.S.J. Russell, D. Atkin, Optics Lett., 21 (1996) 1547-1549.

[58] Y. Zhu, P. Shum, J.-H. Chong, M.K. Rao, C. Lu, Optics Letters, 28 (2003) 2467-2469.

[59] Y.J. Rao, T. Zhu, Z.L. Ran, Y.P. Wang, J. Jiang, A.Z. Hu, Optics Comm., 229 (2004) 209-221.

[60] D. Davis, T. Gaylord, E. Glytsis, S. Kosinski, S. Mettler, A. Vengsarkar, Elec. Lett. 34 (1998) 302-303.

[61] B.D. Fabes, Sol-Gel Optics, Springer, 1994, pp. 483-510.

[62] T.C. Zaugg, B.D. Fabes, L. Weisenbach, B.J. Zelinski, Int. Soc. Optics Photo. 1991, pp. 26-35.

[63] L.C. Klein, Sol-gel optics: processing and applications, Springer, 1994.

[64] J. Andrew, P. Dyer, D. Forster, P. Key, Appl. Phys. Lett., 43 (1983) 717-719.

[65] P. Schwab, J. Heitz, S. Proyer, D. Bäuerle, Appl. Phys. A: Mater. Sci. Pro., 53 (1991) 282-283.

[66] E. Hunger, H. Pietsch, S. Petzoldt, E. Matthias, Appl. Surf. Sci., 54 (1992) 227-231.

[67] A. Jadin, I. Filiouguine, M. Wautelet, L. Laude, Appl. Surf. Sci., 46 (1990) 375-377.

[68] E. Matthias, M. Reichling, J. Siegel, O. Käding, S. Petzoldt, H. Skurk, P. Bizenberger, E. Neske, Appl. Phys. A, 58 (1994) 129-136.

[69] T. Chia, L. Hench, C. Qin, C. Hsieh, Appl. Optics, 33 (1994) 3486-3492.

[70] T. Bloomstein, D. Ehrlich, Appl. Phys. Lett., 61 (1992) 708-710.

[71] J.L.H. Chau, K.L. Yeung, Chem. Comm., (2002) 960-961.

[72] E. Mateo, R. Lahoz, G.F. de la Fuente, A. Paniagua, J. Coronas, J. Santamaría, Chem. Mater., 16 (2004) 4847-4850.

[73] G. Calzaferri, H. Li, D. Brühwiler, Chem. Eur. J., 14 (2008) 7442-7449.

Part II: Optical Characterization of Silicalite-1 Films

Chapter 5: Introduction to Part II of Thesis

5.1 Introduction

Utilization of inherent properties like uniform porosity and ion-exchange capabilities of zeolites has paved the way for its wide variety of nontraditional applications. Identification of the critical needs of the new fields is usually unrelated to the already explored/studied areas. Apart from the fields where zeolites have established its wide spread usage since decades the newer applications have enormous implications for air, water, mobility, communication and energy, all comprising vital components for sustainable civilization [1]. Development of zeolite thin films for future generation computer chips, corrosion resistant coatings for aerospace alloys or hydrophilic and microbiocidal coatings for gravity-independent water separation in space stations encompasses taking advantages of some unique properties of zeolites that have not been extensively exploited so far; such as, high elastic modulus, mechanical strength and hardness, heat conductivity and biocompatibility [1, 2].

Unlike amorphous silica and polymers which have low *k* values due to presence of air in the pores but poor mechanical strength, hence most likely unable to withstand the much required chemical mechanical polishing (CMP) processes for industrial usage, the intrinsic crystalline structure and uniform microporosity of silicalite-1 shows high mechanical strength/integrity along with desirable thermal conductivity, porosity and

hydrophobicity. Research in zeolite like porous nanomaterials can pave the way to create two-dimensional and three-dimensional structures with intrinsic pores and channels as membranes and supports [3-6]. This increases their potential for use not only use as dielectric material but also being converted to small features for use in next generation microprocessors [7].

5.2 Introduction to Microporous Zeolite as Optoelectronic Materials

Owing to the ever increasing need for greater device density and decrease in feature sizes, insulators with dielectric constant lower than silicon dioxide are required and porous materials like zeolites (silicalite-1) has already been proven to be of paramount importance [7, 8]. However, to understand the potential of zeolites as optical materials and to be able to tune their properties in desired way based on need and application it is essential to understand the energy transport properties. The excition transport dynamics theoretically have the parameters of dimension and direction of excitons transport, similar to excition diffusion length [9] e.g. zeolite (L), which is similar in several aspects apart from having characteristic hexagonal channel structures. Observation reports that to increase the diffusion length we have to choose suitable donor and acceptor molecules. Large pore/cavity size causes the choromophore to align themselves in multiple orientations leading to non-cooperative modes. Owing to intrinsic charges of zeolite channel wall there is influence on the sensitivity of optical property of the dye/guest molecules [9]. The lattice contraction in the crystalline structure of zeolites, change in location of cation and pore opening; observed on account of X-ray diffraction

and powder neutron studies inflicted the idea about presence of framework flexibility in small pore titano-silicates (ETS-4), which in turn would mean that tailoring the absorption characteristics of such form of zeolites is achievable [10-13]. Cazaferri *et al.* mentioned that such materials with inorganic hosts are not only highly stable chemically, mechanically and thermally but have the potential of optical and electrical variation. Owing to the characteristic host guest chemistry in zeolites they are used for introduction of metal clusters and organic functionalization. Semiconducting material in nanoscale have been synthesized within the pores of zeolite Y and sodalite, which includes cadmium selenide, cadmium sulfide, lead sulfide and gallium phosphide [14]. These studies have definitely paved the path for application of novel materials with nanostructured compounds, allowing host-guest interactions with objectives of immobilizing fluorescent materials at high concentrations, which actually get attached to otherwise inert channels and pores of sub-nanometer dimension. These might find application in improving and widening the area of optoelectronic devices [9]. Potential for use as optical information storage material of sodalite films encapsulated with silver have been reported long back [14-16].

With these concepts in mind it is practical to envision zeolite-dye micro-laser, which is essentially incorporation of an organic dye in the micropores of crystalline zeolite as aluminophosphate. These molecular sieves acting as lasers have been found to be governed by the size, shape and arrangement of the pores in their microstructure [8, 17-19]. These confined materials are known to exhibit properties distinct to quantum confinement effects along with effects due to surface states. Due to characteristic and

specific refractive indices (RI) of materials like sapphire, ZnO and air they act as mirror and it is feasible to create optical cavity rather an optical resonance cavity at nanoscale. Hence, this leads to two-fold objective; i) obtaining lasing action without any intricate fabrication steps ii) understanding the lasing actions and effects of the components by optical characterization. With success of these approaches we should be able to obtain similar miniaturized one-dimensional lasers applicable as optical devices [20, 21].

Badini *et al.* first proposed the application of sol-gel process to fiber optics chemical sensor [22]. Consequently Avnivet *et al.* successfully trapped organic dyes in sol-gel matrix which acted as solid support for chemical sensor in optical sensing [23]. The possibility of immobilization of organic macromolecules in zeolite network with importance in areas of fiber optic chemical sensors further fosters the need to study the optical properties of the host zeolites and how it varies based on deposition techniques and extent of densification. One of the challenging issues for synthesis of porous materials like zeolites is towards achieving films with unidirectional orientation of pores given that the effects and consequences it causes are phenomenal for light interaction and optical characterization [24, 25].

5.3 Synthesis of Zeolites for Optical Applications

The objective is to form a transparent material which is easy to prepare in various forms namely; films, monoliths, fibers, easily impregnable by a dopant. For e.g. polystyrene has good transparency in the visible range, has high refractive index (1.59) however, cannot be used based on application and is hazardous to fabricate [23].

Synthesis of continuous polycrystalline zeolite film is challenging with regard to attaining desired type and level of crystallization. To overcome this it becomes essential to synthesize highly oriented films with unidirectional crystal orientation, intergrown, minimum defects and grain boundary and reduced surface roughness [26]. Though *in situ* grown films and membranes have higher quality and promises e.g. better permeation characteristics (for adsorption purposes) the fact that it have in most cases randomly oriented crystals with less control over the microstructure arrangement cannot be overlooked. It has been studied that in-spite of seeding the substrate it is possible to have final films with different crystal orientation; however, the most commonly observed final orientation is *c*- axis perpendicular to the surface of the substrate for zeolite MFI. Given that the nanocrystals used as seeds prior to secondary growth has no distinct faces, hence is equivalent to random orientation. Thus, based on observations and understanding it can be said that there will be anisotropic crystal growth on the crystals with their fastest growing faces (*c*-axis for zeolite MFI) unhindered (i.e. away from the seeds) having highest growth. This will dominate the final orientation of the film with majority of grown crystals being perpendicular to the plane [25]. At the same time the desired films thickness based on many applications is < 1 μm, hence precise control of every reaction parameter needs to be considered critically to attain this. Though there are several publications addressing modifications that has led to ideal, highly intergrown, very thin (300 nm), continuous *in situ* grown films; however, thin films with absolute no porosity or inter-zeolitic spaces with desired crystal orientation for eliminating any light absorption is yet to be achieved with repeatability [27]. Also in some cases this *in situ* technique is considered impractical for thin film applications (e.g. low-*k* films etc.) where

immersion of the entire wafer in the corrosive reaction gel is an issue. Tasaptasis *et al.* has proposed the technique of making zeolite nanocrystals and zeolite nano-sol which can be coated on intended substrate to obtain films or membranes with almost no inter-zeolitic pores at very minute scale, they have a unique process of homogeneous nucleation in the reaction gel, which gets deposited subsequently on the substrates through self-assembly. To combat this limitation manufacture friendly spin-on processes has gained immense importance wherein nanoparticles of silicalite-1 (PSZs) suspensions are hydrothermally synthesized and later spin coated on substrates (e.g. Si wafer). The nanoparticle suspension could be formed either by using ethanol as dispersion media or with aged amorphous silica precursor. The resultant spin-coated film would form bimodal pore size distribution owing to the presence of intraparticle zeolite micropores and interparticle voids or mesopores between adjacent crystals along with formation of intercrystalline grain boundaries. The added mesoporosity further acts by holding more air in the film thus are significant in affecting the overall optical nature/character (reduction in *k* value, elastic modulus etc.). Also, presence of intercrystalline boundaries could be vital when the application is for optical components and these boundaries would modulate light interaction at the boundaries and crystal itself. For spin-coated (*ex situ*) films the zeolite content/yield can be increased by increasing the synthesis time (typically crystallization) however, longer crystallization time results in larger particles which leads to undesirable films roughness and striations [1, 28].

While using aged amorphous silica precursor (TEOS gel) as the dispersion media before spin coating, there is reduction in pore size distribution owing to filling of the

mesopores/ intercrystalline voids by TEOS thus imparting further uniformity of composition in the film. This provides improved result for optical studies [29]. With increases in the TEOS content in the dispersion there is inevitably higher TEOS loading in the film and reduced pore size and porosity [1, 29].

The films formed by spin coating (or dip coating) are white in color. XRD data confirms that there are zeolite crystals forming the films (with thickness > 500 nm). With increase in number of coating, concentration of zeolite suspension used for coating, or dipping time in the casting dish we can control the thickness of the film. These films are calcined post formation which improves its mechanical robustness and chemical stability without causing change in their color, crystals size, shape or orientation; which has also been proven with post-calcination XRD data [26, 30, 31].

5.4 Characterization of Zeolites for Optical Applications

Zeolite like materials suitability in optical systems could be derived from that of silica-optics and some of the most relevant points can be summarized as; (1) shows excellent optical transmission from ultraviolet (170 nm) to near infrared wavelength (3400 nm), (2) possess isotropic optical properties with very low co-efficient of thermal expansion and high thermal stability and (3) high chemical and environmental durability with negligible amount of impurity inclusion and can be polished to high standards. The various processes to synthesize silicalite-1 thin films and perform their characterization are shown in step-wise manner in **Figure 5-1**.

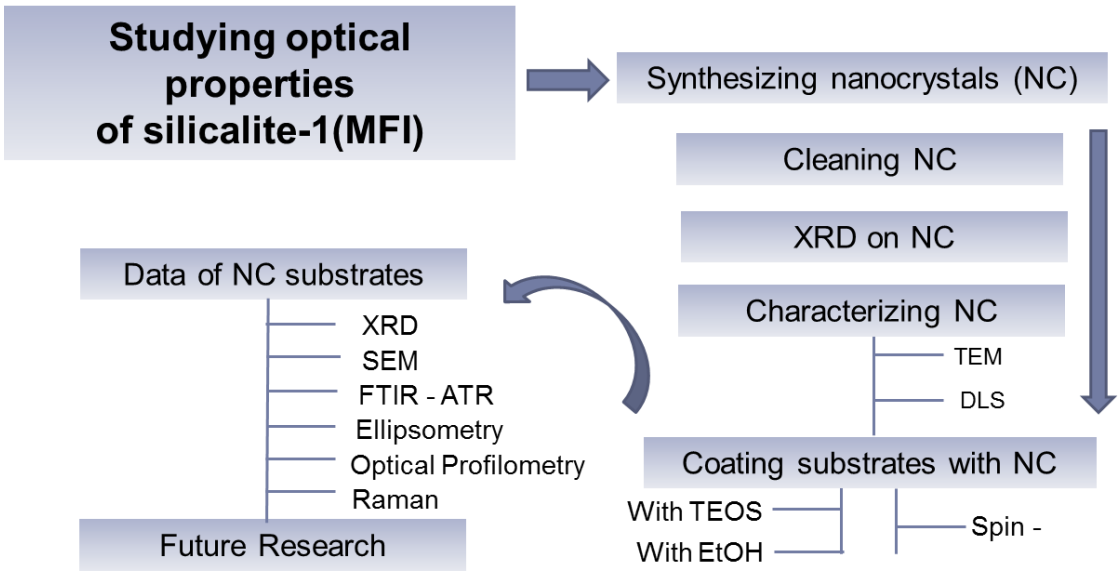

Figure 5-1: Steps for preparation and characterizations of *ex situ* grown silicalite-1 films using silicalite-1 NC for optical studies.

(NC - Nanocrystals).

5.4.1 Determination of Refractive Index

We know refractive index (RI) is a complex number n = n` + *i*n", where the real part n` indicates the measure of decrease in phase velocity of light in the interacting media (compared to vacuum) however the imaginary part n" measures the amount of light lost or absorbed in the media i.e. extinction [23]. Application of single coated zeolite film has been established for different V-type antireflection purposes for e.g. silicalite-1 films of 120 nm thickness has shown antireflection property with change in reflectance from bare Si to silicalite-1 film i.e. 34.3% to 23% [32]. Based on such observations we intend to further dwell into extensively studying the optical properties (RI, IR and Raman transmission) of silicalite-1 films.

Most literature has reported optical parameters obtained from studying sol-gel/silicalite-1 coated on silicon substrates. In all these studies the thickness of the film has been built-up by repeated coating; however, this technique of repeated/multiple coating is often associated with formation of internal defects or cracks in the final film, incorporation of impurity or its migration and uneven densification [33]. In this thesis, for the first time, based on our knowledge we have reported optical properties on *in situ* grown silicalite-1 films. With control over the film synthesis steps we were able to form *b*-oriented silicalite-1 thin films, providing further insight into interaction of light with fully intergrown, uniformly laden crystals and minimizing the factors of crystal boundaries and film roughness. We also compared the various optical parameters with spin-coated (*ex situ* grown) silicalite-1 films and with reported literature. The results obtained for *in situ* grown films and spin-coated (*ex situ*) films taken at different spots on

the film and their standard deviation values show that there is RI homogeneity, which further confirms silicalite-1 as optical material.

The optical properties or possibly RI of these materials could be varied on account of non-homogeneous mixing of the different components or varying molar composition of the reaction gel. The method of synthesis also offers control over the degree and extent of porosity of these materials hence their effective RI. Variation in RI for applications as stepped index type waveguides can be imparted to *in situ* or NC coated (different sizes) films and by using different composition of spinning solutions/dispersion media. The mode of operation of Bragg stacks is through change in RI independently or coupled with change in film thickness of each or certain layers comprising the Bragg stack [32, 34]. This kind of changes has so far been accomplished through physical processes like ion-exchange, physisorption and condensation of adsorbed molecules. Change in pore-diameter and corresponding pore-volume accomplished either by the typical ion-exchange process or molecular grafting has been used to modify and tune the desired characteristic of the final materials chemically/thermally/physically and optically, by changing the way the modified zeolite crystals interact with light [3]. Research has also been focused on tuning the morphology of the zeolite crystals so as to increase the density of pore on the surface of the crystals which is believed to improve/ease the accessibility to the channels [3].

5.4.2 Infra-red Transmission and Raman Characteristics

IR and Raman spectroscopy has been used to study and characterize silicalite and pre-crystalline zeolite solutions. IT and Raman vibrations ranging between 1200-300 cm^{-1} are characteristic of vibrations from crystalline zeolite structural units. IR spectroscopy has been used as early as 1976 by Flanigen *et al.* as a spectroscopic technique to examine changes and study evolution in the solid phase of the reaction gel during the entire process of crystallization for FAU zeolite [35]. The IR bands that were most structure sensitive with growth of crystallinity were near 360, 555, 665, 745 and 1060 cm^{-1}.

The peak intensity at 850 cm^{-1} assigned to a Si-OH bending vibration, decrease with increase crystalline material. It was first observed by Beard *et al.* that with increase in SiO_2/Al_2O_3 ratio, the vibrations from absorption maxima shifted from near 950 cm^{-1} (due to monomer and dimer species) to 1120 cm^{-1}, primarily due to growth of extended chains of silicalite species having molecular weights of about 1 million [36]. IR spectroscopic information could be obtained to study the changes occurring in the reaction gel prior to starting of crystal growth; however, the water present in the reaction gel, as we know strongly absorbs in the IR region of interest hence imposing obvious limitations on extensively used this technique in the presence of water to study the crystallization phases of zeolite synthesis. In order to combat this limitation, use of Raman spectroscopy was proposed due to its advantages of having strong intensities for aluminate and silicate anions at the same time having weak scattering owing to water in the aqueous phase. Various monomeric, dimeric, trimeric and tetrameric cyclic species in the silicate reaction solutions were studies by Dutta and Sheih [37].

The limitations and difficulties associated with Raman and IR spectroscopy studies of zeolite crystals (solid phase) in its heterogeneous system is challenging owing to the lack of full-proof experimental technique to successfully isolate or prepare zeolite solid phase i.e. crystals. In order to address this issue one might think of the obvious routes of drying or heating the solid crystals. Irradiation of the films using a high power laser can accomplish such a task. In this thesis we have introduced the study on CO_2 laser densified silicalite-1 films.

5.5 CO_2 Laser Densification

CO_2 lasers have been used to achieve variation in refractive index (RI) in photonic crystal fibers (PCF) by creating long period grating (LPG) owing to relaxation of the irradiated regions from mechanical stress [38]. The exposed region also shows signs of geometric deformation on the surface of the fiber, which essentially causes stronger coupling mode compared to when such LPG are created using ultraviolet (UV) light as the source instead of CO_2 laser [38]. In general the advantages of CO_2 laser over UV laser for creating variations in optical fibers for applications in optical communications has been known for a while, due to less expenses involved, simpler patterning steps, not requirement of specialized material as compared to UV protective materials (photosensitive fibers or H_2-loaded fibers) and temperature stability [39, 40]. Intricate and complicated profiles can also be fabricated using CO_2 laser irradiation due to its point-to-point ablating abilities that do not use expensive masks. Laser processing of sol-gel films has been studied for various applications in optics including electro-

chromic films, channels and slab-waveguides [41-44]. Several hybrid gels prepared by hydrolysis of metal oxide to produce metal hydroxides, followed by poly-condensation of hydroxide groups has shown applications as laser dye hosts, optical memory material, photochromic materials, catalyst carriers etc. Hybrid gels reported since 1978 with silica, alumina or aluminosilicate gel as hosts and their applications can be found in reference [23].

In order to meet the requirements as components on integrated optical systems (IOS) etc., we are interested in determining if densified regions of the films can act as different propagation media for optical applications of sol-gel films, created via a CO_2 laser-based, serial writing process. We envision that silicalite-1 films may also result in formation of rod like fiber waveguide with graded RI when differentially densified using CO_2 laser irradiation, hence form slightly different composition and optical property e.g. RI, IR or Raman. Versatility and maneuverability in terms of optical properties of the material can be achieved by imparting variation in the sol-gel processing steps, modifying the surface of the transparent film, thin film deposition steps or varying extent of their densification.

Based on studies of formation of optical fiber grating using femtosecond laser, we tried densification of *in situ* grown silicalite-1 films [45]. However, the regions of densification by femtosecond laser (CLARK-MXR, generating 150-fs laser pulses, central wavelength 775 nm, repetition rate 1 kHz) irradiation when ran under XRD for determination of their crystallinity, did not seem to retain the original form. However, when we check XRD data of CO_2 laser densified films, they have preserved crystalline

structure. Hence based on this observation we further carried out our study using CO_2 laser. **Figure 5-2** shows XRD pattern for femtosecond and CO_2 laser densified films for *b*-oriented *in situ* grown silicalite-1 films.

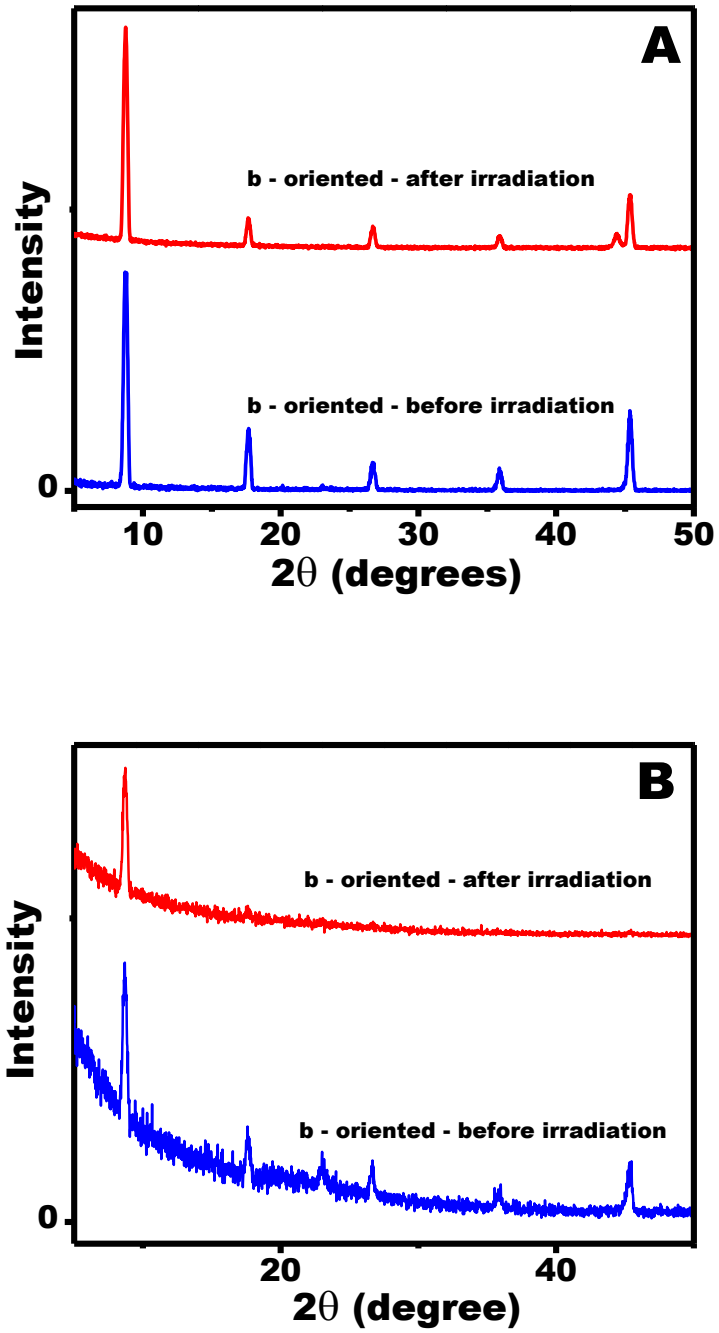

Figure 5-2: XRD have retained MFI crystal framework structure of silicalite-1 films after (A) CO_2 laser ablation but not for (B) femtosecond laser ablated films.

Our main focus in this section is to study changes in transmission and absorption characteristics of the laser densified *in situ* grown silicalite-1 films depending on extent of heating and heat diffusion at different laser powers. Since it is well established in the earlier section **(Chapter 4:)** that with respect to the distance from the point of laser irradiations the three distinct regions formed (Elastic, Viscoelastic and Plastic), these regions must have altered degree of porosity. The heat radiated on the film at different laser power causes difference in amount of release of internal stress, hence could cause RI profiles, i.e. gradient index changes along with changes in transmission and absorption in the IR wavelengths [38]. These regions could possibly give rise to RI profiles, which could be achieved reproducibly using this simple, single-step laser writing method on zeolite films. Since laser exposure causes intense heating of the irradiated regions, completely removal of any remaining water (from intra-zeolitic pores) and collapsing of the surface silanols groups might led to changes in the IR and Raman spectrum. Further changes in degree of crystallinity can also be estimated and studied by doing spectroscopic studies in the laser densified regions. **Figure 5-3** shows a schematic representation of the direct laser irradiation of silicalite-1 film to create regions of densification. **Figure 5-4** shows densification on regions of laser irradiation of silicalite-1 films at lower (10%) and higher (20%) laser powers respectively.

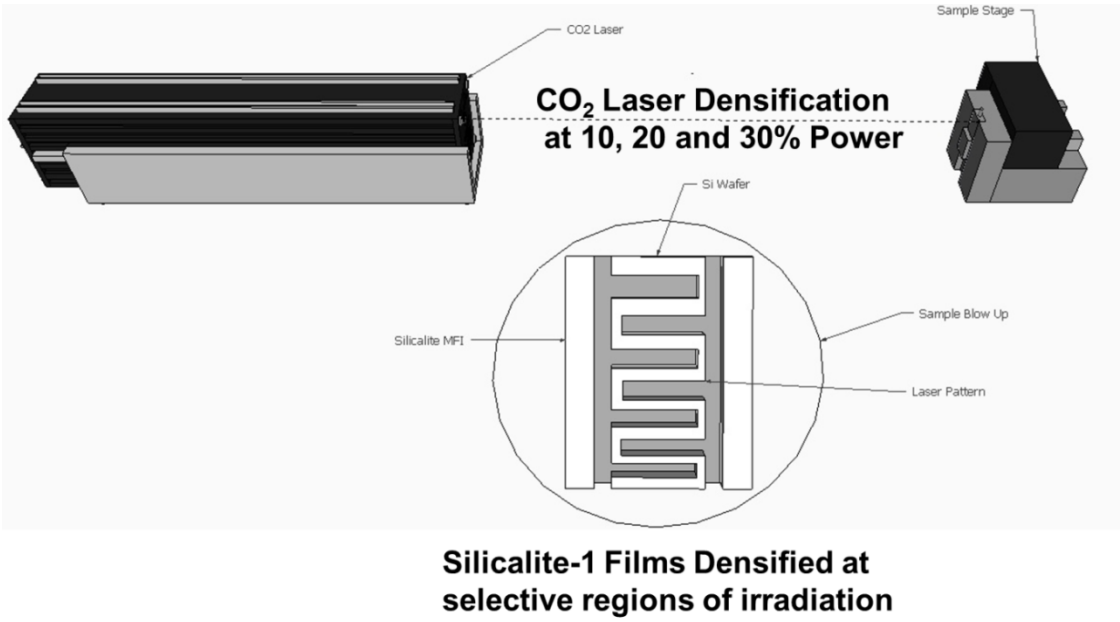

Figure 5-3: Schematic representation of CO_2 laser irradiation of silicalite-1 films forming regions of densification.

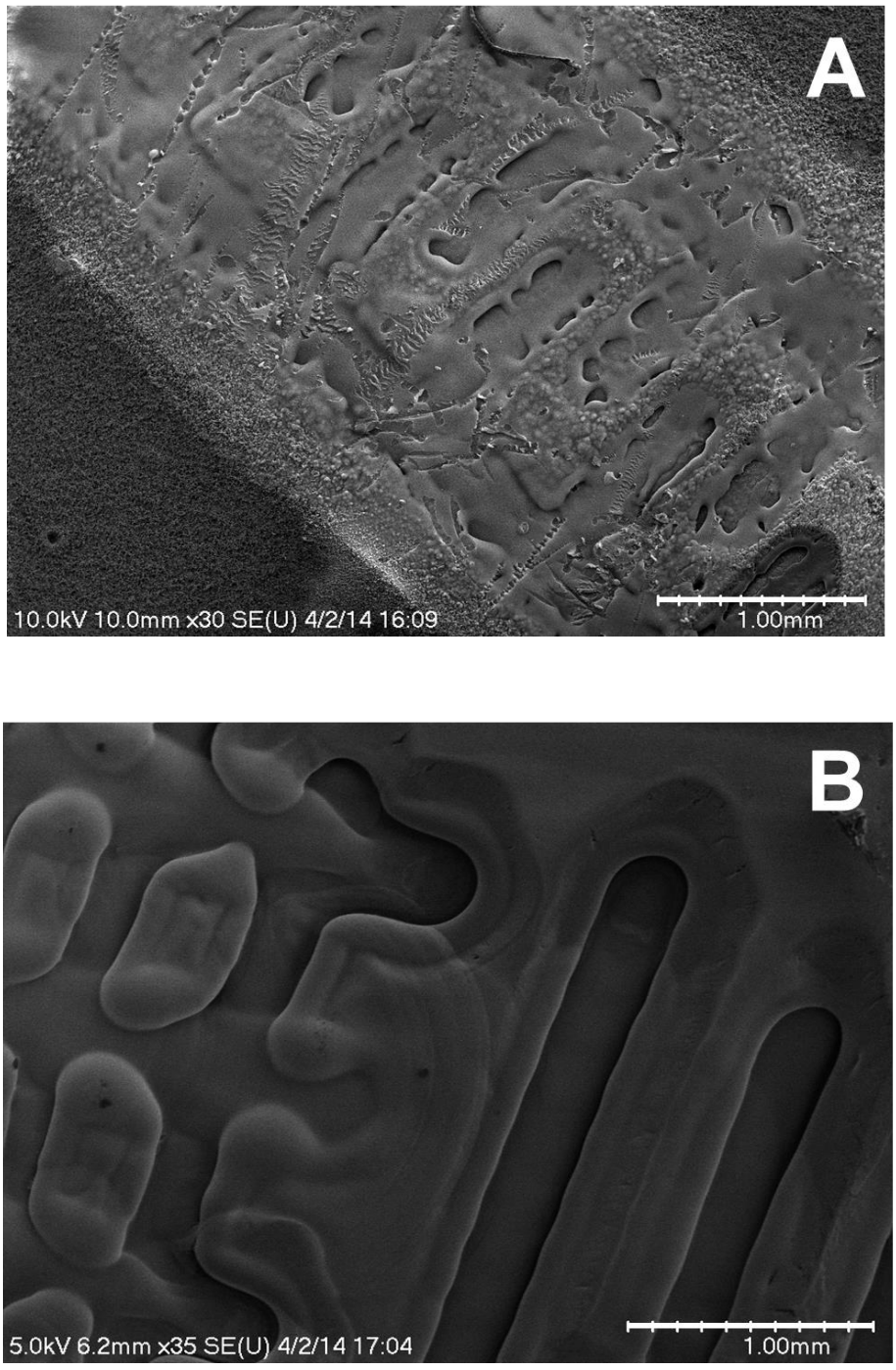

Figure 5-4: Shows silicalite-1 film densification using CO_2 laser at (A) 10% and (B) 20% laser power irradiation respectively.

5.5.1 Determination of Infra-red Transmission

Narrow band transmission systems has been fabricated using simple all dielectric systems [46]. The already described systems with maximum transmission at around 545 nm goes as per with silicalite-1 materials with the several advantages. However, with CO_2 laser densification of the films we expect to have altered degree of transparency on the different IR wavelengths of the silicalite-1 films, along with considerable reduction in optical loss which arises on account of crystal boundary and its effects on light interaction. Thus improving the chances of optical data storage/information storage and optical processing, which encumbers high speed modulators and demodulators which allows highly enhanced parallel processing.

We know that MFI type zeolites with IR spectroscopy shows band a 550 cm^{-1} which suggests 97% crystallinity with pentasil structure and another band at 972 cm^{-1} occurs due to high concentration of terminal Si-OH group which should decrease after the sample is calcined, suggesting cross-link of external surface silanols group. We are interested in studying the changes in peak position and intensity based on extent of densification of the silicalite-1 films, which again is varied based on the irradiated CO_2 laser power. The IR spectrum will also help to determine compositional uniformity in the pre- and post- densified films. For e.g. band at 972 cm^{-1} provides insight into the extent of packing of the NC coated films, which changes on laser densified films due to loss of external silanols groups, water or remaining organics. We are also interested in retaining the films optical transparency post- laser densification for their application as advanced photoconductive materials and optical fibers [47, 48]. In order to study the effects of CO_2

laser irradiation on silicalite-1 films certain specific regions that were evaluated and facts that were considered are summarized below [49]:

The IR spectra of zeolite lattice vibration modes are found in the mid-IR range (1400-400 cm^{-1}) where, bands at 1221 and 1095 cm^{-1} correspond to TO_4 asymmetric stretching vibrations, bands at 792 cm^{-1} correspond to TO_4 symmetric stretching, 546 cm^{-1} due to double ring, 453 cm^{-1} due to bending vibrations and Internal asymmetric stretching vibration at 1095 cm^{-1}. Bands around 808, 555 and about 462 cm^{-1} (most intense), are directly related to the materials structure. The latter signal is assigned to T-O (T: Si, Al, etc.) bending while the signal around 808 cm^{-1} arises from internal stretching of T-O-T bonds, this signal is sensitive to the Si/Al ratio and it may get displaced accordingly. Sharp band at 555 cm^{-1} is due to the structural double rings, which have been pointed out for several zeolites having five-membered double ring blocks variations (i.e. MFI, MOR, FER). This band is sensitive to the crystalline nature of the materials.

Typical stretching band of water around 3421 cm^{-1}, band at 1627 cm^{-1} is due to scissor type band arising from the proton vibration in the water molecules and intense band at 967 cm^{-1} correspond to stretching vibrations of the terminal silanols group. However, triplet observed at about 2971 cm^{-1} is due to residual organic matter in the sample, related to the double band at 1400 cm^{-1}. 1111 cm^{-1}, well defined shoulder on the high energy side is not distinct at lower degree of crystal effect.

5.5.2 Determination of Raman Characteristics

Evolution of the solid phase in the reaction gel can also be determined using Raman spectroscopy where scattering due to water is minimized. Keeping this idea in mind we studied for the first time based on our knowledge the Raman spectra (1200-200 cm^{-1} and 3000-2500 cm^{-1}) of CO_2 laser densified silicalite-1 films [50, 51]. The intense heat generated during laser irradiation will not only remove any remaining water and organic template from the films but cause changes in crystalline structure. By comparing peak intensity at 380 and 495 cm^{-1} we can estimate amount of amorphous to crystalline material in the irradiated silicalite-1 film. Corresponding non-homogeneity on the film and mechanical strength which is correlated with the amount of crystalline material in the sample etc. at different laser power were studied [51].

5.6 References

[1] C.M. Lew, R. Cai, Y. Yan, Zeolite Thin Films: From Computer Chips to Space Stations, Accounts of Chemical Research, 43 (2009) 210-219.

[2] T. Babeva, H. Awala, M. Vasileva, J. El Fallah, K. Lazarova, S. Mintova, Pure silica MFI zeolite films as antireflection coatings, Bulgarian Chemical Communications, 45 (2013) 18-22.

[3] V. Valtchev, L. Tosheva, Porous Nanosized Particles: Preparation, Properties, and Applications, Chemical Reviews, 113 (2013) 6734-6760.

[4] V. Valtchev, S. Mintova, Layer-by-layer preparation of zeolite coatings of nanosized crystals, Microporous and Mesoporous Materials, 43 (2001) 41-49.

[5] V. Valtchev, Silicalite-1 Hollow Spheres and Bodies with a Regular System of Macrocavities, Chemistry of Materials, 14 (2002) 4371-4377.

[6] V. Valtchev, B.J. Schoeman, J. Hedlund, S. Mintova, J. Sterte, Preparation and characterization of hollow fibers of silicalite-1, Zeolites, 17 (1996) 408-415.

[7] H.K. Hunt, C.M. Lew, M. Sun, Y. Yan, M.E. Davis, Pure-silica zeolite thin films by vapor phase transport of fluoride for low-k applications, Microporous and Mesoporous Materials, 128 (2010) 12-18.

[8] M.E. Davis, Ordered porous materials for emerging applications, nature, 417 (2002) 813-821.

[9] J. Gierschner, Directional exciton transport in supramolecular nanostructured assemblies, Physical Chemistry Chemical Physics, 14 (2012) 13146-13153.

[10] G. Calzaferri, Nanochannels: Hosts for the Supramolecular Organization of Molecules and Complexes, Langmuir, 28 (2012) 6216-6231.

[11] G. Calzaferri, A. Devaux, V. Ramamurthy, Y. Inoue, Manipulation of Energy Treansfer Processes within the Channels of L-Zeolite, John Wiley & Sons, Hoboken, NJ2011.

[12] G. Calzaferri, S. Huber, H. Maas, C. Minkowski, Host–guest antenna materials, Angewandte Chemie International Edition, 42 (2003) 3732-3758.

[13] G. Calzaferri, H. Li, D. Brühwiler, Dye-Modified Nanochannel Materials for Photoelectronic and Optical Devices, Chemistry-A European Journal, 14 (2008) 7442-7449.

[14] M.E. Davis, Zeolites and molecular sieves: not just ordinary catalysts, Industrial & Engineering Chemistry Research, 30 (1991) 1675-1683.

[15] G.A. Ozin, Nanochemistry: Synthesis in diminishing dimensions, Advanced Materials, 4 (1992) 612-649.

[16] G.A. Ozin, A. Kuperman, A. Stein, Advanced Zeolite, Materials Science, Angewandte Chemie International Edition in English, 28 (1989) 359-376.

[17] D.E. Kuechl, A.I. Benin, L.M. Knight, H. Abrevaya, S.T. Wilson, W. Sinkler, T.M. Mezza, R.R. Willis, Multiple paths to nanocrystalline high silica beta zeolite, Microporous and Mesoporous Materials, 127 (2010) 104-118.

[18] C. Martínez, A. Corma, Inorganic molecular sieves: Preparation, modification and industrial application in catalytic processes, Coordination Chemistry Reviews, 255 (2011) 1558-1580.

[19] P. Sharma, P. Rajaram, R. Tomar, Synthesis and morphological studies of nanocrystalline MOR type zeolite material, Journal of Colloid and Interface Science, 325 (2008) 547-557.

[20] Y. Xia, P. Yang, Y. Sun, Y. Wu, B. Mayers, B. Gates, Y. Yin, F. Kim, H. Yan, One-Dimensional Nanostructures: Synthesis, Characterization, and Applications, Advanced Materials, 15 (2003) 353-389.

[21] M. Wolkin, J. Jorne, P. Fauchet, G. Allan, C. Delerue, Electronic states and luminescence in porous silicon quantum dots: the role of oxygen, Physical Review Letters, 82 (1999) 197.

[22] G. Badini, K. Grattan, A. Palmer, A. Tseung, Development of pH-sensitive substrates for optical sensor applications, Proc. OFS1989, pp. 436-442.

[23] L.C. Klein, Sol-gel optics: processing and applications, Springer1994.

[24] J. Caro, M. Noack, J. Richter-Mendau, F. Marlow, D. Petersohn, M. Griepentrog, J. Kornatowski, Selective sorption uptake kinetics of n-hexane on ZSM 5-a new method for measuring anisotropic diffusivities, The Journal of Physical Chemistry, 97 (1993) 13685-13690.

[25] J. Caro, M. Noack, Zeolite membranes–recent developments and progress, Microporous and Mesoporous Materials, 115 (2008) 215-233.

[26] M. Tsapatsis, Molecular sieves in the nanotechnology era, AIChE Journal, 48 (2002) 654-660.

[27] J. Jansen, D. Kashchiev, A. Erdem-Senatalar, Preparation of coatings of molecular sieve crystals for catalysis and separation, Studies in Surface Science and Catalysis, 85 (1994) 215-250.

[28] S. Eslava, M.R. Baklanov, A.V. Neimark, F. Iacopi, C.E.A. Kirschhock, K. Maex, J.A. Martens, Evidence of Large Voids in Pure-Silica-Zeolite Low-k Dielectrics Synthesized by Spin-on of Nanoparticle Suspensions, Advanced Materials, 20 (2008) 3110-3116.

[29] G. Dubois, R.D. Miller, W. Volksen, Spin-on Dielectric Materials, Dielectric Films for Advanced Microelectronics, John Wiley & Sons, Ltd2007, pp. 33-83.

[30] M. Tsapatsis, M. Lovallo, T. Okubo, M.E. Davis, M. Sadakata, Characterization of zeolite L nanoclusters, Chemistry of Materials, 7 (1995) 1734-1741.

[31] M.C. Lovallo, M. Tsapatsis, Preferentially oriented submicron silicalite membranes, AIChE Journal, 42 (1996) 3020-3029.

[32] T. Babeva, H. Awala, M. Vasileva, J. El Fallah, K. Lazarova, S. Thomas, S. Mintova, Zeolite films as building blocks for antireflective coatings and vapor responsive Bragg stacks, Dalton Transactions, 43 (2014) 8868-8876.

[33] L. Lakiss, I. Yordanov, G. Majano, T. Metzger, S. Mintova, Effect of stabilizing binder and dispersion media on spin-on zeolite thin films, Thin Solid Films, 518 (2010) 2241-2246.

[34] B. Gospodinov, J. Dikova, S. Mintova, T. Babeva, Tunable Bragg stacks from sol-gel derived Ta2O5 and MEL zeolite films, Journal of Physics: Conference Series, IOP Publishing2012, pp. 012026.

[35] E.M. Flanigen, J. Rabo, Zeolite chemistry and catalysis, ACS monograph, 171 (1976) 80.

[36] W. Beard, Molecular Sieves, Meyer and Uytterhoeven (eds.). ACS Adv. Chem. Series, 121 (1973) 164.

[37] P.K. Dutta, D. Shieh, Crystallization of zeolite A: A spectroscopic study, The Journal of Physical Chemistry, 90 (1986) 2331-2334.

[38] Y. Zhu, P. Shum, J.-H. Chong, M.K. Rao, C. Lu, Deep-notch, ultracompact long-period grating in a large-mode-area photonic crystal fiber, Optics Letters, 28 (2003) 2467-2469.

[39] Y.J. Rao, T. Zhu, Z.L. Ran, Y.P. Wang, J. Jiang, A.Z. Hu, Novel long-period fiber gratings written by high-frequency CO2 laser pulses and applications in optical fiber communication, Optics Communications, 229 (2004) 209-221.

[40] D. Davis, T. Gaylord, E. Glytsis, S. Kosinski, S. Mettler, A. Vengsarkar, Long-period fibre grating fabrication with focused CO 2 laser pulses, Electronics Letters, 34 (1998) 302-303.

[41] D. Taylor, B. Fabes, Laser processing of sol-gel coatings, Journal of Non-Crystalline Solids, 147 (1992) 457-462.

[42] B.D. Fabes, Laser processing of sol-gel coatings, Sol-Gel Optics, Springer1994, pp. 483-510.

[43] B.D. Fabes, D.J. Taylor, L. Weisenbach, M. Stuppi, D. Klein, L.J. Raymond, B.J. Zelinski, D.P. Birnie III, Laser processing of channel waveguide structures in sol-gel coatings, San Dieg-DL Tentative, International Society for Optics and Photonics1990, pp. 319-328.

[44] T.C. Zaugg, B.D. Fabes, L. Weisenbach, B.J. Zelinski, Waveguide formation by laser irradiation of sol-gel coatings, Submolecular Glass Chemistry and Physics, International Society for Optics and Photonics1991, pp. 26-35.

[45] Y. Kondo, K. Nouchi, T. Mitsuyu, M. Watanabe, P.G. Kazansky, K. Hirao, Fabrication of long-period fiber gratings by focused irradiation of infrared femtosecond laser pulses, Optics Letters, 24 (1999) 646-648.

[46] H. Schroeder, Physics of thin films, Advances in Research and Development, 5 (1969) 87.

[47] H.J.H. Chen, C.-J. Huang, Nonvolatile Polycrystalline-Silicon Thin-Film-Transistor Silicon–Oxide–Nitride–Oxide–Silicon Memory with Periodical Finlike Channels Fabricated Using Nanoimprint Technology, Applied Physics Express, 6 (2013) 024201.

[48] K.T. Jung, J.H. Hyun, Y.G. Shul, D.S. Kim, Synthesis of fibrous titanium silicalite (FTS-1) zeolite, Zeolites, 19 (1997) 161-168.

[49] I.O. Ali, A.M. Ali, S.M. Shabaan, K.S. El-Nasser, Isomorphous substitution of Fe in the framework of aluminosilicate MFI by hydrothermal synthesis and their

evaluation in p-nitrophenol degradation, Journal of Photochemistry and Photobiology A: Chemistry, 204 (2009) 25-31.

[50] G. Deo, A.M. Turek, I.E. Wachs, D.R. Huybrechts, P. Jacobs, Characterization of titania silicalites, Zeolites, 13 (1993) 365-373.

[51] L. Tosheva, V. Valtchev, J. Sterte, Silicalite-1 containing microspheres prepared using shape-directing macro-templates, Microporous and Mesoporous Materials, 35–36 (2000) 621-629.

Chapter 6: Impact of Deposition and Laser Densification of Silicalite-1 Films on their Optical Characteristics

Abstract

Although the field of integrated optics has advanced tremendously in the past two decades, the state-of-the-art still lags behind its electronic counterpart, particularly in the development and integration of new optical materials systems. Nanostructured materials, and in particular, porous, nanostructured materials, often have unique and complex relationships between their structure and their resulting optoelectronic properties. These relationships may be tailored during or after synthesis or deposition, leading to potentially intriguing new material systems that may be suitable for various applications in integrated optics (tunable lasers, waveguides, transmitters, etc.) in the visible or near infrared regions. Zeolites represent a unique example of this material class; with their uniform microporosity and structural symmetry, their physicochemical and optoelectronic properties may be tailored to present a broad range of structures, compositions, surface areas, chemical and thermal stabilities, refractive index, dielectric constants, etc. Here, we synthesize a model zeolite system, silicalite-1 (MFI), in film form and characterize the resulting films both before and after partial laser densification to evaluate its potential for integrated optics. We use scanning electron microscopy, X-ray diffraction, and ellipsometry to determine the crystallinity, film thickness, surface coverage, crystal size, and crystal habit of the MFI films. We explore the fundamental optical properties of these films, such as index of refraction, and absorption and transparency windows, as a function of deposition method and film orientation. Within

these parameters, we evaluate their optical versatility that may arise from small changes in the structure that are induced via CO_2 laser-assisted densification using their resulting IR and Raman characteristics. The resulting randomly and *b*-oriented films of thickness (94.324-410.313 μm), showed the ability to reach a range of refractive indices (1.327-1.678), depending on film orientation and deposition technique. The intensities of their IR (1400-400 cm^{-1}) and Raman (1500-600 cm^{-1}) absorption regions indicate an increase in crystallinity with laser irradiation from 10 to 20% power, however, crystallinity then decreases above 30% laser irradiation. These changes are all possible without changes in the overall composition. Determining these fundamental optical properties will allow us to explore the functionality of these materials for a wider array of applications in optics and electronics, where nanostructured materials can make a significant difference in scale, cost, efficiency, and overall performance. The results of this study will help determine the suitability of zeolites for optoelectronic materials, and will broaden their usage in optical computing, signal processing, and a new generation of optical components.

*Mandal *et al.* Manuscript Submitted to Microporous and Mesoporous Materials, 2015

6.1 Introduction

The high demand for very fast communication and information processing systems has stimulated research towards the study of novel optical materials and devices for integrated optics, specifically those that are compatible with laser-assisted photonic systems/devices, e.g. optical switches, modulators, waveguides, interconnects, couplers, and micro-lens arrays [1-8]. Nanostructured optical materials have been studied extensively for applications in optoelectronics, including computing, communication, and sensing [9, 10]. For instance, nanostructured materials like carbon nanotubes (CNT), graphene, quantum dots, nanowires, superlattices, and nanoshells have all been used to create high-functionality optical devices [11]. Although less frequently exploited, nanocrystalline materials, such as ordered, microporous materials like zeolites, often have unique optical properties that arise due to either their nanoscale confinement or nanoscale features, and are fundamentally different than those of the same material composition at the bulk scale or in an amorphous configuration[12, 13]. When realized in the form of discrete, three-dimensional structures, these materials have very interesting and potentially useful applications in the fields of electronics, photonics, phononics, and microfluidics [14, 15]. The use of nanostructured, porous materials in these applications allows a number of new interactions that current material systems may not allow, including guest-host interactions [8, 16, 17]. For example, the presence of one-dimensional pores in zeolite-like materials has been used for building highly-ordered, guest-host systems [18, 19]. In these systems, the excitation energy in dye molecules captured within the zeolite's porous framework can be efficiently transferred and

harvested, owing to the confined volume of the pores [18, 19]. It is unsurprising, then, that these materials could be a practical matrix for hosting a number of species, not limited to dye-molecules, resulting in, for example, the generation of zeolite-dye micro-lasers, where the laser properties are governed by the size, shape, and arrangement of the pores in their microstructure [13, 20]. Alternatively, when used as a fiber-optic sensor, the microporous, high surface area characteristics of these film-based materials increases the surface area of the fiber and its subsequent light interaction by orders of magnitude, thus enhancing the sensitivity of the device by one hundred fold [20, 21]. Lastly, the zeolite matrix has the potential to act as a 3D well of dielectric material, which may confine the excitons of its guest semiconductor particles [1, 15, 22, 23].

Moreover, zeolites, which are typically synthesized through a sol-gel process, are potentially well-suited as optical materials since they can be made in a variety of forms, including membranes, films, fibers, fine powders, and monoliths. The ability to control zeolites' film/membrane thickness, along with their 3D crystal arrangement, into a desired, pre-determined hierarchy, has pushed the boundaries of their applications beyond their traditional uses as industrial catalysts, separation membranes, ion-exchange networks, etc., to next-generation electronics, with applications as insulators, as well as next-generation coatings, such as antimicrobial coatings, corrosion resistant coatings, etc. [2, 24, 25]. Additionally, the crystalline material structure of these materials possesses greater mechanical strength compared to their nanostructured amorphous counterparts of similar composition, thus increasing their potential for use in a variety of applications that require mechanical strength or durability, such as optical polishing [13, 26]. Lastly, their

application as optical materials is further based on their optical transparency characteristics, modifiable hydrophilicity, controllable porosity and compositional purity, and doping ability [27, 28].

In order to extend the application of these nanostructured, porous materials in optoelectronics and integrated optics, it is necessary to have a detailed understanding of their relevant material properties, e.g. refractive index (RI), absorption, etc., in addition to strict control of these properties [4]. For example, silicalite-1 (MFI) is a commonly used and well-understood zeolite system, primarily due to its robust and facile synthetic techniques. It has been synthesized by direct hydrothermal or secondary growth in the form of powder, films, and membranes on different substrates [15]. Over the past two decades, scientists have optimized its synthesis, surface characteristics, molar composition, substrate, crystal orientation, and film thickness in order to alter its physicochemical, electronic, and mechanical properties [1, 13]. However, there have not been many attempts to study its optical properties on the basis of the aforementioned optimization or to evaluate this material for its suitability as an optoelectronic material.

For this material system, previous literature has reported its potential for both waveguide materials and waveguide-based sensors. Based on its unique electronic properties, silicalite-1 (MFI), when synthesized with high purity and low water content, and in the appropriate form, may be a promising material for optical waveguides [1, 26]. As a demonstration of this, silicalite-1 has been used as a fiber optic chemical sensor (FOCS) [28].

Based on this work, as well as more recent work, it is easy to extrapolate that, for instance, this material system could act as an effective V-type antireflection coating, or as the basis for Bragg stacks or more complex Gradient Refractive Index (GRIN) materials **(Figure 6-1)** [2, 29-31].

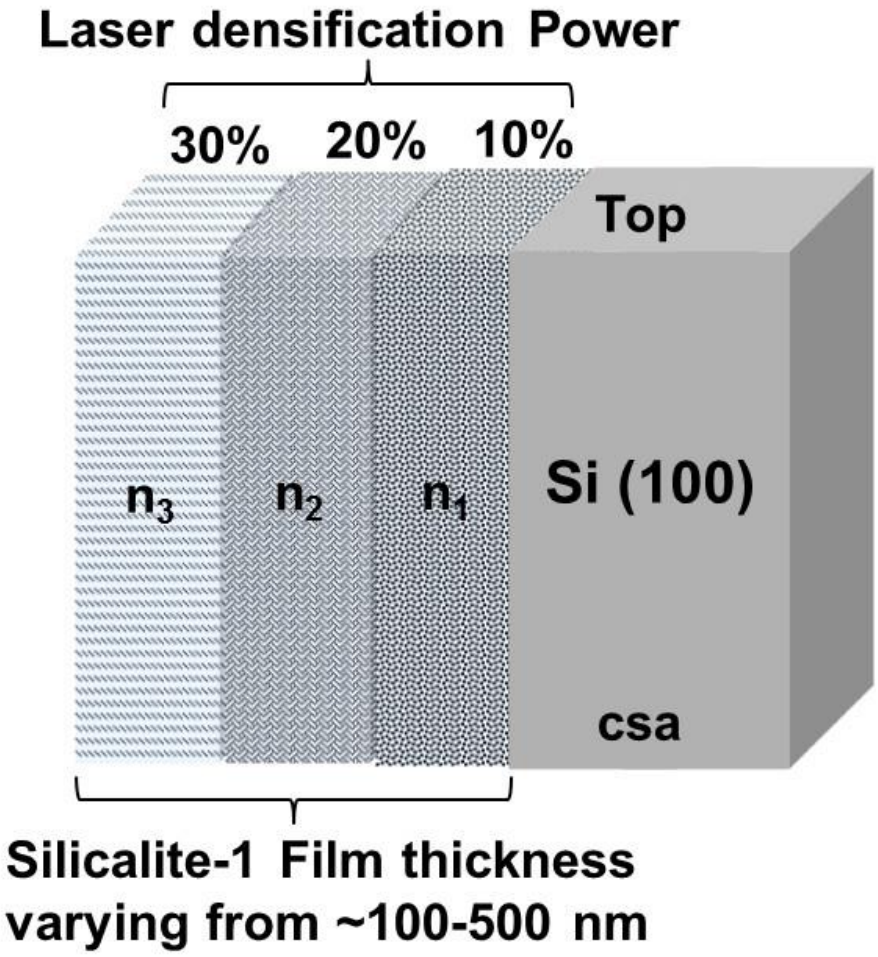

Figure 6-1: Cross-sectional (csa) illustration showing formation of different RI regions on silicalite-1 film when irradiated at different laser power (10, 20 and 30%), due to different degree of porosity, densification and ratio of amorphous to crystalline material.

For example, the potential effectiveness of silicalite-1 films as V-type antireflection coating with low spectral coverage with percentage of reflection at wavelength, λ for a film-substrate system is given by **equation 6.1**, below [28]

$$R = (n_1^2 - n_o n_s) / (n_1^2 + n_o n_s) \quad \textbf{6.1}$$

where, n_1 is the RI of the film (i.e. silicalite-1), n_s is the RI of the substrate (i.e. Si (100)), and n_o is the RI of the medium, commonly air, (n=1). Typically Equation (1) is simplified to **equation 6.2**:

$$R = (n_1^2 - n_s) / (n_1^2 + n_s) \quad \textbf{6.2}$$

This relation requires a detailed understanding of the wavelength-dependent RI of the silicalite-1 material, which could vary based on film deposition method, crystal size, number of defects, etc., all of which must be explored in detail to verify the material's use in this type of application.

Beyond simple anti-reflection coatings, Bragg stacks, which are based on a simple periodic design of alternating layers of high and low RI materials, could be obtained for applications requiring wavelength-selective reflectance, according to the conventional optical design where the optical thickness of the individual layer is given by λ/4, **(equation 6.3)**. [28].

$$nd = \lambda/4 \quad \textbf{6.3}$$

where n is the RI, d is the physical thickness of film, and λ is the wavelength of incident light.

Previously, work has been done to incorporate such designs with amorphous titania/silica polymeric sols or alkoxide derived sols of silica/zirconia [32, 33].

Given that Bragg stacks operate by changes in the thickness and RI values of layered films comprising the stack, these types of layered materials could be created with nanostructured, porous materials through not only compositional and synthetic changes, but also post-synthetic physical processes like ion-exchange, physisorption, or adsorption [2, 34]. To reproduce the functionality and exact operation of zeolite films for the purposes of creating Bragg stacks, it is mandatory to synthesize films with constant/reproducible thickness and controllable optical properties **(Figure 6-1)** [15].

This understanding of the complex relationships between structure, composition, synthesis, and properties becomes even more important when complex systems like Gradient Refractive Index (GRIN) materials are considered. These materials have continuous variation in their RI in the radial, axial or spherical direction, thus resulting in light beam transforming and imaging characteristics [35, 36]. GRIN materials with flat surfaces have found tremendous application in many optical systems, and could theoretically be derived index-modified SiO_2 materials, such as silicalite-1 films [2, 28, 30, 35, 36].

Across all the aforementioned applications, the processing conditions and the structural homogeneity of the synthesized material contribute largely to the resulting optical properties. At the simplest level of application, an optical waveguide, the optical losses in the final optical device must be minimized by reducing both absorption and

scattering. The effects of optical loss and optical non-linearity can be combined to define the susceptibility of a material for wavelength non-linearity **(equation 6.4)** [37]:

$$W = \Delta n_{max} / \lambda\alpha \qquad \textbf{6.4}$$

where, Δn_{max} denotes the maximum change in RI that occurs in the material during its interaction with irradiated light (e.g. a laser), and α is the total waveguide loss. Hence, Equation 4 denotes that in order to increase W, i.e. the material's suitability as a waveguide, Δn_{max} must increase and/or α must decrease, which also means there must be increase in the non-linear coefficient and optical quality of the guiding material. This yet again implies that there must be control over the materials' linear RI, since for wave-guiding applications; the guiding material must have a higher RI than the surrounding medium, such as a substrate in the case of a channel or planar waveguide.

In this study, our interest lies in primarily in creating zeolite films with tunable optical properties, e.g. RI, either by modulating the processing conditions (e.g. crystallization time) or post-synthetic modifications of selective regions e.g. (CO_2 laser based-densification). CO_2 lasers can be used to densify such zeolite films, which have a uniform microstructure that facilitates uniform densification. This causes a density gradient cross the film, and minimizes loss due to optical scattering at crystal boundaries, hence altering the film's optical properties as well as its porosity, film thickness, and roughness [38-41]. Moreover, in this work, we have also incorporated similar changes in RI and thickness of silicalite-1 films through modulation of growth conditions.

In this paper, we explore the model zeolite system, silicalite-1 (MFI)'s optical properties (RI, as well as IR and Raman absorption spectra) and evolution of IR and Raman spectra upon in response to modification to synthetic or deposition parameters. Furthermore, we explore the effect of densification or ablation via CO_2 laser irradiation on these properties. This process could be used to fabricate waveguides and other structures from the materials, and has the potential to convert silicalites-1 into GRIN in less than 30 min using laser assisted densification [38-43]. Moreover, for these applications, laser irradiation could be used as a final step to remove excess water from the material, as the water content of the as-made materials (often several hundred ppm) may hinder the potential of using these materials in optoelectronics We have used *ex situ* solution chemistry synthesis as well as *in situ* hydrothermal synthesis of silicalite-1 (MFI) films to establish a reference point for understanding and interpreting the optical and spectroscopic responses of film deposition techniques, and how the FTIR and Raman responses change with laser-assisted densification. Past literature on this topic remains sparse, and has been limited to evaluating basic optical properties, such as the RI, of only one sample type (silicalite-1 films deposited by spin-coating on silicon substrates) [2, 15]. Here, we expand upon this work, and compare as-made, *in situ* and *ex situ* films of silicalite-1 (MFI) with laser-irradiated counterparts for a variety of optical properties [15].

6.2 Experimental

6.2.1 *In situ* hydrothermal synthesis of silicalite-1 films on Si (100) wafers

Silicon wafers (100) (University Wafers, 0.008-0.02 Ω-cm, 600-700 μm thick) were used for *in situ* synthesis of silicalite-1 (pure-silica, MFI) films. The substrates were cleaned with piranha solution [1Hydrogen peroxide (H_2O_2) (40 wt%, Aldrich): 4Sulphuric acid (H_2SO_4) (98 wt%, Aldrich)] and dried in N_2 gas to remove any surface contamination. This also populated the surface with hydroxyl groups. The reaction gel was prepared by first mixing DDI H_2O (still) and tetrapropylammonium hydroxide (TPAOH, 1.0 M in H_2O, Aldrich), followed by slowly adding tetraethylorthosilicate (TEOS, 98%, Aldrich) under stirring. The mixture was then aged for 1-2 h while stirring at room temperature. The molar ratio of the reaction gel was $99.0H_2O$: 0.14TPAOH: 0.84TEOS. After aging, the synthesis solution was charged into a 23 ml Teflon©-lined Parr autoclave. A piranha-cleaned silicon substrate was also placed in the lined autoclave, either horizontally or slightly tilted, with the polished surface facing upwards. Film crystallization, as well as the concomitant powder crystallization, was then carried out at 165 ^oC for times ranging from 2-4 h. At the end of the crystallization time, the samples were recovered and washed with DDI water, and air-dried at room temperature. The films were then calcined in air at 400 ^oC for 4 h at a 0.5 ^oC/min ramp rate in a tube furnace (Lindberg Blue M Tube Furnace).

6.2.2 *Ex situ* synthesis of silicalite-1 films on (100) Si wafers

Nanosized silicalite-1 crystals (NC) were prepared from a reaction gel with molar composition 9TPAOH: 25SiO_2: 680H_2O: 100EtOH, following the procedures outlined by Mintova *et al.* [44]. The reaction mixture was pre-hydrolyzed at room temperature for 24 h on a slow shaker (VWR Signature Incubating Rocker Platform Shaker, 32 ^oC, 20 rpm, 10 ^{o} tilt angle). The aged mixture was charged into a 23 ml, Teflon©-lined Parr autoclave and placed into a 90 ^oC oven for 12-48 h (Heratherm General Protocol Oven, mechanical convection). After the appropriate amount of time, the reaction was quenched by removing the autoclaves and placing the hot autoclaves under running tap water. The NC were collected and purified by three rounds of centrifugation, following a method described by Mintova *et al.*[44]. After each centrifugation step, the NC were re-dispersed in DDI water and ultrasonicated for 3 h. At the end of 3rd centrifugation step, the cleaned silicalite-1 NC was dispersed in either EtOH (98%, Aldrich) or TEOS gel (25SiO_2: 408H_2O and 25SiO_2: 680H_2O, aged overnight). The concentration of NC was kept constant in all suspensions at 3 wt%. Si (100) substrates (2 cm X 2 cm) were cleaned using ethanol and acetone, and dried with N_2. The NC suspension was spin-coated (Laurell Technologies, 3000 rpm, 1000 rpm/s ramp rate, 35 s total spin time) onto the substrates and the coated substrates were thermally aged at 450^oC in air at 0.5 ^{o}/min ramp rate in a tube furnace for 4 h (Lindberg Blue M Tube Furnace). Only one coat was applied because of the inverse relation between film thickness and the number of coatings with decrease in film quality, due to the formation of cracks [28].

6.2.3 Laser densification of calcined silicalite-1 films

Laser densification of the films was carried out using a class IV, air-cooled CO_2 laser (SYNRAD, USA) at 10, 20, and 30% power. The laser has an average power output of ~29.31 W (calculated over 5 minutes, with a 30 second warm up at 30 V), a power stability of ± 4.14%, a peak power of 40.80 W (measured with a 100 Hz, gating signal with 10% positive duty cycle), and a respective rise and fall time of 86 and 88 μs (measured at 1000 Hz at 50% duty cycle). The power of the laser was controlled using a controller (Intelligent PC control), which acts by modulating the RF drive circuit that excites the plasma tube and causes lasing at a power density of 8.8 W/cu-in (PS-2 DC Power Supply-Emersion iMP4-3S0-00-A). The sample was held using an XYZ stage, fixed for translational movement in one direction only during experiments, which was controlled using a DC-motor (2-phase stepper) stage with 25 mm travel-stepper actuator with ¼ in-80 threads, and a lead screw pitch of 0.5 mm. The laser-irradiated samples were used to study the evolution of the silicalite-1 films' IR and Raman spectra.

6.2.4 Characterization:

The purity of the calcined, silicalite-1 NC and calcined, *in situ* films grown on Si (100) were confirmed using X-ray diffraction (XRD) (Rigaku, 40 kV, 44 mA, 5-50 ^{o} two theta, step size-0.02, 2 ^{o}/min). For the NC, the particle size distribution within the ethanol and TEOS suspending media was measured using dynamic light scattering measurements (Horiba-LB-550). The particle size and morphology was also checked with Transmission Electron Microscopy (TEM, FEI Tecnai F30 Twint). The morphology, quality, and

nature of the films generated by both *ex situ* and *in situ* synthesis were studied using Scanning Electron Microscopy (SEM) (Hitachi S4700). A VASE JA Woollam ellipsometer was used to determine the film thickness and refractive index of different films, at 65, 70 and 75^{o} in the 400-1200 nm wavelength range. Optical profilometry was used to determine the roughness of the measured films (Veeco -NT9100). The samples' Raman spectra were taken with a Renishaw microscope equipped with a HeNe laser (115-230 V, 50/60 Hz), with a maximum power of 50 W. A grating 2400 l/mm^{-1} grating was used in conjunction with a Renishaw CCD camera as the detector, laser 633 nm, an edge exposure time of 60/s, a laser power of 10%, and a 50X objective. The IR spectra of the laser-irradiated films were obtained using Thermo Electron Corporation, Nicolet 4700 (KBr crystal, resolution 0.5 cm^{-1}). All the measurements were performed at room temperature.

6.3 Results and Discussion

6.3.1 Film synthesis

Two different deposition methods were used to create films of silicalite-1 on Si (100) wafers: *in situ* hydrothermal synthesis and *ex situ* synthesis via the deposition of suspension of silicalite-1 NC. The deposition of a suspension of pre-made NC onto a substrate via spin-coating (*ex situ*) is a quick and convenient technique that is commonly used for the preparation of commercial sol-gel optical coatings e.g. antireflection, corrosion resistant coatings. For spin-coated films in an ideal system, the thickness of the film formed is inversely proportional to the square root of the rotation speed **(equation 6.5)**:

$$\text{Thickness} \propto \sqrt{\frac{1}{speed}} \qquad \textbf{6.5}$$

Using the standard, non-templated, sol-gel method, the film thickness is typically limited to about 1 μm. However, films up to 10 μm can be obtained by the application of multiple coatings, with appropriate drying or evaporation steps in between the coating steps [28].

Thicker films, which could be used as the basis for multimode planar waveguides, would require thicknesses ranging from 6-10 μm. In that case, *in situ* hydrothermal film syntheses might be a more appropriate choice, since these syntheses typically result in thicker films whose thickness is easily controlled via the crystallization time. However, prior research has shown that, for electronic properties (which are closely related to

optical properties), the synthesis and deposition methods can have a significant impact on the resulting properties [45-47]. Therefore, we explored the refractive index of *in situ* grown silicalite-1 films and compared those values with *ex situ* silicalite-1 films. The IR and Raman spectra of *in situ* grown films were then evaluated after laser irradiation.

6.3.1.1 Silicalite-1 films grown by in situ hydrothermal synthesis

Changes in the synthesis parameters of continuous, polycrystalline zeolite films alter the resulting films' mechanical properties, such as their mechanical integrity and robustness, crystalline nature, and grain boundaries, all of which affect the way light interacts with and transmits through the material [1, 13, 26]. In order to impose control on these properties, it is essential to synthesize highly intergrown films with unidirectional crystal orientation, minimal defects and grain boundaries, and reduced surface roughness [48]. Using the method discussed, we were able to create uniform, intergrown, well-adhered, reflecting (i.e. thin films compatible for ellipsometry) films of silicalite-1 on (100) Si wafers. **Table 6-1** summarizes the various experimental parameters evaluated in this work.

Table 6-1: Summary of the different parameters used for making *in situ* grown films, characterization done and properties studied.

Molar Ratio	99.0H_2O: 0.14TPAOH: 0.84TEOS
Substrate	Si (100)
Aging time (h)	1, 2
Crystallization time (h)	2, 2.3, 2.7, 3, 3.2
Calcination	450 ^oC at 1 ^{o}/ min ramp rates for 4 h
Film characterization Techniques	XRD, SEM, Optical profilometry, Ellipsometry
Laser densification	Yes
Film properties determined	Thickness, RI, FTIR and Raman spectra

6.3.1.2 Silicalite-1 films grown by ex situ synthesis

Using the method by Mintova *et al.*, we were able to create a stable suspension of nanosized, porous crystals with the MFI-type structure, containing mono-disperse particles with a mean hydrodynamic radius (RH) ranging from 50-80 nm [44]. The monodispersed nature of the silicalite-1 NC in the suspension was confirmed using TEM images **(Figure 6-2)**. The particle size distribution and stability of the coating suspension did not alter at prolonged storage times (~30 days at ambient conditions) **(Figure 6-3)**. By tuning the crystallization time, we were able to obtain NC of different sizes **(Table 6-2)**. By doing single step spin-coating (*ex situ*) of this suspension, silicalite-1 films with different thicknesses (~150-550 nm) can be obtained [44]. The thickness range of silicalite-1 film of the *ex situ* grown films were higher when we used TEOS gel (217-550 nm) as the dispersion media as compared to when we used ethanol (153-339 nm) as the dispersion media. This is likely due to the higher viscosity of TEOS gel and greater NC packing density. **Table 6-3** summarizes the various experimental parameters evaluated in this work.

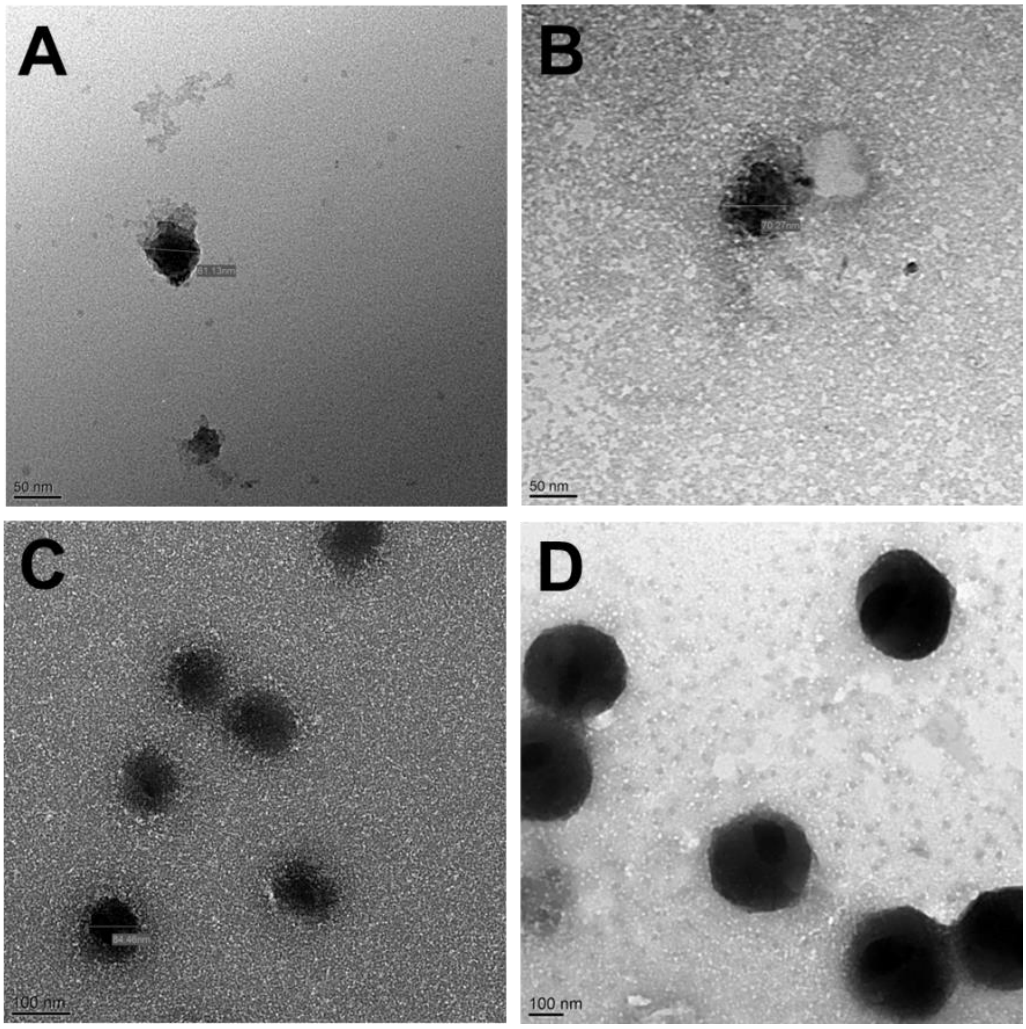

Figure 6-2: Transmission electron microscopic (TEM) images of silicalite-1 nanocrystals (NC) formed by crystallization at (A) 20 h, (B) 22 h, (C) 24 h and (D) 36 h respectively.

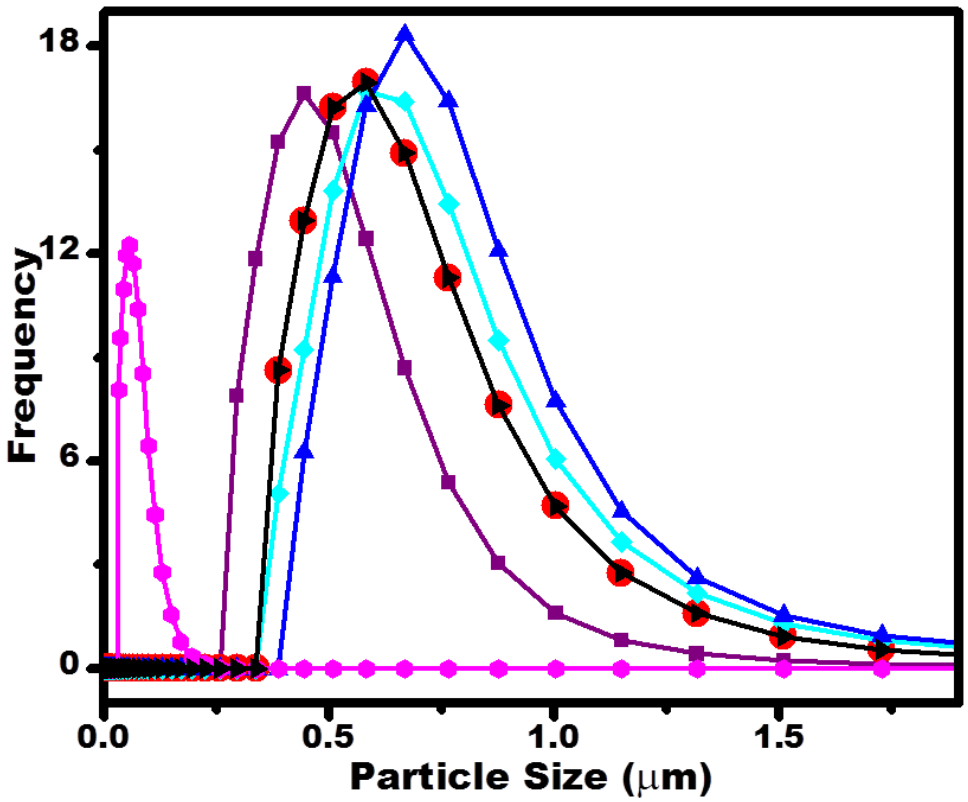

Figure 6-3: DLS data of silicalite-1 nanocrystals (NC) showing monodispersed suspensions. These suspensions were stable for a prolonged period of time (~30 days) under ambient conditions, according to repeated DLS measurements.

Table 6-2: Dynamic light scattering (DLS) data of the silicalite-1 nanocrystals (NC) used for preparation of *ex situ* samples showing their mean sizes below 100 nm. Increasing crystallization time results in increased crystal sizes.

Sl no.	Crystallization time	Median (nm)	St. Dev	Mean (nm)	St. Dev.
1	16 h	47.914	6.542	51.142	5.640
2	20 h	55.029	6.612	61.686	6.799
3	22 h	66.81	11.957	71.67	10.561
4	24 h	73.6	7.14	80.6	6.18
5	36 h	192.525	10.583	207.65	8.384
6	48 h	567.15	93.7955	631.45	110.05

Table 6-3: Summary of the different parameters used for making *ex situ* grown films, characterization done and properties studied.

Molar Ratio of NC	9TPAOH: 25SiO_2: 680H_2O: 100EtOH
Substrate	Si (100)
Aging time (h)	24
Crystallization time (h)	12, 16, 20, 22, 24, 36, 48
Molar Ratio of sol-gel (TEOS)	25SiO_2: 680H_2O
ex situ parameters	3 wt%, 3000 rpm, 1000 rpm/s, ramp rate, 35 s
Calcination	450 ^oC at 1^o / min ramp rates for 4 h
Film characterization Techniques	XRD, TEM, DLS, SEM, Optical profilometry, Ellipsometry, FTIR-ATR, Raman
Laser densification	None*
Film properties determined	Thickness, RI

* Note: Only *in situ* grown films were studied for laser densified IR and Raman spectroscopy

6.3.2 Film Characterization

The typical Bragg reflections, obtained via XRD, of the silicalite-1 NC and the *in situ* grown, *b*-oriented thin films are shown in **Figure 6-4**. Note that, as is typical for films with thickness < 500 nm, no distinct Bragg reflections were obtained using standard XRD methods for either *in situ* or *ex situ* grown silicalite-1 films of less than 500 nm (obtained for *in situ* films via short crystallization times). For *ex situ* grown films created from the deposition of a suspension of NC, only the powder pattern of the calcined NC, prior to deposition, was obtained [44]. The *in situ* films showed the expected *b*-oriented XRD pattern reported in previous literature [26, 44, 49] For *ex situ* grown films, the XRD pattern is obtained from the NC grown according to technique described in **section 6.2.2**, with 24 h crystallization and 80.6±6.18 nm sizes, to confirm the desired structure of silicalite-1 (MFI).

As expected, with an increase in crystallization time the resulting film thickness increases, which again affect the effective optical path. SEM was used to confirm the formation of intact, intergrown, uniform, and well-adhered films of the desired thickness for optical measurements. Thus, as long as the *b*-orientation of the crystals can be preserved, along with the final film properties, the choice of crystallization time should be determined by the film's resulting application. We have used films with crystallization times of 2, 2.3, 2.7 and 3 h for determination of specific film thickness **(Figure 6-5)** and their respective RI **(Table 6-4)** using ellipsometry.

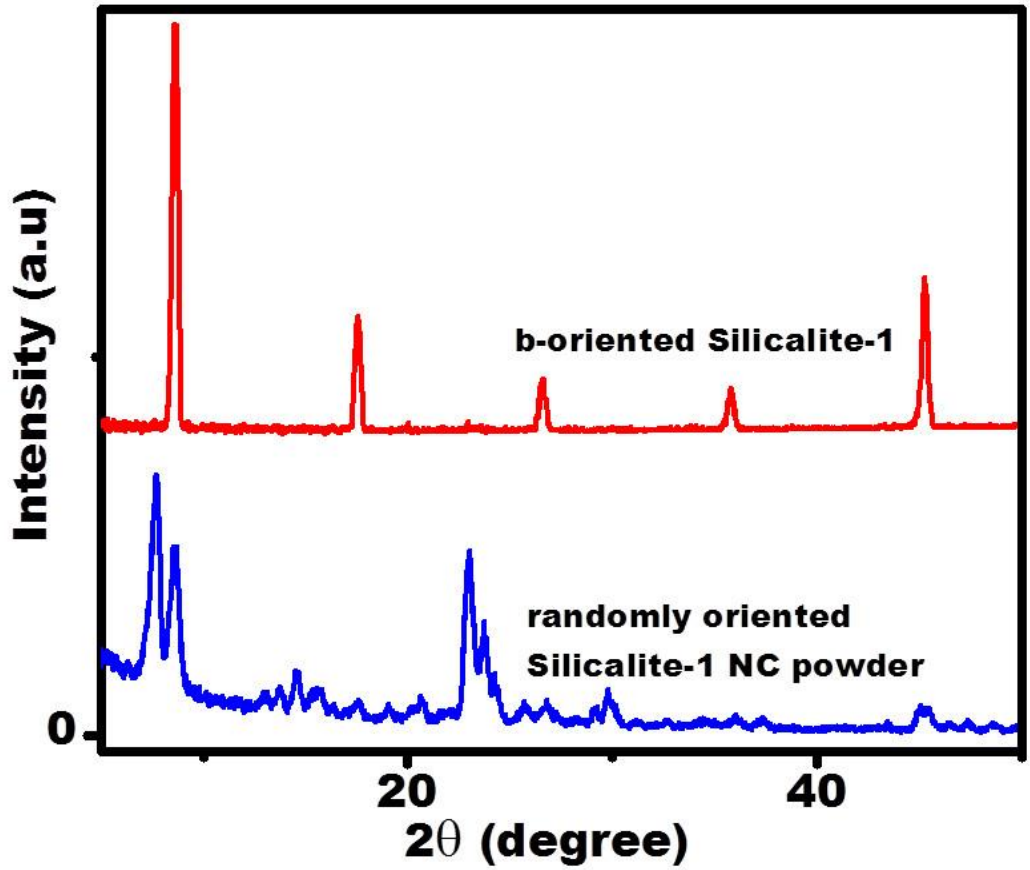

Figure 6-4: XRD pattern of *b*-oriented silicalite-1 (MFI) film and randomly distributed silicalite-1 NC powder. The 3.2 hour crystallization time for the *in situ* hydrothermal synthesis yielded the best results, of the times evaluated, in terms of crystallinity.

Figure 6-5 compares the thicknesses of *in situ* grown films on Si (100) at crystallization times from 2-3 h. The film thicknesses were measured using ellipsometry (630 nm) with 3-5 repetitions at a minimum of 3 different points on the sample. The various mean thickness values are shown in the graph **(Figure 6-5)**. It can be seen that the thickness of the *in situ* silicalite-1 films increases from 279.62±1.998 nm to 320.056±31.165 nm with a corresponding increase in crystallization time from 2 to 2.7 h. At 2.7 h, the film thickness showed comparatively large standard deviations (SD). Given that it takes about 1 h for the reaction gel to reach the crystallization temperature (165 ^{o}C), the formation of MFI nuclei, becomes uniform around 2 h, which concurs with our results [50]. As the reaction gel is further heated and the nuclei grow due to Ostwald ripening, there are increased collisions amongst the growing NC, leading to film formation and a corresponding increase in the SD of the film thicknesses, which appears to reach a maximum at around ~2.7 h for these samples. At the end of the 2nd hour (i.e. 3 h total crystallization time), the reaction gel again reaches an equilibrium temperature and continues sustained growth of the crystals, thus reducing the SD of the resulting film thicknesses and at the same time not showing marked changes in the film thickness values (320.61±2.76 nm) as compared to 2.7 h.

For the silicalite-1 films formed via *ex situ* synthesis, the film thicknesses can be fine-tuned by the number of coatings, as well as the speed of the coating. However, we found that with an increase in the number of coatings, the quality of the resulting film is compromised i.e. the occurrence of cracks between adjacent coatings increased the chances of film peeling, and the introduction of inhomogeneity in the film could be

detrimental for applications where thin, homogeneous coatings are required, such as optical coatings. Therefore, as mentioned in the methods, only one coat was applied because of the inverse relation between film thickness and the number of coatings/decrease in film quality, due to the formation of cracks [28]. The benefit of this single coating stage is that it allowed the formation of a uniform, and compact, film with homogeneous particle distribution. The size of the NC chosen is another important factor in determining the thickness of the final *ex situ* film. With an increase in the size of the NC used to coat the substrates, the film formed after one coating had higher thickness, as we would expect. Hence, depending on the thickness requirement, the crystallization time for obtaining the NC can be tuned **(Table 6-5)**.

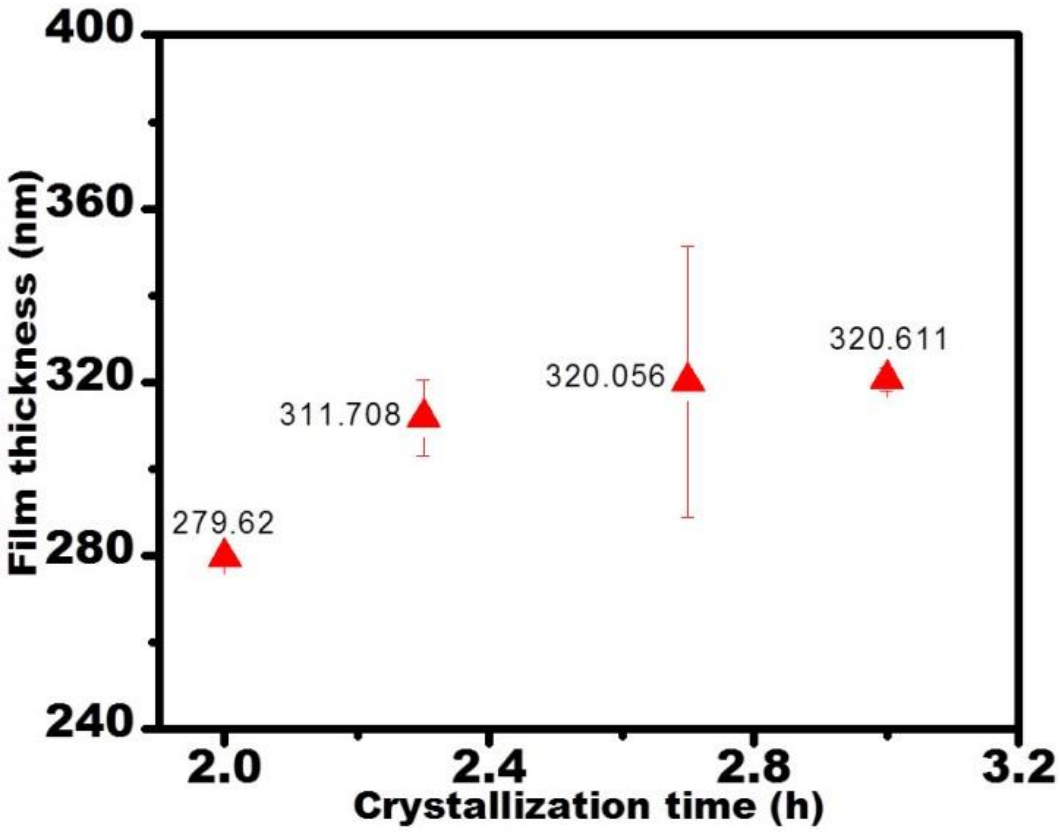

Figure 6-5: By tuning crystallization time ranging from 2-3 h films of thickness ranging from ~ 279-320 nm were made by *in situ* synthesis on Si (100) wafer.

The uniformity and quality of the calcined films was confirmed using SEM **(Figure 6-6)** [15]. Fully intergrown *b*-oriented film were made by *in situ* technique **(Figure 6-6A)** and the *ex situ* grown films also shows compact binding between NC with reduced intercrystalline spaces and surface roughness with TEOS as dispersion media **(Figure 6-6B)** Using SEM the thickness of the *ex situ* grown films were also confirmed to be in the nanometer range **(Figure 6-6C)**.

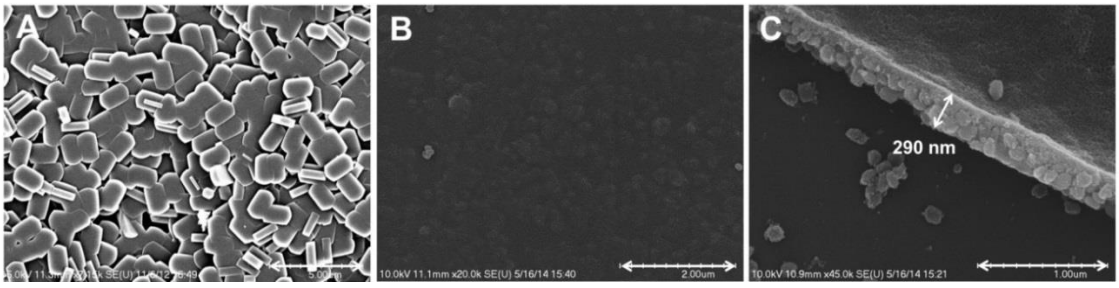

Figure 6-6: (A) *In situ* grown *b*-oriented silicalite-1 film; silicalite-1 film made by one-step *ex situ* technique with TEOS as dispersion media showing; (B) top view (C) cross-sectional view with film thickness ~ 290 nm.

These films were then subjected to optical profilometry measurements to obtain their typical surface roughness. For silicalite-1 films grown via *in situ* hydrothermal synthesis, the average roughness is 13±0.827nm. However, silicalite-1 films formed via *ex situ* synthesis had an average roughness in the order of 14.18±0.834 nm (with TEOS, **Figure 6-7B**) and as expected, the roughness of the film reduces from 54.49±1.714 nm (with ethanol), which implies that TEOS acts to bind the nanocrystals to a greater degree, hence improving the compactness, mechanical strength and uniformity of the film. **Figure 6-7A** shows that film formed with TEOS as the dispersion media binds the individual crystals to a much greater degree, i.e., high enough to cause film curling with NC.

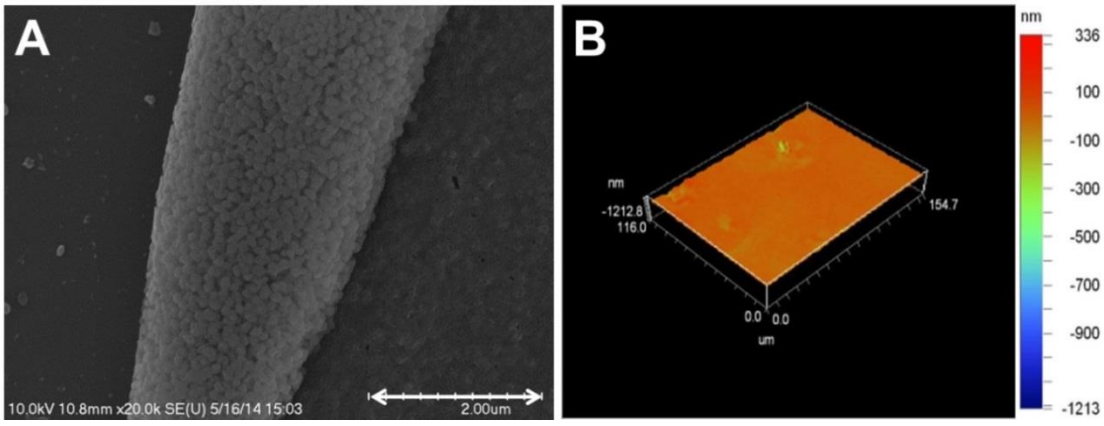

Figure 6-7: (A) Curling of TEOS coated film showing greater NC binding; (B) Representation of an optical profilometry on *ex situ* grown silicalite-1 for determination of surface roughness.

6.3.3 Optical Properties of Silicalite-1 Films

To the best of our knowledge, there are no reports on the optical parameters of direct *in situ* grown silicalite-1 films. Reports exist for *ex situ* and secondary hydrothermal grown silicalite-1 films [2, 15, 51, 52]. In this paper, for the first time, we have studied the refractive index of *in situ* grown films and have compared it with NC spin-coated (*ex situ*) silicalite-1 films. We have also compared the RI values obtained from *ex situ* films with that of reported values in the literature. The *in situ* grown films tend to minimize several limitations associated with *ex situ* grown films, addressed in **section 6.3.3.1**. In line with various methods by which the optical properties of sol-gel materials are varied, the optical properties of these materials can also be varied. Variation in their RI, and transmission or absorption properties can be obtained by changes in synthesis strategies or post-synthesis processes. Hence, *in situ* films grown at different crystallization times are expected to show variations in RI. The effect of presence of water on the RI of porous zeolites has been pointed out, and it is understood that porous material with large volume of water will invariably have greater effective RI owing to the high RI of water (1.33) compared to that of air (1.0) [28]. Silicalite-1, when made appropriately, tends to have minimal water in its pores; usually 1-2 weight % according to thermogravimetric analysis (TGA) arising from water present in the pores, cracks, or defects of a spin-coated film [28]. CO_2 laser based densification of the *in situ* grown films is expected to cause changes in the form of: altered degree of porosity, extent of remaining organic and water in the intercrystalline (meso-) and intracrystalline (micro-) pores. Such changes are likely to cause variation in transmission, absorption properties. The large amount of heat generated owing to laser irradiation is also likely to cause

variation in ratio of crystalline to amorphous nature of the films, which in turn could have effect on the way light interacts with the film. We will discuss this in the following sections.

6.3.3.1 Refractive Index

The ellipsometry data was modeled by assuming the material to be a Cauchy layer on top of which lies a porous rough layer with Bruggeman effective medium approximation (EMA). The Si (100) wafers of fixed thickness are used as the substrate. The correlation between the experimental data and modelled data varied from film deposition technique (*in situ*/*ex situ*) and across suspending media for the *ex situ* samples.

Table 6-4: Refractive index (RI) and thickness data obtained from ellipsometric modelling shows in *in situ* grown films we can tune film thickness and RI by changing synthesis parameters. *Ex situ* grown films also shows range of thickness and RI when coated with NC of different sizes or different dispersion media.

Sl no.	Film deposition method	Thickness (nm)	RI at 630 nm	Comparison with Literature	
				Thickness (nm)	RI
1	*in situ*	94.324±8.035-510.313±14.563	1.335±0.015-1.638*±0.037	-	`
2	*ex situ*[#] in EtOH	153.157±4.235-339.819 ± 1.575	1.098±0.014-1.210± 0.019	150-400 **	1.20-1.26 **(smallest=1.172)
3	*ex situ*[#] in TEOS	217.691 ± 6.74-550.89 ± 1.577	1.403±0.161-1.765±0.027	190-520***	1.38-1.39***

[#] *ex situ* films formed by coating silicalite-1 (MFI) NC with sizes 61.686±6.799 nm.

Reference; * [52], **[2, 15], ***[15]

Unlike in some recent publications where spin-coating deposition step (*ex situ*) is repeated to increase the film thickness, we performed a single coating step [15]. Given that, depending upon the type of binder used and the number of coatings applied, the final orientation of crystals, and the degree and extent of porosity of the final film might vary, as well as the potential for cracking and peeling due to multi-layer formation, we chose to use a single deposition step (*ex situ*) to keep the resulting film samples as uniform as possible for comparison. Babeva *et al*. pointed out that after one deposition step (*ex situ*) all films formed have similar thickness, about 50 nm, which is dependent on the spinning condition and the concentration of NC in the deposition solution [2]. Film thickness in the range 50-170 nm were achieved on *ex situ* films formed by 2-5 times coating of silicaite-1 NC sizes ~35 nm [2]. Since we are using 3 wt% coating suspension with minimum NC sizes ~50 nm (compared to 1 wt%, 35 nm NC size) and applying one-step coating, the thickness of the films are expected to be, at minimum, 150 nm [2, 7].

For the *ex situ* films, the RI values increase from 1.183 to 1.201 with an increase in size of the NC from 51.143 nm to 61.686 nm; however, when the *ex situ* film is made by mixing these two NC sizes the RI of the film obtained is 1.098, which is lower than the endpoint RIs of either of the sizes. Using the Bruggeman EMA (which considers the film to be an effective medium comprised of two phases i.e. pure silica and air in the free pores), the volume fraction of the free pores in silicalite-1 film is 61%, however, for individual silicalite-1 NC it is 19%. The reason for this marked increase in porosity from crystals to *ex situ* films, is the presence of inter-particular spaces in the film that significantly increases the total porosity, since the volume of these spaces are in the

mesopore size range [2, 29]. This observation led to the insight that silicalite-1 NC, when spin-coated; do not form compact films with no inter-particular spaces. Frisch *et al.* also found that there is an increase in ion-conductivity when the sizes of silicalite-1 crystals decrease to the nanosize domain compared to the micrometer domain, thus suggesting that the optical properties could follow the same trend [28]. When NC of different sizes are dispersed in same dispersion media and coated on Si (100) substrate, variations in RI can be obtained, as shown in **Table 6-5**.

Table 6-5: Film thickness and RI values obtained from *ex situ* films made by using different NC sizes.

NC size (nm)	No. of coating	Dispersion media	Thickness (nm)	RI ±SD
51.143±5.640 (16 h)	1	Ethanol	198.188 ± 2.265	1.183 ± 0.265
61.686±6.799 (20 h)	1	Ethanol	339.819 ± 1.575	1.201 ± 0.575
Mixing 1 and 2	1	Ethanol	300.48 ± 1.481	1.098 ± 0.235

The smallest reported value of the RI for *in situ* silicalite-1 coated films is 1.172 [2]. In this work, we have observed samples with an even lower RI value i.e. 1.098, obtained when NC of two different sizes were mixed and spin-coated onto a substrate in an ethanol suspension. In principle, this can occur due to the unique combination of the deposition through evaporation and the sol-gel synthesis process. Here, metal alkoxide is converted to form an infinite molecular weight oxide network through the sol-gel process. The oxide network condenses to reject the solvent, thus forming interconnected porosity upon drying. Several factors affect the product film formed by coating. For example, with a change in molar composition of the reactive gel, it is possible to affect the amount of water absorbed, thus modifying the evaporation time needed. In this work, the water content was kept constant in each type of synthesis, i.e. *in situ* and *ex situ* of redispersed silicalite-1 NC. Typically for sol-gel film formation, condensation continues to occur during the entire process and the rates of condensation and solvent evaporation affect the extent of cross-linking. The deposition conditions, such as temperature, pressure, and humidity also affects the evaporation and condensation rates. Although we performed a single coating step, multiple coating steps can cause overlap of the deposition and evaporation stages, which establishes a competition between the compaction and the stiffening of structure. This could be advantageous in cases where specific wave modes or volumes are required. In comparison, the *in situ* technique yields films with the best uniformity and intergrowth, which likely prevents variations of the modes' effective indices.

The technique of *in situ* deposition deals with fewer number of steps and can incorporate variation in final film properties compared to coating method, which distinctly involves three major steps; (1) making the nanocrystals through hydrothermal synthesis (variation in molar ratio, aging crystallization time, temperature) followed by cleaning, (2) making final colloidal suspension (variation in, wt%, stability, mono vs poly dispersion) and (3) coating steps [28].

6.3.3.2 Absorption and Transmission Characteristics

Our main focus in this section is to study changes in transmission and absorption characteristics of the densified *in situ* grown silicalite-1 films. The effect of laser irradiation is expected to vary depending on extent of heating and heat diffusion at different laser powers.

It is well understood that these regions possess different degrees of porosity and density owing to differences in the amount of internal stress that is relaxed during their heating and cooling steps [28]. Since laser exposure causes intense heating of the irradiated regions, complete removal of any remaining water (from intra-/inter-zeolitic pores) and collapsing of the surface silanols groups might led to changes in the IR and Raman spectrum. Further changes in degree of crystallinity can also be estimated and studied by doing spectroscopic studies in the laser densified regions.

Figure 6-8 shows the IR spectra of zeolite lattice vibration modes seen in the mid-IR range (1400-400 cm^{-1}) on laser densified (10, 20 and 30%) *in situ* grown

silicalite-1 films on Si (100). All spectra show a typical silicalite-1 structure associated with minor changes. The intensity ratio of the 550-450 cm^{-1} bands is indicative of the degree of crystallinity [53]. The spectrum for silicalite-1 film densified at all the three laser powers, clearly shows that the one with 20% laser densification has most distinct peak at this region. Band near 1200 cm^{-1} is indicative of presence of double five-membered ring containing structures i.e. MFI-type zeolites. **Figure 6-8** shows that the peak intensities increases for the bands near 1200 cm^{-1} for films densified at 10 to 20% laser power; however, these characteristic structural bands have lower peak intensity for films densified at 30% laser. This indicated that, at 20% laser power, the *in situ* grown silicalite-1 film receives enough heat so as to complete crystallization and retain its MFI topology; however, at 30% irradiated laser power the MFI crystallites dissociate causing reduced peak intensity [54]. It is also seen that when the irradiated laser power is 20%, the intensity of peaks for silicalite-1 at 795, 812 and 820 cm^{-1} splits into three distinct components, due to symmetric T-O stretch, which is completely absent when we raise the laser power to 30% [55].

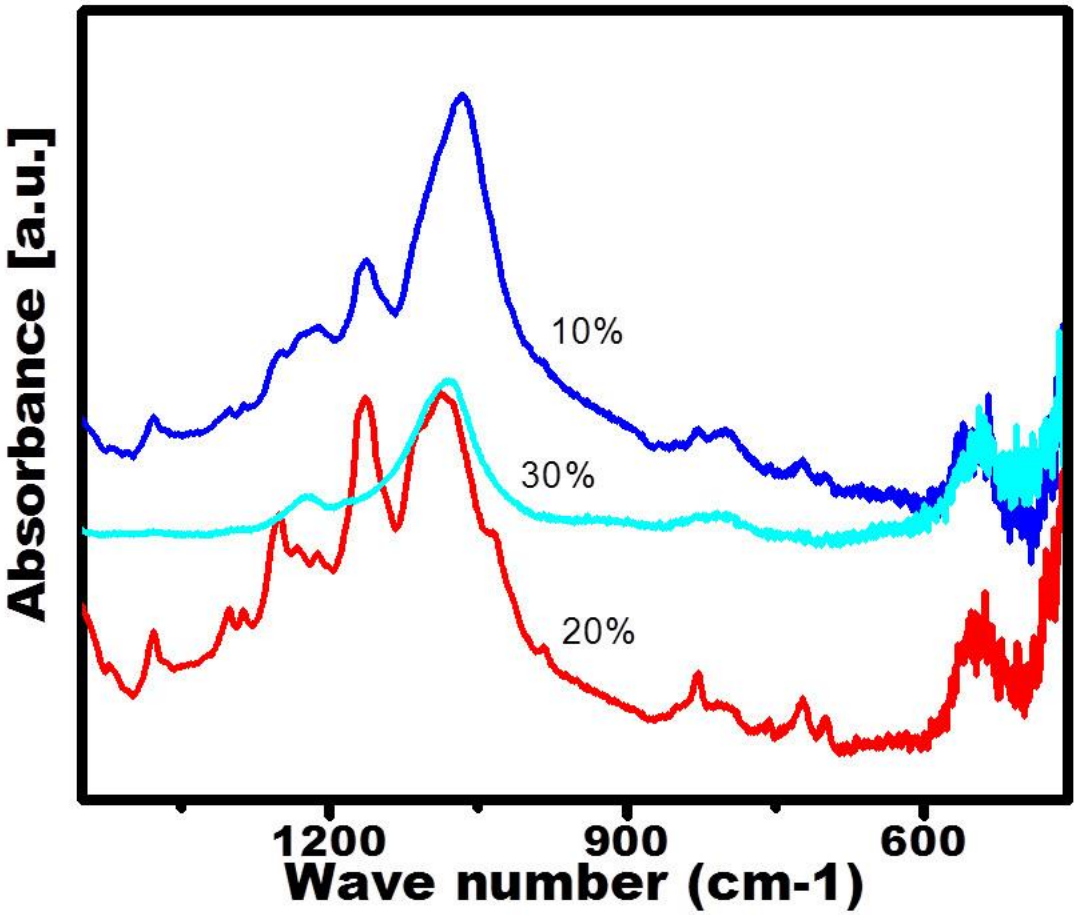

Figure 6-8: FTIR spectrum of *in situ* grown *b*-oriented silicalite films when densified at CO_2 laser powers 10, 20 and 30% respectively.

The intensity of the transmitted light through a film may be manipulated by varying the thickness of the deposited film, i.e. by varying the path-length of the transmitted light. However, the transmitted wavelength is determined by the absorbing characteristics of the MFI material composition (in this case, pure silica). Manipulation of the transmitted wavelength range can be achieved by deposition of films of non-absorbing materials, films of varying optical thicknesses, or films with different compositions. These layers formed with multiple deposition steps (*ex situ*) often lead to selective reflection/transmission of the irradiated wavelength owing to interference effects. Silicalite-1 films with specific optical performance are all dielectric systems with absorbing components (oxides, metals) that can be formed in multilayer stacks [28]. Thus by combining layers with different thicknesses and deposition methods, or by combining an absorbing layer with a non-absorbing layer, flexibility in the final optical properties can be obtained. For instance, if a silicalite-1 film is deposited in a large number of layers, the resulting structure could result in broad-band antireflection, i.e. reduced transmission at the specific wavelength.

In this paper, along with the IR spectra of *in situ* grown, laser densified silicalite-1 films, we have also studied the Raman spectra of laser densified *in situ* films. **Figure 6-9** and **Figure 6-10** shows the Raman spectra of *in situ* grown silicalite-1 films on Si (100). Sharp peaks at 619 cm^{-1} are due to the three-membered rings of SiO_4-tetrahedra. **Figure 6-9A** shows that peaks intensity at 619 cm^{-1} increases from 10 to 20% laser irradiation; however, it decreases at 30%; the possible reason for this occurrence could be due to improve in crystal effect/formation which reverses with an increase in laser power (30%)

as the crystallinity is reduced. Along with the intensity of peaks at 619 cm^{-1} measurements of the amounts of the crystalline and amorphous phases present can be estimated through the intensity of the peaks at 960 $cm^{-1}$and, both supports the observation that the samples irradiated at 20% laser power have the highest crystallinity, since strong intensity of both the 606 and 970 cm^{-1} peaks is typical of chain-like silicalite. In **Figure 6-9A, B** small peak at 606 cm^{-1} with the shoulder at 495 cm^{-1} indicates the presence of non-crystalline silica in the sample [56]. The formation of the peak at about 960 cm^{-1} is also characteristic of point defects in the Si-O network, which indicates formation of amorphous silica (SiO_2) **(Figure 6-10A)**.

The difference in the extent of inhomogeneity in the laser densified samples, i.e. the ratio of amorphous to crystalline material, can be also determined through the occurrence of poor spectral resolution in the spectral range from 400-500 cm^{-1} due to Rayleigh scattering caused by the presence of sample inhomogeneity **(Figure 6-9B)**. Intensity ratio between the broad band at about 435 cm^{-1} and the sharp peak at about 495 cm^{-1} is also used as measure of crystallinity, which also validates the same conclusion **(Figure 6-9B)**. Raman intensities at 380 cm^{-1} and 495 cm^{-1} are also subject to changes with relative crystallinity and amorphous phase. Intensity of peak at 380 cm^{-1} defines the amount of silicaite-1 hence, the peak intensity at 380 cm^{-1} must increase or remain the same to designate increase in crystallinity or structural collapse respectively on account of laser treatment **(Figure 6-9B)**.

The broad band at about 445 cm^{-1} as well as the formation of a new peak at 435 cm^{-1} (weak peak) in the Raman spectra is characteristic of the crystallization of silicalite-

1. The peak at 435 cm^{-1} has been attributed to the 6-membered ring that connects to the chains of five-membered rings (of MFI structure). The five membered rings of silicalite-1 gives the most intense Raman peak at 435 cm^{-1}, due to increase in cooperative long-range rearrangement leading to the formation of MFI structure, hence with increase in laser power from 10-20% there is further improvement in crystal effect due to increase in peak intensity at 435 cm^{-1} **(Figure 6-9B)**; however, with further increase in laser power i.e. at 30% the peak intensity recedes [56].

In **Figure 6-9B** presence of broad bands or peaks from 380 to 460 cm^{-1}; suggests existence of metastable phases. MFI peak at 380 cm^{-1} in the spectrum is overlapped in the Raman spectrum. The Raman bands at 375 and 290 cm^{-1} are probably related to 10-membered rings present in the silicalite-1 structure, the amount of which, as determined from the peak intensities is the highest at the 20% laser densified film **(Figure 6-9B)** [57].

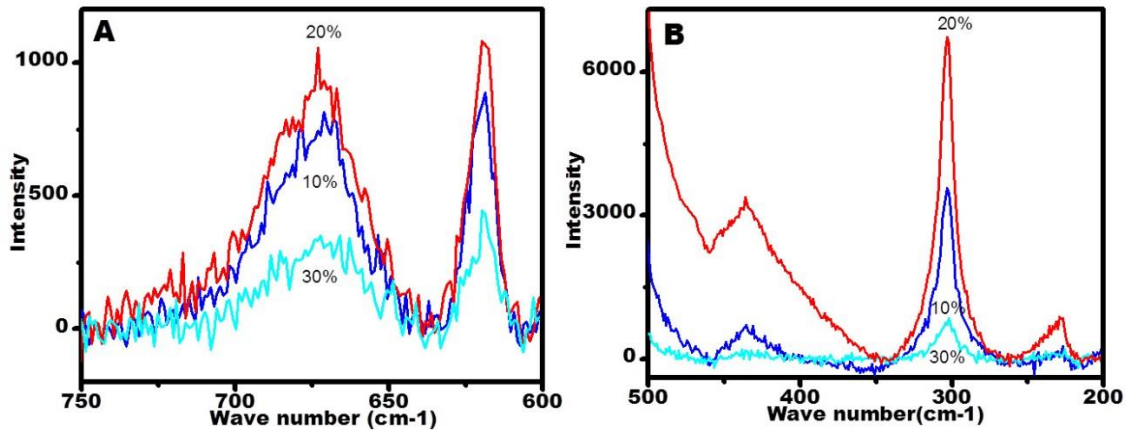

Figure 6-9: Shows Raman spectrums on *in situ* grown silicalite-1 films laser densified at 10, 20 and 30 % powers respectively in (A) 600-750 cm^{-1} and (B) 200-500 cm^{-1} spectral range.

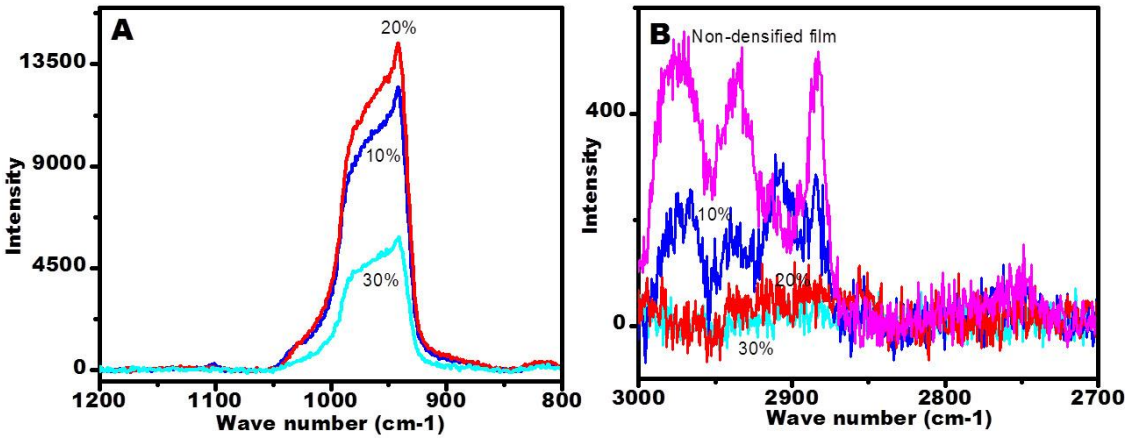

Figure 6-10: Shows Raman spectrums of *in situ* grown silicalite-1 films laser densified at 10, 20 and 30 % powers respectively in; (A) 800-1200 cm^{-1} and (B) 3000-2700 cm^{-1} spectral range.

Figure 6-10A shows Raman spectrum from *in situ* grown silicalite-1 film in the high frequency region of 800-1200 cm^{-1} due to symmetric silicon-oxygen stretching notions of silicate units having 1, 2, 3 and 4; non-bridging oxygen. Raman spectra from these silicalite-1 show band at 967-977 cm^{-1} due to ≡Si-OH vibrations **(Figure 6-10A)**. A similar peak at 978 cm^{-1} in the Raman spectra occurs from amorphous SiO_2 arising from silanols vibrations [57]. At higher laser power which also means heating the samples to higher temperature does not influence the Raman band at ~970 cm^{-1} implying that his band arises from dehydrated species **(Figure 6-10A)** given that silicalite-1 are hydrophobic in nature they readily lose any remaining water on account of laser heating. 910 and 1180 cm^{-1} is due to Si-O and does not provide further information/insight into the structure. CH stretching shows peaks at 2890, 2940, 2980 cm^{-1} for bound TPA i.e. entrapped organics. **Figure 6-10B** shows that the intensity of these peaks is highest for non-densified silicalite-1 films as we would expect followed by 10% laser densified films, which decreases significantly for both 20% and 30% laser densified films. This could be due to removal of the entrapped TPA at both 20 and 30% laser power; however, at 20% the peaks are still discernible. Additional peak shift from 2980 to 2991 cm^{-1} (for CH_3) and 2892 cm^{-1} for TPA from non-densified to laser densified samples is seen in **Figure 6-10B**. Based on these data, we observed that changes in laser densified *in situ* silicalite-1 films could act towards solving a major factor that contributes significantly to attenuation and optical loss due to scattering at crystalline or grain boundaries of individual crystals by reducing the boundary effect of individual crystals through a melting process [58].

Zeolites show large optical nonlinear susceptibility and are on par with inorganic glasses in terms of use due to transparency, ease of fabrication to form waveguides and other optical components, chemical and thermal stability, mechanical strength (hardness 6000 MPa, strength 100 MOR sigma in MPa) and resistance i.e. durability to laser irradiation strength comparable to silica and both are environmentally stable [28]. Thus far most methods have failed to achieve the theoretical minimum loss properties of the glasses and the minimum optical loss values obtained are with silicate-based compositions of glass in the order of 0.1 dB/km [59]. Thus the pure silica composition for zeolites (silicalite-1) is expected to possess optical loss in similar order, although this will likely vary with topology. Moreover, this composition eliminates the possibility of optical absorption/attenuation due to impurities such as transition metal and hydroxide ions [58].

6.4 Conclusions

The notion of all optical or optoelectronic computer technology has attracted much attention recently because of its potential for extreme speeds and parallel processing capabilities in areas such as computing, switches and image recognition. To convert this envisioned idea into reality and foster its growth and proliferation starts with recognition of basic optical materials for the construction of components and devices which can effectively operate and mimic as per their electronic counterparts e.g. optical transistor or amplifier. Nanostructured materials like zeolites (silicalite-1) owing to their unique relationship between structure and properties along with the flexibility to tune

their properties of refractive index (RI), absorption and transmission characteristics on changing processing and post-processing modifications have been a major area of research.

Silicalite-1 films synthesized by *in situ* hydrothermal growth had shown RI in the range 1.335-1.638 however, films formed by *ex situ* synthesis in ethanol had a range of 1.098-1.210. The RI observed while using TEOS as the dispersion media for spin coating had the highest values ranging from 1.403-1.765, which is believed to depend on the molar ratio of the TEOS thus affecting the property of binding the NC in the film. It is also reported that with change in NC sizes from 51.143-61.656 nm the RI of the resulting spin coated film in ethanol varies from 1.183-1.201. This technique of modulation of RI will allow us to judiciously select RI based on the specific waveguide mode thus allowing confinement of the wave field distribution and operational versatility with different substrates. This control also improves optical quality and inhomogeneity in RI.

We believe that a multistep process involving sol-gel synthesis of silicalite-1 film, followed by CO_2 laser irradiation/treatment can be used to prepare densified films/monoliths of silicalite-1 films with significantly reduced crystal boundaries. *In situ* grown silicalite-1 films irradiated at 20% laser power had highest crystallinity. Raman intensity at 619 cm^{-1} increases from 10 to 20% laser irradiation; however, it reduces when the laser power is raised to 30%. Raman peak at 960 cm^{-1} further showed that samples irradiated at 20% laser power had highest crystallinity. Improvement in crystal effect (long range MFI order) was also observed owing to increase in Raman peak intensity at 435 cm^{-1} (10-30% laser power).

Another interesting area of study could be observation of rigidochromism which is essentially a vast area to probe the rigidity of the matrix i.e. silicalite-1 film. For these materials we envision applications in telecommunication and laser applications like optical collimators, switches and fiber optic couplers for optical fiber communication [60-62]. In order to evaluate the suitability of silicalite-1 as optical materials the factors that needs to be considered are (1) to what degree/extent their optical properties (RI) can be tailored (2) light transmission characteristics (3) attainable material homogeneity that reduces optical loss (<0.1 dB/cm) (4) patternability to be able to produce patterned components.

6.5 References

[1] H.K. Hunt, C.M. Lew, M. Sun, Y. Yan, M.E. Davis, Microporous and Mesoporous Materials, 128 (2010) 12-18.

[2] T. Babeva, H. Awala, M. Vasileva, J. El Fallah, K. Lazarova, S. Thomas, S. Mintova, Dalton Transactions, 43 (2014) 8868-8876.

[3] T. Babeva, R. Todorov, S. Mintova, T. Yovcheva, I. Naydenova, V. Toal, Journal of Optics A: Pure and Applied Optics, 11 (2009) 024015.

[4] Y. Ikemoto, T. Nakano, Y. Nozue, O. Terasaki, S. Qiu, Materials Science and Engineering: B, 48 (1997) 116-121.

[5] L.H. Wee, Z. Wang, L. Tosheva, L. Itani, V. Valtchev, A.M. Doyle, Microporous and Mesoporous Materials, 116 (2008) 22-27.

[6] A.E. Espinal, L. Zhang, C.-H. Chen, A. Morey, Y. Nie, L. Espinal, B.O. Wells, R. Joesten, M. Aindow, S.L. Suib, Nature materials, 9 (2009) 54-59.

[7] M. Zaarour, B. Dong, I. Naydenova, R. Retoux, S. Mintova, Microporous and Mesoporous Materials, 189 (2014) 11-21.

[8] G. Schulz-Ekloff, D. Wöhrle, B. van Duffel, R.A. Schoonheydt, Microporous and Mesoporous Materials, 51 (2002) 91-138.

[9] A.S. Arico, P. Bruce, B. Scrosati, J.-M. Tarascon, W. van Schalkwijk, Nat Mater, 4 (2005) 366-377.

[10] H. Gleiter, Nanostructured Materials, 6 (1995) 3-14.

[11] T. Humplik, J. Lee, S. O'Hern, B. Fellman, M. Baig, S. Hassan, M. Atieh, F. Rahman, T. Laoui, R. Karnik, Nanotechnology, 22 (2011) 292001.

[12] A. Gusev, Inorganic Materials-New York, 35 (1999) 1318-1319.

[13] M.E. Davis, nature, 417 (2002) 813-821.

[14] Y. Zhao, B. Liu, L. Pan, G. Yu, Energy & Environmental Science, 6 (2013) 2856-2870.

[15] L. Lakiss, I. Yordanov, G. Majano, T. Metzger, S. Mintova, Thin Solid Films, 518 (2010) 2241-2246.

[16] A. Dong, Y. Wang, Y. Tang, N. Ren, Y. Zhang, Z. Gao, Chemistry of Materials, 14 (2002) 3217-3219.

[17] A. Dong, Y. Wang, D. Wang, W. Yang, Y. Zhang, N. Ren, Z. Gao, Y. Tang, Microporous and Mesoporous Materials, 64 (2003) 69-81.

[18] V. Valtchev, L. Tosheva, Chemical Reviews, 113 (2013) 6734-6760.

[19] L. Tosheva, V.P. Valtchev, Chemistry of Materials, 17 (2005) 2494-2513.

[20] G.A. Ozin, Advanced Materials, 4 (1992) 612-649.

[21] G.A. Ozin, A. Kuperman, A. Stein, Angewandte Chemie International Edition in English, 28 (1989) 359-376.

[22] J. Gierschner, Physical Chemistry Chemical Physics, 14 (2012) 13146-13153.

[23] N. Herron, Zeolites as hosts for novel optical and electronic materials, in: Inclusion Chemistry with Zeolites: Nanoscale Materials by Design, Springer, 1995, pp. 283-298.

[24] M. Pina, R. Mallada, M. Arruebo, M. Urbiztondo, N. Navascués, O. De La Iglesia, J. Santamaria, Microporous and Mesoporous Materials, 144 (2011) 19-27.

[25] I. Pellejero, J. Agustí, M.A. Urbiztondo, J. Sesé, M.P. Pina, J. Santamaría, G. Abadal, Sensors and Actuators B: Chemical, 168 (2012) 74-82.

[26] Z. Wang, H. Wang, A. Mitra, L. Huang, Y. Yan, Advanced Materials, 13 (2001) 746-749.

[27] C.M. Lew, R. Cai, Y. Yan, Accounts of Chemical Research, 43 (2009) 210-219.

[28] L.C. Klein, Sol-gel optics: processing and applications, Springer, 1994.

[29] T. Babeva, H. Awala, M. Vasileva, J. El Fallah, K. Lazarova, S. Mintova, Bulgarian Chemical Communications, 45 (2013) 18-22.

[30] B. Gospodinov, J. Dikova, S. Mintova, T. Babeva, Journal of Physics: Conference Series, 398 (2012) 012026.

[31] X. Li, J. Gao, L. Xue, Y. Han, Advanced Functional Materials, 20 (2010) 259-265.

[32] I.M. Thomas, Applied Optics, 26 (1987) 4688-4691.

[33] D. Kundu, P.K. Biswas, D. Ganguli, Journal of Non-Crystalline Solids, 110 (1989) 13-16.

[34] B. Gospodinov, J. Dikova, S. Mintova, T. Babeva, Tunable Bragg stacks from sol-gel derived Ta2O5 and MEL zeolite films, in: Journal of Physics: Conference Series, IOP Publishing, 2012, pp. 012026.

[35] D.T. Moore, Applied Optics, 19 (1980) 1035-1038.

[36] I. Kitano, Applied Optics, 29 (1990) 3992-3997.

[37] G.I. Stegeman, R.H. Stolen, Journal of the Optical Society of America B Optical Physics, 6 (1989) 652-662.

[38] B.D. Fabes, Laser processing of sol-gel coatings, in: Sol-Gel Optics, Springer, 1994, pp. 483-510.

[39] B.D. Fabes, B.J. Zelinski, D.J. Taylor, L. Weisenbach, S. Boggavarapu, D.Z. Dent, Laser densification of optical films, in: San Diego'92, International Society for Optics and Photonics, 1992, pp. 227-234.

[40] D. Taylor, B. Fabes, Journal of Non-Crystalline Solids, 147 (1992) 457-462.

[41] S. Mandal, D. Macoubrie, H.K. Hunt, Microporous and Mesoporous Materials, 204 (2015) 81-90.

[42] Y.J. Rao, T. Zhu, Z.L. Ran, Y.P. Wang, J. Jiang, A.Z. Hu, Optics Communications, 229 (2004) 209-221.

[43] Optics & Laser Technology, 58 (2014) 114.

[44] S. Mintova, T. Bein, Advanced Materials, 13 (2001) 1880-1883.

[45] A. Reina, X. Jia, J. Ho, D. Nezich, H. Son, V. Bulovic, M.S. Dresselhaus, J. Kong, Nano Letters, 9 (2009) 30-35.

[46] C.T. Campbell, Surface Science Reports, 27 (1997) 1-111.

[47] K.L. Chopra, S. Major, D.K. Pandya, Thin Solid Films, 102 (1983) 1-46.

[48] M. Tsapatsis, AIChE Journal, 48 (2002) 654-660.

[49] Z. Wang, Y. Yan, Chemistry of Materials, 13 (2001) 1101-1107.

[50] J.D. Wright, N.A. Sommerdijk, Sol-gel materials: chemistry and applications, CRC press, 2000.

[51] R.B. Bjorklund, J. Hedlund, J. Sterte, H. Arwin, The Journal of Physical Chemistry B, 102 (1998) 2245-2250.

[52] J.F. Gaynor, Nanocrystals, low dielectric constant, porous binder, in, Google Patents, 2001.

[53] I.O. Ali, A.M. Ali, S.M. Shabaan, K.S. El-Nasser, Journal of Photochemistry and Photobiology A: Chemistry, 204 (2009) 25-31.

[54] C.L. Angell, The Journal of Physical Chemistry, 77 (1973) 222-227.

[55] A. Miecznikowski, J. Hanuza, Zeolites, 7 (1987) 249-254.

[56] L. Tosheva, B. Mihailova, V. Valtchev, J. Sterte, Microporous and Mesoporous Materials, 39 (2000) 91-101.

[57] G. Deo, A.M. Turek, I.E. Wachs, D.R. Huybrechts, P. Jacobs, Zeolites, 13 (1993) 365-373.

[58] D. Tran, G. Sigel, B. Bendow, Lightwave Technology, Journal of, 2 (1984) 566-586.

[59] P. France, S. Carter, M. Moore, C. Day, British Telecom technology journal, 5 (1987) 28-44.

[60] W. Tomlinson, Applied Optics, 19 (1980) 1127-1138.

[61] I. Kitano, H. Ueno, M. Toyama, Applied Optics, 25 (1986) 3336-3339.

[62] K. Nishizawa, J. Optics16, 189 (1987).

Chapter 7: Conclusions and Future Work

7.1 Conclusion

In this research we tried to emphasize the importance of zeolites using silicalite-1 (MFI) as proof of concept material as nanoporous materials. We discussed the wide variety of non-traditional applications and the emerging properties of zeolites. We studied, compared and evaluated various techniques of converting zeolites into usable small- scale devices, most of which encumbers limitations discussed in **Chapter 3**: and **Chapter 4**: Part I of the thesis evaluates the several existing techniques for patterning of zeolites in micro-scale. We discussed methods involving patterning with etching and lithography followed by deposition of zeolite nanocrystals or incorporation of zeolite seeds into prefabricated patterns. These encumber the concerns of obtaining desired zeolite loading or multiple steps of coating or deposition. The post coating of the patterned substrates also pose the chances of uneven surface coverage by coating with several spots on the microchannel devoid of zeolite crystals. In **Chapter 4**: we introduced the technique of patterning silicalite-1 films using a high frequency CO_2 laser. This technique of patterning using CO_2 laser ablation takes care of several existing limitations. Channels and waveguides were created on silicalite-1 films of different crystal orientation and thickness. Being a direct laser writing (DLW) technique this patterning strategy acts as a rapid, inexpensive, flexible to sample size and shape fabrication for various applications. This technique also alleviates the need of time consuming, labor intensive, post-processing, complex clean-room operations etc. Since no physical contact

is involved between the material and the tool the chance of film contamination and defect formation is also largely minimized and allow us to patterns zeolite like films with control over feature location, morphology, aspect ratio, roughness etc. It is seen that feature dimension, roughness, quality and resolution is of the same order as the existing techniques. We believe that this study will contribute towards the transition in using zeolites in micro-scale devices and components for purposes other than their conventional ones which mostly encumbers large scale consumption.

Though patterning using CO_2 laser addresses one of the primary criteria in the selection process of optical material there remains second criteria of optical transparency to be studied. The knowledge about material properties of zeolites should go in parallel with that of ways to converted into usable components or features so as to harness their benefits for real world applications. Along with successful patterning of various features (design and sizes) determining their optical behavior and how they can be tuned will pave the way to use these patterns to tailor light as waveguides which will further give us insight about the way light interacts with these materials and their efficiency in acting as waveguides. The notion that illumination of such a material with intense laser light will cause change of its refractive index thus forming a switching action at the same time denoting change in nature of transmission from opaque to transmissive state fostered our interest to conduct study reported in part II of the thesis.

Part II of this thesis encompasses studying the optical properties of silicalite-1 films. In this thesis for the first time we reported the refractive index of *in situ* grown silicalite-1 films. The *in situ* film provides us with several benefits compared to *ex situ*

grown films **(Chapter 6:)**. Range of RI were reported along with their corresponding film thickness values at different crystallization times, which were compared with both *ex situ* grown film in our laboratory and in literature. The films synthesis strategies were also evaluated in details in order to minimize defects for applications of these films as optical coatings **(Chapter 5:)**. Silicalite-1 films synthesized by *in situ* hydrothermal growth had shown refractive index (RI) in the range 1.335-1.638; however, films formed *ex situ* technique i.e. by spin-coating of NC in ethanol as dispersion media had a range of 1.098-1.210. The RI observed while using TEOS as the dispersion media for spin coating had the highest values ranging from 1.403-1.765, which is believed to depend on the molar ratio of the TEOS thus affecting the property of binding the NC in the film. It is also reported that with change in NC sizes from 51.143-61.656 nm the RI of the resulting *ex situ* film in ethanol varies from 1.183-1.201. This technique of modulation of RI will allow us to judiciously select RI based on the specific/intended waveguide mode thus allowing confinement of the wave field distribution and operational versatility with different substrates. For these materials we envision applications in telecommunication like optical collimators, switches and fiber optic couplers. In order to evaluate the suitability of silicalite-1 as optical materials the factors that needs to be considered are (1) to what degree/extent their optical properties (RI) can be tailored (2) light transmission characteristics (3) attainable material homogeneity that reduces optical loss (<0.1 dB/cm) (4) patternability to be able to produce patterned components.

We believe that a multistep process involving sol-gel synthesis of silicalite-1 film, followed by CO_2 laser irradiation/treatment can be used to prepare densified

films/monoliths of silicalite-1 films with significantly reduced crystal boundaries. In this thesis we have also studied the densification effects of CO_2 laser irradiation on *in situ* grown silicaite-1 films. *In situ* grown silicalite-1 films irradiated at 20% laser power shows highest crystallinity based on its IR and Raman spectrum. In the IR spectrum intensity ratio of the 550-450 cm^{-1} bands is indicative of the degree of crystallinity and the spectrum for silicalite-1 film densified at all the three laser powers indicates that the one with 20% laser densification has most distinct peak at this region. The IR peak intensities increases for the bands near 1200 cm-1 for films densified at 10 to 20% laser power; however, these characteristic (MFI-type zeolites) structural bands have lowed peak intensity for films densified at 30% laser most likely due to laser assisted dissociation of the crystalline structure. Raman intensity at 619 cm^{-1} increase from 10 to 20% laser irradiation; however, it reduces when the laser power is raised to 30%, which could be due to at first increase in crystal effect (from 10-20%) followed by their disintegration (30%). This observation is also supported by poor spectral resolution around 400-500 cm^{-1} due to presence of both crystalline and amorphous (disintegrated crystallinity) phase. Highest Raman peak at 960 cm^{-1} on CO_2 irradiated samples further showed that samples irradiated at 20% laser power had highest crystallinity. Improvement in crystal effect (long range MFI order) was also observed owing to increase in Raman peak intensity at 435 cm^{-1} as effect of laser densification (10-30%). Observations in the Raman spectra supporting our observations are discussed in detail in

Chapter 6:

7.2 Future Direction

The notion of all optical or optoelectronic computer technology has attracted much attention recently because of its potential for extreme speeds and parallel processing capabilities in areas such as computing, switches and image recognition. To convert this envisioned idea into reality and foster its growth and proliferation, requires several basic optical materials for the construction of components and devices which can efficiently mimic their electronic counterparts e.g. optical transistor or bi-stable device acting as light switches or amplifier. However, in these materials must possess certain basic properties in order to function as optical or optoelectronic devices with extreme efficiency and acuity; for e.g. very rapid optical switching (to the order of picosecond), photo-stability and thermal-stability (to be able to perform trillions of switching actions per second and for long period of time).

The idea of being able to realize material with the above stated properties is to involve the use of third-order non-linear optical properties, x^3 to cause a transient refractive index change. Optical Kerr effect is based on non-linear polarization with effective applications in photonic devices. This effect arises due to third-order optical non-linearity/susceptibility [1]. The relation can be represented as below also known as Miller's rule:

$$X^{(3)} = (X^{(1)})^4 \text{ X } 10^{-10} \text{ esu} \qquad \textbf{7.1}$$

Where $X^{(3)}$ is known as 3rd order optical non-linear susceptibility which is related to linear susceptibility through Miller's rule and $X^{(1)}$ is the linear susceptibility. $X^{(1)}$ has

linear correlation with linear refractive index, 'n'; thus implying the fact that, $X^{(3)}$ must increase with increase in RI of the material i.e. $X^{(3)}$ should be large in materials with high 'n'. Optical properties measured using PbO-TiO_2 glass plates of about 0.5 mm thickness revealed that with decrease in porosity or in porous PbO-TiO_2 glass the value of $X^{(3)}$ is higher since $X^{(3)}$ is directly related or is positively dependent on RI. Hence, we can derive form this observation that silicalite-1 films could possibly give rise to high values of optical non-linearity. In order to implement nonlinear materials to perform optical/optoelectronic functions the material need to have high optical quality with large and stable optical nonlinearity. Zeolites are primarily materials with optical linearity as bulk effect. The response time for such 3rd order nonlinear materials with non-absorptive optical nonlinearity is in sub-picosecond time range, thus suitable for rapid optical switching [1]. Hence, we envision that with further studies on optical properties and means to convert them into useful optical components will have significant impact on our knowledge of optical materials at fundamental levels well as extend the current library of techniques and material systems that can be used to improve the overall performance of integrated optics components. Here we propose the following approaches.

7.2.1 Patterning using Pulsed Laser

In order to extend the application of micro-scale patterning of silicalite-1 films using simple laser (CO_2) writing process we propose different methodology. Since the preciseness and resolution of the features made using CO_2 laser is not limited by the basic film properties, but due to limitations imposed by the instrument, we believe using a

differ laser and lens system with short pulse duration (e.g. femtosecond laser) and minimum diffraction of the laser beam; reduced spot size can considerably improve the quality and feature resolution. Using an objective with higher numerical aperture will significantly reduce the diffraction limit of the spot size thus provide smaller spot hence greater feature resolution, The proposed technique can also led to scaling-down of the feature sizes with reduced surface roughness compared to the minimum feature sizes reported in this these. Using an automated stage along with computer-aided design (CAD) interfaced with a LabView program can lead patterning with much complicated design imparting control over the rate of material removal.

7.2.2 Optical Studies on Densified Zeolites with Different Zeolite Compositions

As we discussed in **Chapter 6:**, the potential of silicalite-1 materials to show change in RI, caused due to change in microporous nature, degree of densification, structural and compositional inhomogeneity, can be further studied to observe novel properties and applications. Along with changing silicalite-1 film processing conditions (in situ/ex situ), techniques of microwave heating, using secondary growth can led to useful insight about their effects on final optical properties.

We propose studying the evolution of RI in zeolite films by changing their synthesis conditions *(in situ*/*ex situ*), compositions (silicalite-1/aluminosilicate etc.) at different molar ratios. CO_2 laser based densification of such films (silicalite-1/aluminosilicate) caused at different laser powers is expected to cause changes in optical

property (RI, IR and Raman) as well its homogeneity. We propose studying similar CO_2 laser densification effects on their transmission and absorption characteristics. For zeolite films made using *ex situ* technique we believe interesting phenomenon could be observed by changing the type, nature and concentration of the dispersion media in the *ex situ* grown silicalite-1 films and study their optical properties. With change in dispersion media i.e. change in molecular weight the effects on GRIN index of refraction can be found using molar refraction, R from the following relation **(equation 7.2)** [1];

$$R_i = [(n_i^2-1)/(n_i^2+2)] / (M_i/\rho_i) \qquad \textbf{7.2}$$

Where n_i is index of refraction, M_i is molecular weight, ρ_i is density for species I, which in case of zeolites vary with framework density and will be constant depending upon the framework type of the zeolite used along with composition and deposition techniques, the specific combination we studied are Silicalite-1 (MFI) with deposition technique *in situ/ex situ*.

Also, $R = \Sigma X_i R_i$ and $\rho = \Sigma X_i \rho_i$, where, X_i is mole fraction of oxide, which is constant across film deposition technique and $n = \Sigma(n_i X_i)$ and $\alpha = \Sigma(\alpha_i X_i)$ where, n refractive index, α thermal expansion co-efficient of silicalite-1 film, which can be easily determined. Performing optical characterizations of films prepared across different molar composition of synthesis gel will provide useful insight into their optical properties and tailoring based on these relations. This can be interesting and very valuable addition to the existing work we have done.

7.3 References

[1] L.C. Klein, Sol-gel optics: processing and applications, Springer1994.

VITA

Swarnasri Mandal was born in a Bengali-speaking, Brahmin Mukherjee family in West Bengal, India. Her father Asok Kumar is a Mining Engineering personnel and worked for Coal India as Deputy General Manager (P&P) and her mother Banani is a home-maker. She has an elder sister, Srirupa who completed her MS in Computer Science from NIT, Durgapur and currently works for VISA, Singapore.

She has achieved academic excellence very early and topped the nationwide examination (Indian Certificate of Secondary Education) in school. She received her Bachelor's degree in Pharmaceutical Sciences from India in 2008 and received scholarship for academic excellence for four consecutive years and received top-student award in the University upon Graduation. Later she joined Indian Institute of Technology, Kanpur under mentorship of Professor Shantanu Bhattacharya and Professor Amitabha Ghosh and worked in areas of BioMEMS, nanotechnology and lab-on-chip. She worked with Dr. John. A. Viator at University of Missouri, Columbia towards extending the application of photoacoustic in detecting cancer cells before joining Dr. Heather K. Hunt and worked towards development and characterization of novel optical and electronic materials. Her interest also lies in

Quantum Mechanics and The Theories of Relativity. Areas of Astrophysics and Cosmic Sciences fascinate her. Tennis is her favorite sport and she is a decent Table Tennis player and admires Roger Federer. She also enjoys doing salsa.